A combined in-vivo/in-vitro approach to study knee injury mechanism

by

Preet Sabharwal

A thesis
presented to the University of Waterloo
in fulfillment of the
thesis requirement for the degree of
Master of Applied Science
in
Mechanical Engineering

Waterloo, Ontario, Canada, 2011

AUTHOR'S DECLARATION

I hereby declare that I am the sole author of this thesis. This is a true copy of the thesis, including any required final revisions, as accepted by my examiners.

I understand that my thesis may be made electronically available to the public.

Abstract

The anterior cruciate ligament (ACL) stabilizes the knee during various sporting activities and has great importance as the knee relies entirely on the ligaments and muscles for stabilization. The ACL commonly gets injured during sports activities such as basketball, soccer, and football. In the United States over 80,000 ACL injuries occur every year. There has been decades of research performed on ACL injuries regarding the injury mechanisms of non-contact ACL injuries, but yet they are still not well understood. This is mainly because trials and tests cannot be conducted on live subjects to understand the injury mechanisms.

Existing in-vivo and in-vitro studies in the literature do not relate the effects of dynamic knee muscle forces and kinematics of sports activities with the strain in the ACL.

In this thesis, in-vivo and in-vitro approaches are combined to quantify the effects of muscle group forces on ACL strain during jump landing. This is done by first obtaining muscle force profiles of the knee by performing motion capture and inputting the ground reaction forces and kinematics into a musculoskeletal model. Using the muscle forces and a six axis sagittal plane dynamic knee injury simulator the jump landing simulation can be performed. Six electromechanical actuators controlled by a multi-axis control system apply dynamic muscle forces at the insertion sites of the hamstrings, quadriceps, gastrocnemius, and a hip moment to simulate the hip flexors. The ACL strain is measured using a differential variable reluctance transducer mounted on the ACL.

Our results show that the simulator is able to successfully perform jump landing. The muscle force-time profiles tracked the input very well. The ACL strain from our studies fell within a reasonable level compared to data from other studies of jump landing. This simulator has proven to be successful in simulating high-risk motions.

Acknowledgements

I would like to thank my supervisor Dr. Naveen Chandrashekar for his help and guidance. I would also like to thank Neil Griffett for his help in trouble shooting the simulator and Iris Levine for her help with the motion capture. Lastly, I would like to thank my family, friends, and fellow graduate students for their help and support.

Dedication

I would like to dedicate this thesis to my family and friends.

Table of Contents

List of Figures

List of Tables

Chapter 1

Introduction

1.1 : Knee Anatomy

1.1.1 : Knee joint and Surrounding Anatomy

The knee joint is the most complex and largest diarthrosis of the body. The joint is similar to a hinge joint with the exception that it is also able to move laterally and have a slight medial and lateral rotation about the axis of the lower leg in the flexed position. The knee joint is composed of the tibiofemoral and the patellofemoral joints. The tibiofemoral joint is between the condyles of the tibia and the femur while the patellofemoral joint lies between the patella and the patellar surface of the femur. See Figure 1.1.

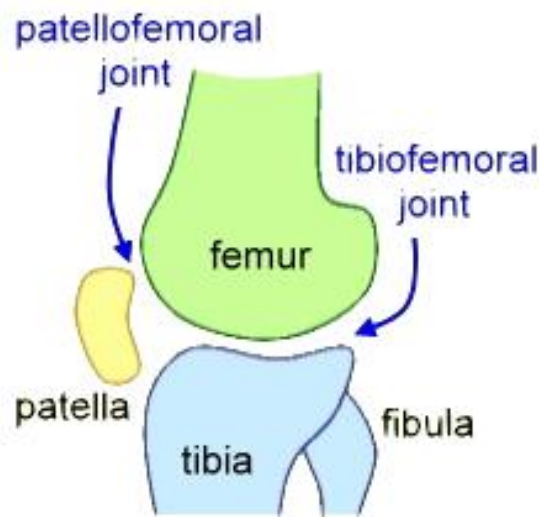

Figure 1.1: Medial view of right knee displaying the tibiofemoral and patellofemoral joints.

The articular capsule of the knee joint encloses the medial, lateral and posterior regions of the knee. The anterior region of the knee is covered by the quadriceps femoris tendon which has the patella

embedded within it. The patellar ligament extends from the patella to the tibial tuberosity of the tibia (McKinley, 2008).

The collateral ligaments are found on the sides of the knee joint. The lateral collateral ligament stabilizes the lateral surface of the joint and extends from the femur to the fibula. The medial collateral ligament reinforces the medial side of the knee joint and runs from the femur to the tibia. The lateral collateral ligament prevents hyperadduction while the medial prevents hyperabduction of the leg at the knee (McKinley, 2008).

Medial and lateral menisci are cushiony C-shaped fibrocartilage pads found on the condyles of the tibia and serve as cushions between the articulating surfaces of the knee joint. The menisci provide partial stability medially and laterally to the joint and continuously change shape to conform to the articulating surfaces (McKinley, 2008).

The cruciate ligaments are two of the most important aspects of the knee joint. The primary mission of the cruciate ligaments is to limit anterior and posterior movement of the femur on the tibia. The anterior cruciate ligament (ACL) runs from the posterior femur to the anterior side of the tibia. The posterior cruciate ligament (PCL) runs from the anteroinferior femur to the posterior side of the tibia. The ACL and PCL cross each other forming an X. During extension the ACL is pulled tight preventing hyperextension and during flexion the PCL becomes tight preventing hyperflexion. The ACL prevents anterior movement while the PCL prevents posterior movement of the tibia on the femur (McKinley, 2008).

The tibia and fibula are located between the knee and the ankle. They are both connected by a dense connective tissue called the interosseous membrane. The tibia is medially placed and is the second largest weight bearing bone in the skeletal system. The head of the tibia is broad and has two flat surfaces called the medial and lateral condyles. These condyles articulate with the medial and

lateral condyles of the femur. The femur is the largest weight bearing body and is located between the knee and the hip (McKinley, 2008).

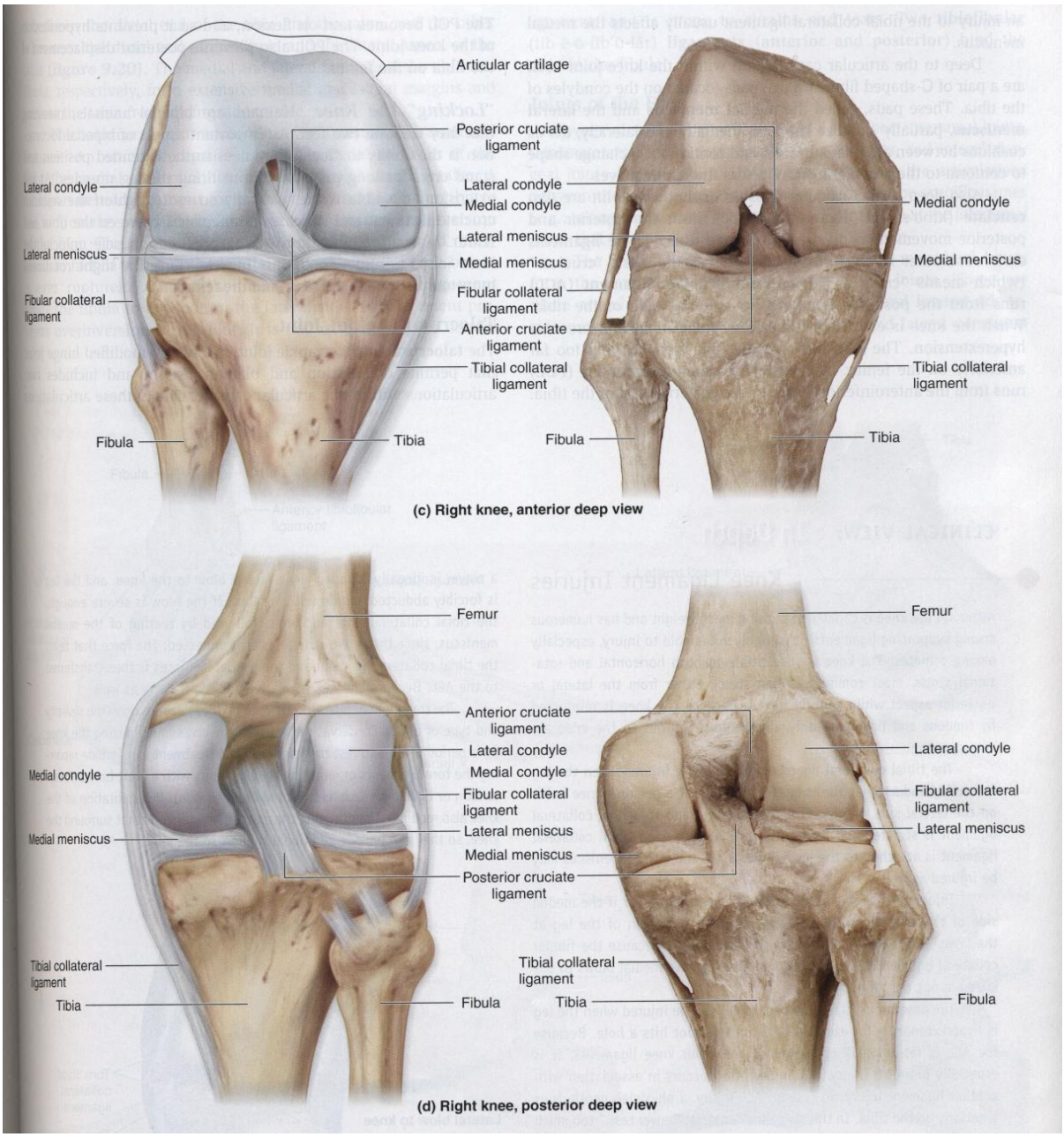

Figure 1.2: Detailed knee anatomy (McKinley, 2008).

1.1.2 : Muscles that move the knee/leg

The leg extensor and flexor muscles are responsible for the flexion and extension of the leg at the knee joint. The leg extensor muscles are the anterior thigh muscles or compartment and composed of the large quadriceps femoris muscle. The flexor muscles are the sartorius, gracilis, and hamstrings (McKinley, 2008).

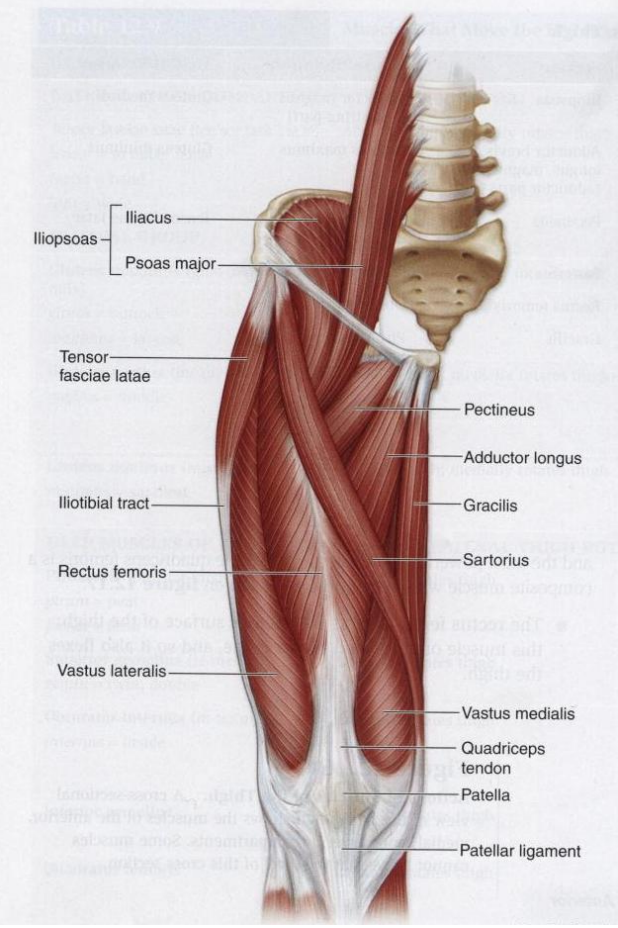

Figure 1.3: Anterior thigh (McKinley, 2008).

The quadriceps femoris is the most powerful muscle in the body and is a composite muscle made up of four extensor muscles that converge on the quadriceps tendon. The four muscles are the rectus femoris, vastus lateralis, vastus medialis, and the vastus intermedius. The rectus femoris is on the

anterior surface of the thigh and both flexes and extends the thigh. The vastus medialis and lateralis are found on the anterior side of the thigh medially and laterally as the name suggests. Finally the vastus intermedius is between the other two vastus muscles and positioned deeper to the rectus femoris. The quadriceps tendon extends inferiorly and attaches to the patella from which the patellar tendon extends to the tibial tuberosity (McKinley, 2008). See Figure 1.3.

The sartorius is a long straplike muscle that extends across the anterior surface of the thigh from the superolateral to the inferomedial side. The Sartorius flexes and rotates the thigh laterally and flexes and rotates the leg medially. The Gracilis is one of the muscles of the thigh that flexes and adducts the leg. It is located in the adductor compartment of the thigh which is the region containing the adductor muscles (McKinley, 2008). See Figure 1.4.

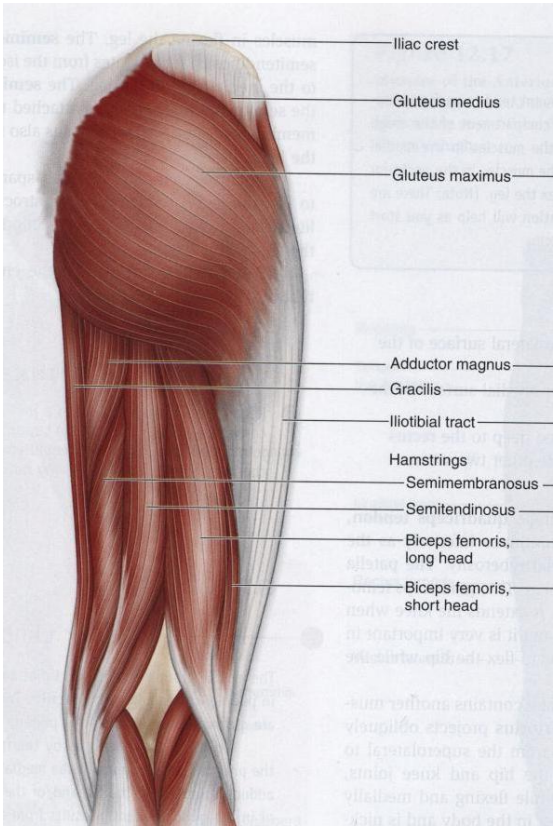

Figure 1.4: Posterior thigh (McKinley, 2008).

The hamstrings are located on the posterior side of the thigh and are the flexors of the thigh. The three hamstring muscles are the biceps femoris, semimembranosus and the semitendinosus. The biceps femoris inserts on the posterior lateral side of the leg and has the ability to laterally rotate the leg when it is flexed. The semimembranosus extends from the ischial tuberosity and attaches to the posterior medial side of the leg. The semitendinosus is superficial to the semimembranosus and it attaches to the posterior medial side of the leg. Both muscles rotate the leg medially when it is flexed (McKinley, 2008). See Figure 1.4 for a more detailed look at the posterior thigh. The knee has six degrees of freedom.

The gastrocnemius has a medial and lateral head commonly referred to as the calf muscle and is another important large muscle that plays a part in the flexion of the leg at the knee. It also plantar flexes the foot. The muscle spans both the knee and the ankle joints. It is the most superficial muscle with two thick bellies. Figure 1.5 displays a detailed look at the posterior lower leg. Figure 1.6 displays the internal/ external rotation, varus/ valgus rotation (adduction/ abduction), and the flexion/ extension of the knee.

1.1.3 : Knee joint stability

The tibiofemoral joint is stabilized by the interaction of both dynamic and passive stabilizers. Dynamic stabilizers are the muscles that cross the tibiofemoral joint. These muscles are the quadriceps, hamstrings, and triceps surae(made up of the gastrocnemius and soleus muscles). The passive stabilizers are the noncontractile parts of the knee. These are the joint capsule, lateral and medial menisci, the medial and later cruciate ligaments, and the ACL and PCL. The function of the cruciate ligaments is to maintain normal movement between the articulating surfaces of the femur and tibia (McKinley, 2008).

When the leg is fully extended at the knee, the ACL and the hamstrings work together to prevent the anterior dislocation of the tibia relative to the femur by resisting forward movement of the tibial plateaus. Likewise, the PCL works with the quadriceps to prevent posterior dislocation of the tibia relative to the femur by resisting backward translation. It is also generally uncommon for the ACL to tear when the knee is flexed since the quadriceps line of action changes to work with the hamstrings and ACL in resisting forward translation of the tibial plateaus. The cruciate ligaments are also responsible for preventing hyperextension of the tibiofemoral joint, medial and lateral displacement of the tibia relative to the femur, and internal rotation of the tibia relative to the femur (Gerwyn Hughes, 2006).

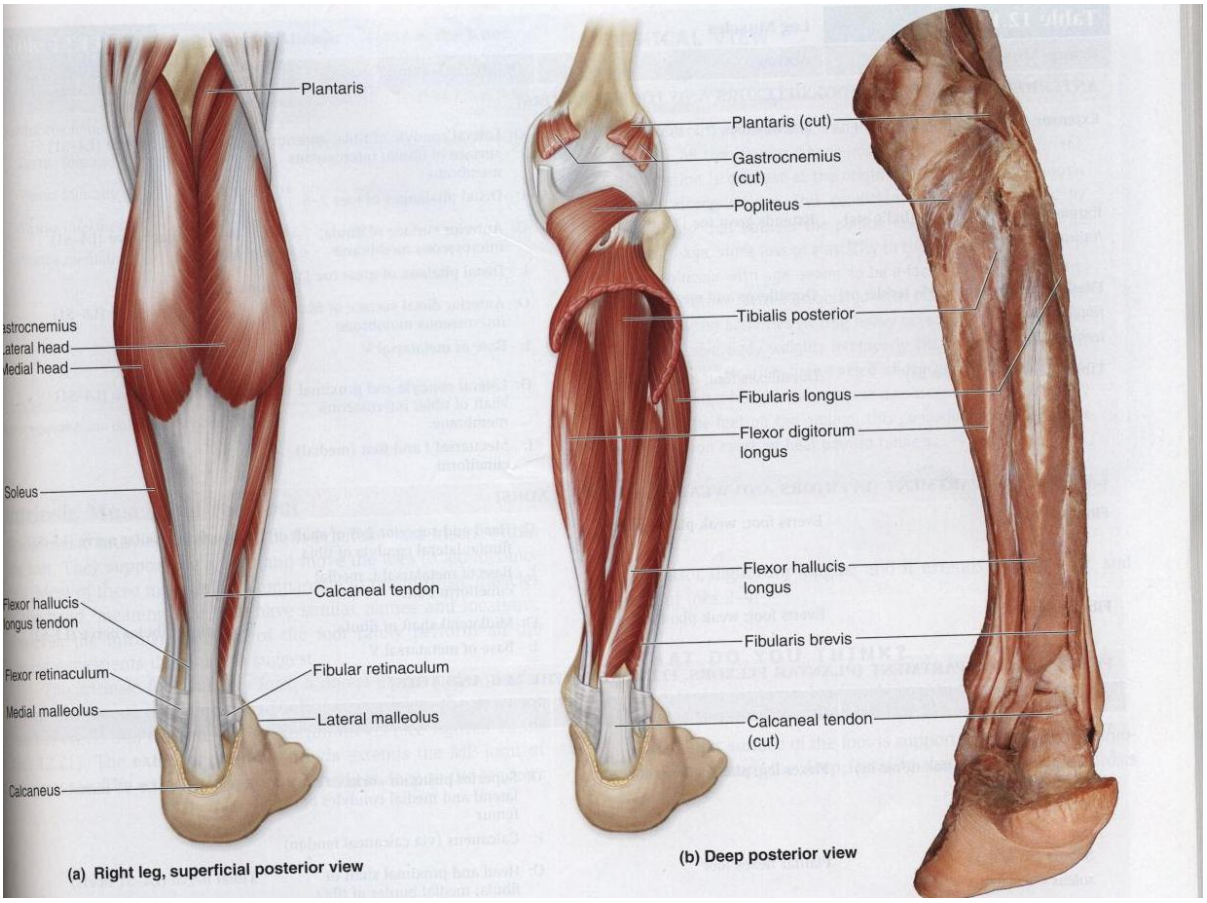

Figure 1.5: Detailed look at posterior lower leg (McKinley, 2008).

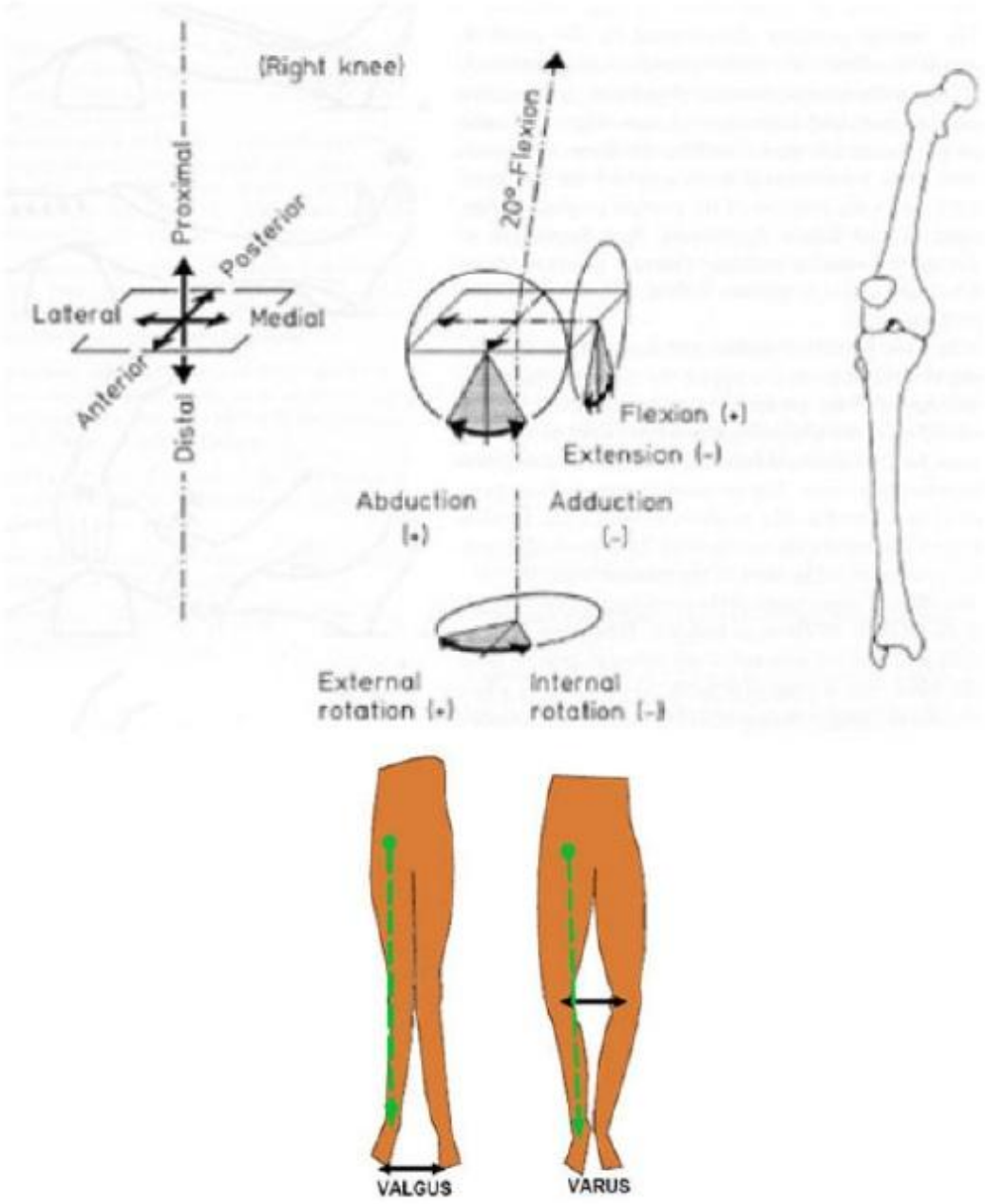

Figure 1.6: Degrees of freedom of the knee.

1.2 : Common non-contact ACL injuries

Non-contact Anterior cruciate ligament (ACL) injury is a common sports related injury. Approximately 80,000 ACL injuries occur annually within the United States, with roughly 50,000 requiring surgical reconstructions (Gerwyn Hughes, 2006). Between 70% and 90% of ACL injuries occur in large volumes as a result of non contact injuries (Gerwyn Hughes, 2006). It has been observed that during decelerating movement types such as jump landing, pivoting, sudden change of direction, or sidestepping there has been an increased risk of ACL injury. The explanation often given for the ACL injury is that at ground contact the leg is in a more extended knee positioning, which results in higher external ground reaction forces (Thomas W. Kernozek, 2005). It also results in a higher resultant force vector between the patellar tendon and the tibia coupled with a large eccentric quadriceps contraction (Thomas W. Kernozek, 2005). This causes an increased anterior translation of the tibia relative to the femur, which mechanically strains the ACL (Thomas W. Kernozek, 2005). This can be seen in Figure 1.7. ACL injury is relatively high in sports such as basketball, handball, netball, soccer and volleyball that are characterized by a high frequency of landing, decelerating, and rapid changes of direction (Gerwyn Hughes, 2006).

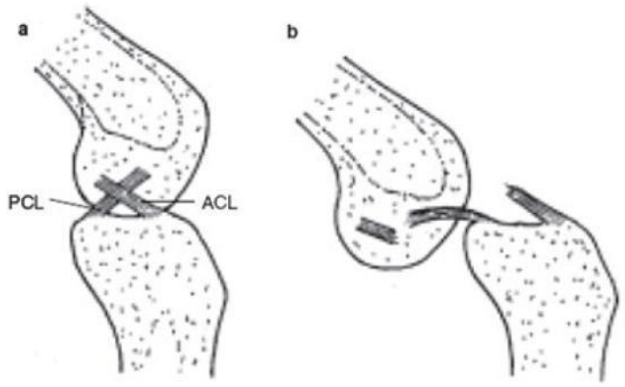

Figure 1.7: Anterior translation of tibia relative to the femur.

1.3 : Purpose of research

The main purpose of this study is to combine in-vivo and in-vitro approaches to quantify the effects of muscle group forces on ACL strain during jump landing. In-vivo and in-vitro studies have been performed in the past but have failed to relate the effects of dynamic knee muscle forces and kinematics of sports activities with the strain in the ACL. The first goal of the study is to perform motion capture on a jump landing task and then to create a biomechanical model of jump landing. The second goal is to simulate jump landing using the dynamic knee simulator. The third goal is to measure ACL strain using a DVRT while performing five trials of jump landing and comparing ACL strain. The final goal is to vary the muscle firing patterns during jump landing simulations and measure the ACL strain during each trial to compare the effects of variable muscle firing patterns on jump landing.

Chapter 2

Literature Review

2.1 : Effects of ACL strain in-vivo

The mechanism of ACL injury has been researched immensely but is still unclear. To gain a better understanding some researchers have studied the healthy ACL in vivo during activities that stress the ligament.

In a study by G. Cerulli et al. ACL strain in vivo was measured during rapid deceleration in a sport like fashion that has been known to cause injuries in healthy individuals. The study was performed by first surgically implanting a differential variable reluctance transducer (DVRT) strain gauge device on the antero-medial band of the intact ACL of a healthy young male as shown in Figure 2.1.

Figure 2.1: DVRT surgically implanted on antero-medial band of the ACL (Cerulli G, 2003).

A DVRT is a half bridge linear variable differential transformer. With the DVRT mounted the subject hopped as quickly as possible 1.5 m from his initial position to a location on a force plate marked with an X. The subject landed with the instrumented leg. Three trials of rapid deceleration were collected and averaged. Each trial was roughly 5 seconds. The rapid deceleration test determined that during flight phase just prior to landing, the strain reaches a peak which corresponds to the peak ground reaction force (Cerulli G, 2003).

Similarly to Cerulli et al., Fleming et al. installed a DVRT on the antero-medial band of the ACL to study the strain in the ligament in vivo. Fleming et al. had a more complex setup for their study. Their study involved monitoring the ACL strain during physical activity on a StairMaster 4000PT with two conditions, at 80 and 112 steps per minute as seen in Figure 2.2. The StairMaster 4000PT is a stepping machine which includes two pedals with independent motion to simulate stair climbing.

Figure 2.2: Test setup for measuring ACL strain during StairMaster activity (Fleming BC, 1999).

Figure 2.2 displays the use of an electrogoniometer to record the knee flexion angles. It can also be seen that the foot pedal was instrumented with a load cell to measure pedal forces and a potentiometer to track pedal position. The study was performed on 14 subjects and produced repeatable results in 5 of the subjects. The other patients were excluded due to technical difficulties and non-reproducible Lachman test data. The antero-medial strain patterns were consistent with the magnitude, increasing as the knee joint was extended. The two climbing conditions did not produce any significant differences in peak strain values (Fleming BC, 1999).

For both studies a Lachman test was performed before testing to determine the reference for strain calculation and after to ensure repeatability of DVRT measurements . In a Lachman test the subject is seated with a t-bar attached to the distal tibia to maintain a knee flexion of 30° with the thigh oriented horizontally. The subjects then relax their muscles while shear loads are applied and the displacement of the DVRT and flexion angles are recorded (Fleming BC, 1999).

Although the results of in vivo testing allow for ACL strain to be recorded on healthy living ligaments, there are ethical concerns with mounting a DVRT or any other transducer or strain gauge on a living subject. Measurements are restricted to simple tasks to prevent injuries to the subjects. These simple tasks limit the understanding of injury mechanisms as the firing patterns of muscles cannot be controlled to study their effects on ACL strain.

In vivo studies have also been performed to study the neuromuscular factors that affect the ACL during injury. Neuromuscular training has the ability to decrease ACL injury rates in athletes. Hewett et al. performed a study in which they monitored 205 female athletes in high risk sports and measured 3D kinematics and joint loads during jump landing tests for neuromuscular control (Timothy E. Hewett, 2005). Analysis of variance and logistic regression were performed to isolate predictors of risk in athletes who injured their ACL. Results of the athletes with normal control were compared

with those who injured their ACL. The females who injured their ACL had altered neuromuscular control characteristics compared to those who were not injured. From the results of Hewett et al. it was evident that during jump landing tasks the injured females had significant increases in valgus and knee abduction loading before their injuries compared to those who were uninjured (Timothy E. Hewett, 2005). Zazulak et al. studied the neuromuscular factors of core stability to predict knee, ligament, and ACL injury risk in athletes. Their hypothesis was that increased trunk displacement in response to sudden trunk force release is associated to increased ACL injury risk (Bohdanna T. Zazulak, 2007). In their study, 277 college athletes were tested to determine their trunk displacement after a sudden force release. Variance and multivariate logistic regression identified predictors of risk in injured athletes (Bohdanna T. Zazulak, 2007). The results showed that athletes with injuries to the ACL had higher trunk displacements than those who were not injured. Zazulak et al.'s model was able to predict injury in female athletes but only history of low back pain was a significant predictor of knee injury risk in males.

2.2 : Use of Musculoskeletal models to study ACL strain

Recently, complex musculoskeletal models have been developed to study ACL strain. Various techniques have been used to collect input data to create these models. The most common method of obtaining the kinematics of dynamic activities is the use of motion capture analysis. Using this data the musculoskeletal models calculate the ACL strain.

Zhang et al quantified ACL strains in vivo by using a biomechanical simulation model (Zhang Y, 2011). The input was body position data and the output was ACL strain. Using motion capture technology, the simulation model estimated ACL strain for a specific subject during jump landing, running, and sidestep cutting activities. Anthropometric parameters were calculated based on marker

positions. These parameters were used to create a lower limb skeletal model which included the geometry of all the bones in the lower limb. The model was subject specifically scaled.

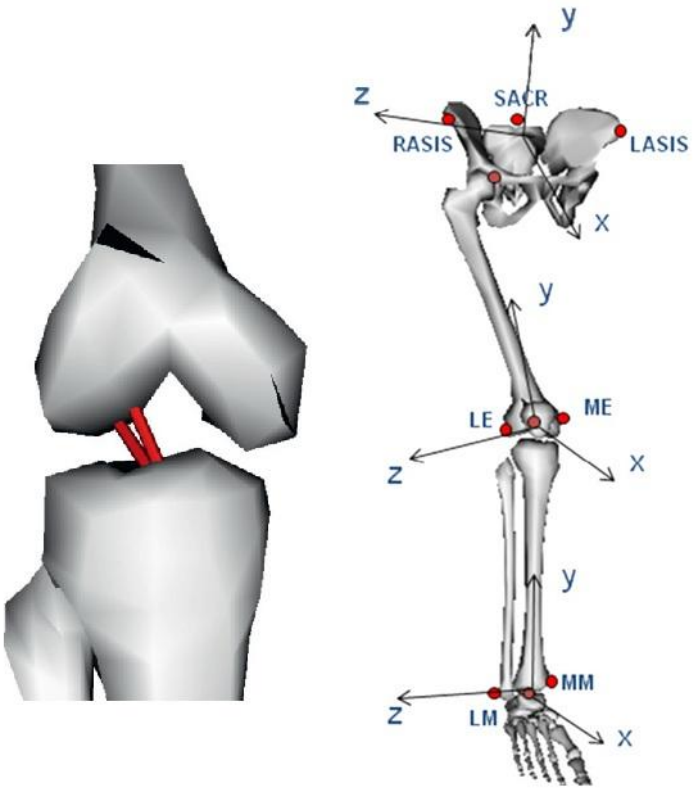

Figure 2.3: Zhang et al. musculoskeletal model (Zhang Y, 2011).

Laughlin et al used musculoskeletal modeling to study the influence of single-leg landing technique on ACL loading in recreationally active females (Laughlin WA, 2011). Participants performed soft and stiff drop landings. Using OpenSim v1.9.1 software a musculoskeletal model with 23 degrees of freedom and 92 Hill-type-muscle tendon units was developed. Fifteen healthy females were subjected to EMG testing as well as motion capture and GRF data collected for the drop landing tasks. Using this data muscle forces and knee joint reaction forces were calculated and served as input data for the knee musculoskeletal model developed by Kernozek and Raymond (Kernozek TW, 2008). The model was used to estimate muscle, joint, and ACL forces. T-tests were performed to determine the

differences in soft and stiff landing techniques. Soft landing resulted in decreased peak ACL force and the hip and knee flexion both had significant increase in force at contact in the initial landing. Laughlin et al believe from their results that simple verbal instruction such as soft or stiff landing may reduce the ACL force experienced by athletes when landing.

Taylor et al quantified ACL strain during jump landing using musculoskeletal modeling (Taylor KA, 2011). There method involved motion capture analysis and fluoroscopic and magnetic resonance imaging techniques to determine ACL strain noninvasively. Eight subjects were involved in the experimentation. Each subjected had an MRI done on their knee. This information was used to determine the ACL attachment sites on the femur and tibia to create 3D models. Then the subjects performed the jump landing tasks while motion capture was performed with markers placed around the knee. With the markers placed around the knee biplanar fluoroscopic images were taken allowing relative positions of the markers to the underlying bone to be quantified as shown in Figure 2.4. From the motion capture the kinematics was input into the model. The results from the model were consistent with previously described neuromuscular patterns.

The method of using a musculoskeletal model has determined some great results but is still limited in helping us understand the injury mechanisms of ACL strain. Although the motion capture subject can land from a jump in various different ways the firing patterns of the subject's muscles cannot be altered to study those effects on the ACL.

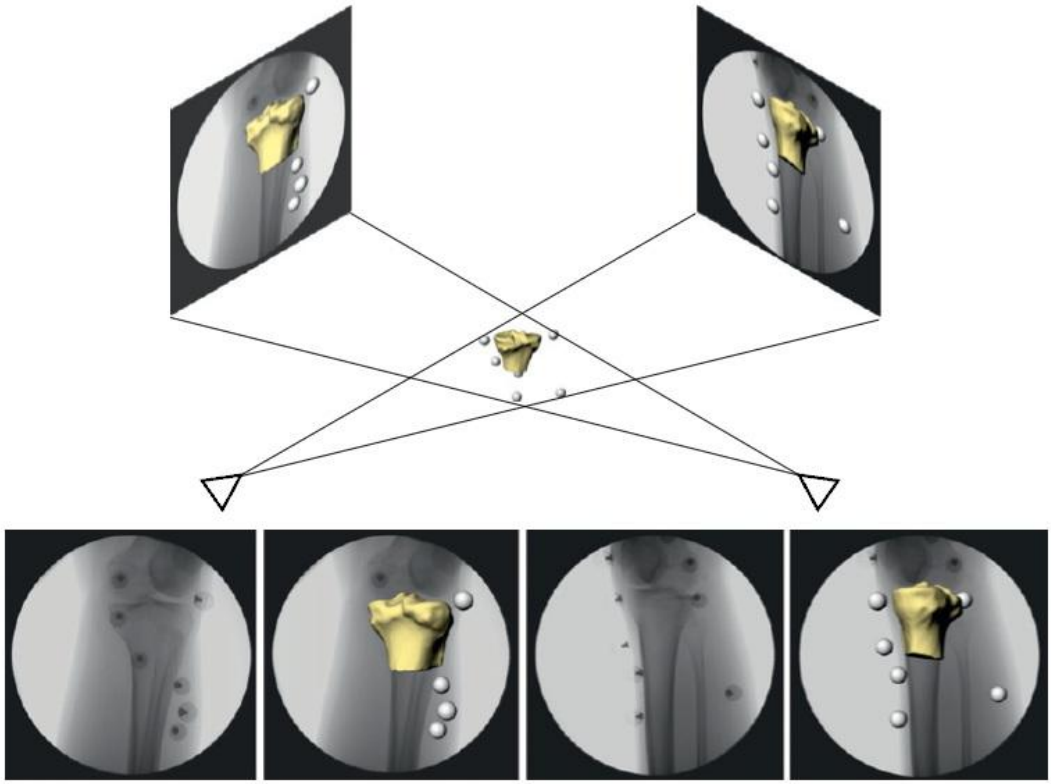

Figure 2.4: Knee biplanar fluoroscopic images were taken allowing relative positions of the markers to the underlying bone to be quantified (Taylor KA, 2011).

2.3 : Use of cadaver knees to determine relationship between muscle forces and ACL Strain

Researchers have used cadaver knees to determine the relationship of muscle forces and ACL strain in vitro. Cadaver studies allow researchers to apply forces to different regions of the knee to study their effects on ACL strain. The ability to study ACL strain in vitro allows for a better understanding of how the mechanical properties of the ACL are affected in various loading conditions.

Demorat et al studied noncontact ACL injury by applying aggressive quadriceps loading (DeMorat G, 2004). They potted thirteen frozen cadaver knees in a jig held at 20 degrees flexion with the femur

positioned inferiorly as can be seen in Figure 2.5. Cryoclamps were applied to the quadriceps tendon. 4500 N quadriceps contraction was then simulated with the knee kinematics recorded. A KT-1000 arthrometer (Medmetric, San Diego, California) and a simulated quadriceps test pre and post 4500 N loading was used to assess the anterior tibial displacement. The results of this test determined that while the knee is flexed 20 degrees and the quadriceps are loaded aggressively a significant anterior tibial translation that leads to ACL injury occurs (DeMorat G, 2004).

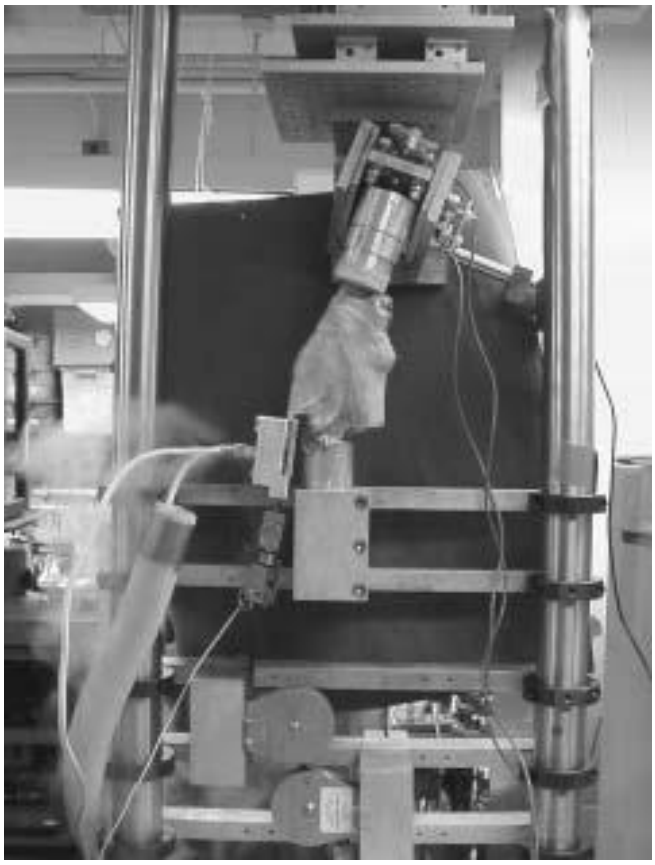

Figure 2.5: Cadaver knee potted in a jig flexed at 20 degrees (DeMorat G, 2004).

Markolf et al performed a study in which they directly recorded forces in the ACL and PCL before and after application of isolated hamstrings and quadriceps loads to the knee (Markolf KL, 2004). Their study involved thirteen fresh frozen cadaver knees with ten of them male and 3 female.

Polymethylmethacrylate was used to pot both the femur and tibia. Load cells were installed to directly measure the resultant forces in the intact ACL and PCL under five different constant loading conditions. The loading conditions were no tibial force, 100 N posterior tibial force, 100 N anterior tibial force, 5 Nm internal tibial torque, and 5 Nm external tibial torque. Weights were hung from a pulley system to cords that were sutured through the quadriceps tendon and hamstrings tendons. This can be seen in Figure 2.6.

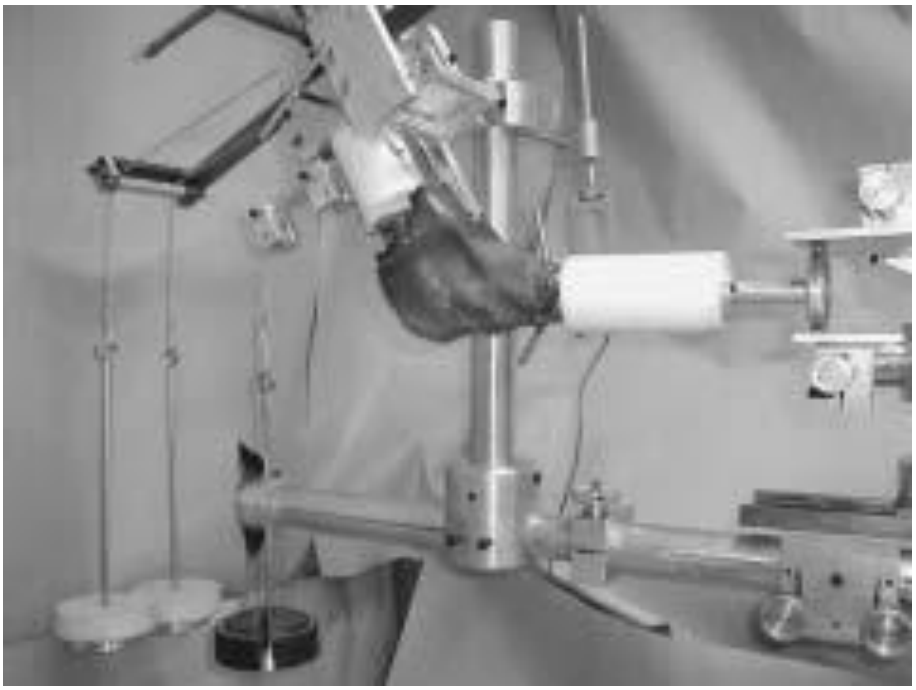

Figure 2.6: Testing apparatus applies muscle loads as the knee is passively extended under various tibial loading conditions. The femur (shown at left) is extended relative to the tibia, which is maintained in a level position throughout the range of motion. The roller at the end of the potted tibia (shown at right) allows unrestrained tibial rotation and varus-valgus angulation (Markolf KL, 2004).

The results from the tests conducted by Markolf et al. showed that the hamstrings load significantly increased the mean PCL force between 30 and 105 degrees of flexion with 100 N of

posterior tibial force. This showed that the hamstrings were more effective than the quadriceps in altering the cruciate forces.

Although these methods determine useful data in understanding the injury mechanisms of the ACL strain they are non dynamic. This means that they cannot simulate the effects of high risk activities seen in sports such as cutting, rapid deceleration, and jump landing. Researchers have loaded cadaver knees and studied the dynamic effects using mechanical simulators.

2.4 : Dynamic knee injury simulators

There have been numerous studies in vitro on the mechanisms of the human knee, but the problem with these studies has been that they've been limited to static joint loads. For the purposes of better understanding and clarification of the pathomechanics of the knee and the design of prostheses, it is important to study the joint response characteristics corresponding to dynamic functional activities (McLean CA, 1993). The issue preventing in vitro evaluation of dynamic response characteristics of the knee is that there is a high level of complexity involved in a dynamic load simulation device.

McLean et al. designed a dynamic knee simulator to allow in vitro studies to be performed on the mechanical response of the knee joint corresponding to dynamic functional activities such as walking. The inputs that were controlled were the time histories of the knee flexion angle, flexion/extension moment, and the tibial axial force components of the foot-to-floor reaction (McLean CA, 1993). Stepper motors and hydraulic actuators were used to apply the load and displacement inputs for a given activity. The simulator was designed with the femur fixed to a force plate. The forces were then applied to a freely moving tibia. The femoral axial component was measured through the force plate. The muscles that surround the knee were combined into flexors and extensors. These were controlled by the flexion angle time histories of the knee joint with the use of flexible cables. The flexor was attached to the potted tibia cup while the extensor was attached to the patella. The displacements of

the muscle cables were controlled by stepping motors. For the floor to foot reaction or the ground reaction, the tibial axial component was measured through the base of the tibia via a hydraulic actuator attached to a cable pulley system (McLean CA, 1993). The simulator can be seen in Figure 2.7.

The performance of the simulator was satisfactory for gait conditions based on measurements from three fresh specimens. The issue with the simulator was that it had to be simplified to limit the complexities. It could only apply in-plane forces and moments. Therefore out of plane loads cannot be considered for the simulations. This limits the types of activities that can be simulated. Also an average location of the flexion axis had to be used for each knee.

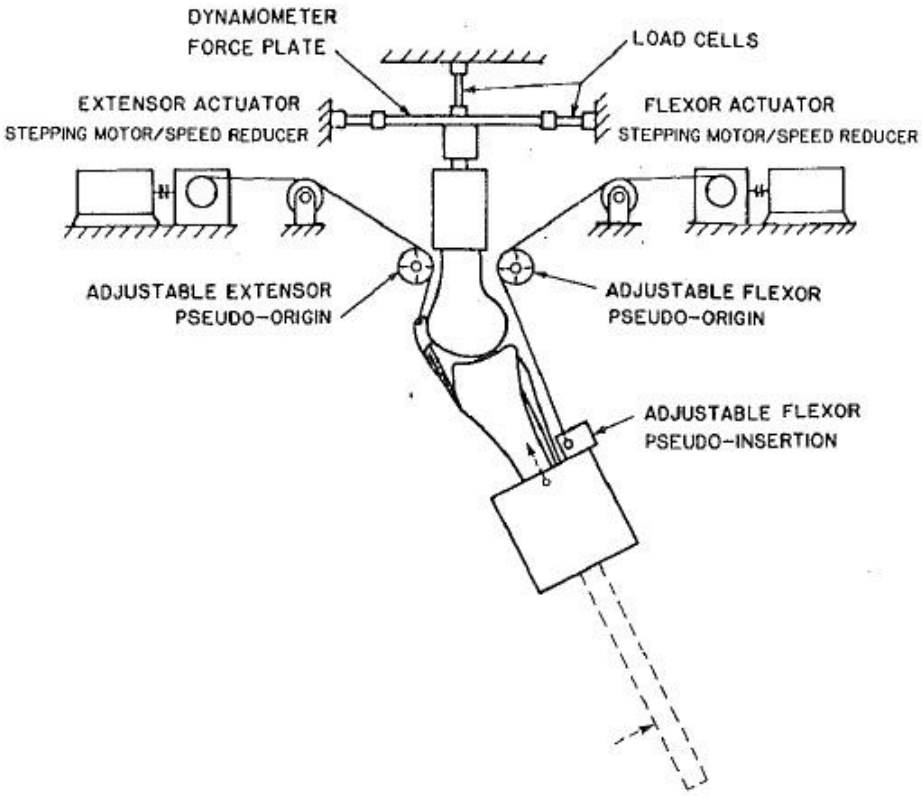

Figure 2.7: McLean et al. dynamic knee simulator (McLean CA, 1993).

Maletsky et al. designed a five axis dynamic knee simulator which could be used to simulate dynamic activities on a cadaver knee or a prostheses knee mounted on fixtures. The simulator was named Purdue Knee Simulator: Mark II. The new simulator was modeled after the original Purdue Knee Simulator built in the 1980s. The simulator was designed to display realistic natural dynamic loading on the knee. It could simulate high loads and rapid motions allowing it to simulate activities such as jogging. The Mark II simulator does not control the kinematics of the knee joint; rather the resultant loads are the results of the applied quadriceps and external loads at the hip and ankle. This allows for a determination of how the knee would react to loading more naturally. The five axis of control were three loads (translations) and two torques (rotations). The simulator did not directly simulate the hamstring and gastrocnemius flexors but incorporated their loading into the tibiofemoral compressive force. The hip sled was designed to allow two degrees of freedom between the femur and the ground. There is vertical translation of the hip and flexion/extension rotation that was fixed relative to the translating hip sled (Maletsky LP, 2005). Downward force was applied to the hip sled via a vertical load actuator. The quadriceps muscle group was simulated using an actuator that was mounted to the femur which caused an extension moment about the knee that extended the hip too. A universal joint was used to provide flexion/extension, adduction/abduction, and internal/external rotation of the tibia at the ankle. The mediolateral translation of the ankle sled was controlled by an adduction/abduction load actuator. Internal/external rotation of the tibia at the ankle was controlled by a vertical torque actuator. Finally the ankle flexion moment actuator applied a torque about the flexion/extension axis between the tibia and ankle sled (Maletsky LP, 2005). The simulator can be seen in Figure 2.8.

The objectives of Maletsky et al were to describe and validate a sigittal plane model of the knee simulator, demonstrate that the knee simulator can duplicate a desired tibiofemoral compressive force, and show that the knee simulator can be used to provide limited control of the patellar forces

(Maletsky LP, 2005). The results from Maletsky et al showed that the tibiofemoral compressive load and quadriceps tension agreed well with the predicted loads from the dynamic model they had used. There were a few issues with this simulator. The patellar loading was tremendously simplified in the dynamic model (Maletsky LP, 2005). There is little understanding in the error between the model and the experimental results which means a modification to the control method would be needed (Maletsky LP, 2005). The flexor muscles were not represented accurately as there was a lack of a direct representation of the hamstring and gastrocnemius muscle groups.

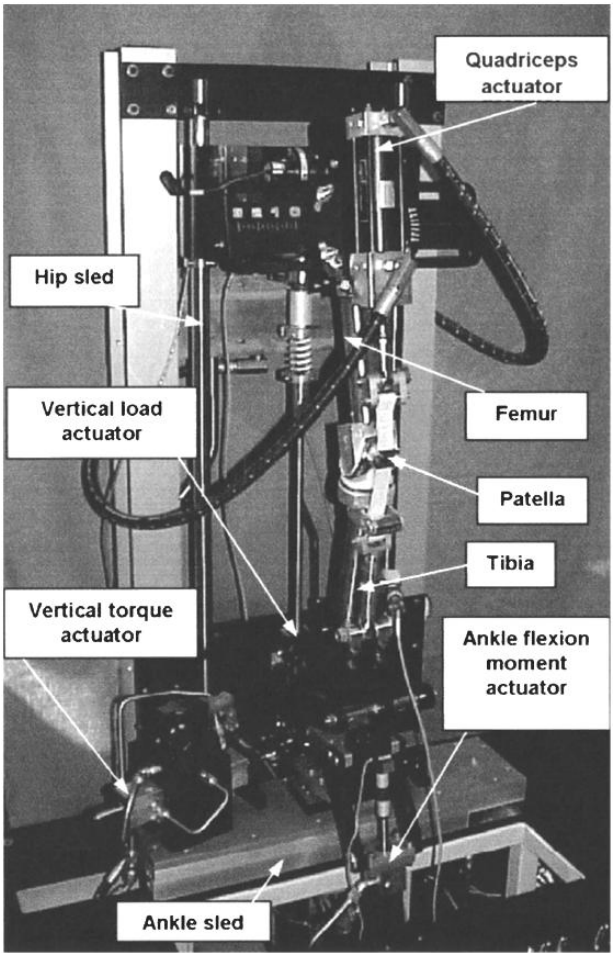

Figure 2.8: Maletsky et al. Purdue Knee Simulator: Mark II (Maletsky LP, 2005).

Weinhold et al. performed a study to determine if the application for a cadaver knee model with female specific loading and movement patterns found in vivo for a stop-jump task would generate higher ACL strain then the load patterns for males (Weinhold PS, 2007). Published kinetic and kinematic results of gender specific loading patterns of stop jump landing were taken from Chappell et al and applied to seven cadaver knees (Chappell JD, 2000). Tibial compression, quadriceps, hamstrings, external posterior tibial shear, and tibial torque loads were applied using a dynamic knee simulator. Strain was measured by mounting a DVRT onto the anteriormedial bundle of the ACL. The knees were cut at the femur and tibia, potted, and subsequently loaded into a knee simulator. The simulator is interfaced with a servohydraulic materials testing system (8500 Plus, Instron Corp., Canton, MA). The simulator allowed knee flexion to be fixed based on the kinematic parameters of the time frame of kinetic results used. Varus/Valgus position was fixed as well at the natural equilibrium point of each knee (Weinhold PS, 2007). Joint compression was applied to the knee using the servohydraulic materials testing machine. All of the other applied loads were applied using pneumatic actuators controlled by pressure regulators with feedback coming from load cells in series with each actuator. The muscle loads for the quadriceps and hamstrings were applied using cryogrips.

The results from the tests showed that there was significantly higher ACL strain for the female loading pattern than the male loading pattern after the posterior tibial shear for was applied.

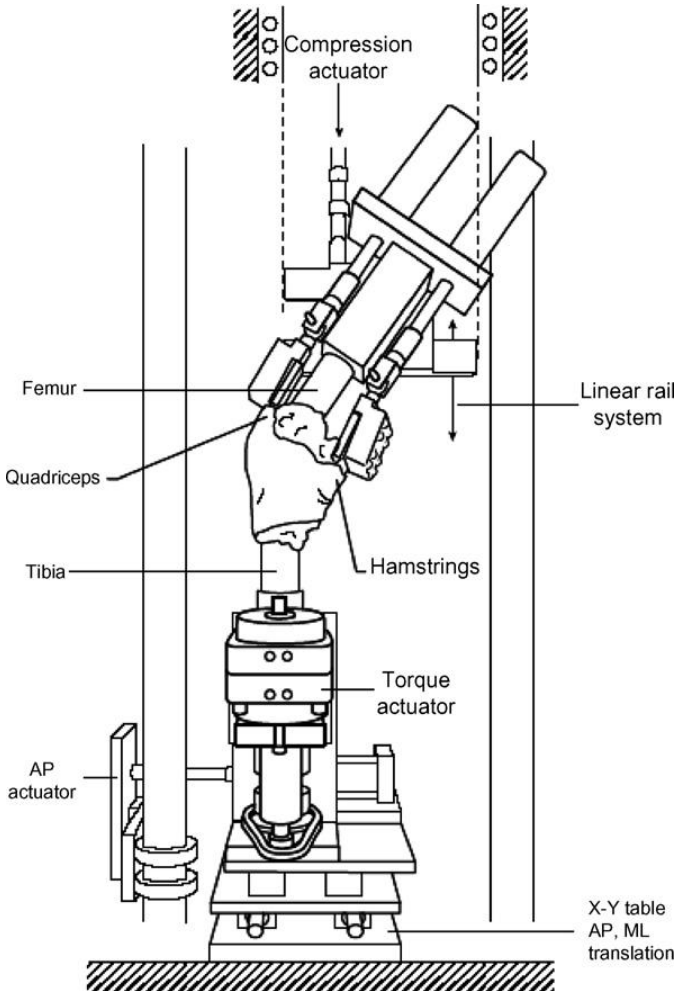

Figure 2.9: Weinhold et al. knee simulator (Weinhold PS, 2007).

2.5 : Simulators used to study ACL strain during jump landing

Withrow et al. tested the hypothesis that during a one legged jump landing task with compressive, flexion, and valgus knee moment loading the peak relative ACL strain would be significantly higher in comparison to loading without the valgus knee moment. A custom dynamic knee simulator was designed to simulate the position of a leg when it is initially about to strike the ground while landing on one leg from a jump. The schematic of the simulator can be seen in Figure 2.10. 5 male and 5 female cadaver knees were potted and mounted in the simulator for testing. Two 3D load cells were mounted on both the tibia and femur to monitor the impulsive force and moments at 2000 Hz. Three

infrared emitting diodes were mounted on both the tibia and femur to measure the kinematics of the knee during loading using the Optotrak 3020 system (Northern Digital, Inc, Waterloo, Canada). Pretensioned steel cables were used to simulate the muscle forces of the quadriceps, hamstrings, and gastrocnemius. A DVRT was mounted on the anteromedial bundle of the ACL and used to measure the strain. 10 trials were performed with the knee in neutral position with 25° flexion and impulsive loading applied 4 cm posterior to the knee joint center in the sagittal plane to cause a flexion moment (Withrow TJ, 2006). The same procedure was repeated with the force applied 15° lateral to the knee in the sagittal plane. Then the 10 neutral trials were repeated again. The impulsive loading was applied as seen by the "W" in Figure 2.10.

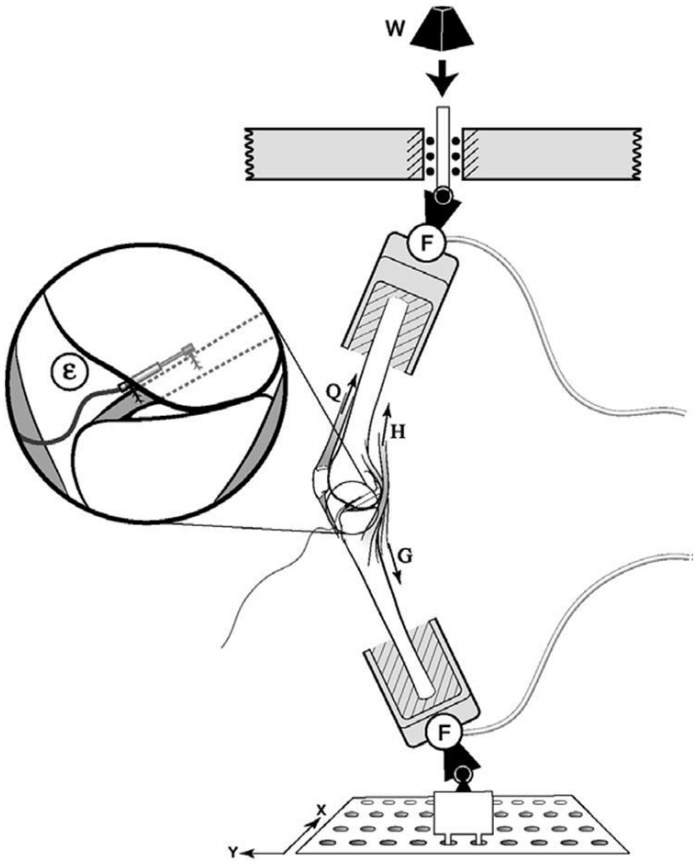

Figure 2.10: Schematic of Withrow et al. dynamic knee simulator (Withrow TJ, 2006).

The results from the Withrow et al. showed that the peak normalized strain in the anterior cruciate ligament was 30% larger for the valgus loading and flexion condition than the neutral loading condition. The issue with this simulator is that the position of the ankle stays constant. The ankle does not move with the motion of the jump landing as it would naturally to stabilize the knee when landing. Another issue with this simulator is that there aren't any muscle profiles that the hamstrings, quadriceps, and gastrocnemius follow. They just remain in tension during loading. This does not simulate realistic muscle loading and reaction.

Hashemi et al presented a dynamic knee injury simulator that was capable of in vitro modeling of the ACL injury during the jump landing activity. The simulator has two servo-electric actuators used to simulate the quadriceps and hamstrings muscle force. An impact plate is setup to measure ground reaction force on the tibia by dropping a weight. The hip and tibia attachment joints are designed as hinge joints. The hip joint is designed with a rotating cylinder allowing for the hip to have anterior/ posterior positioning. The tibia attachment joint is designed to have a yoke joint slotted base allowing for medial/ lateral positioning of the tibia. The schematic of the simulator can be seen in Figure 2.11. The aim of Hashemi et al.'s experiments was to cause ACL injuries on the cadaver knees during the jump landing simulation by controlling the muscle forces and hip flexion to determine which pattern of combinations would cause isolated ACL injury (Hashemi J, 2007). Several trials were performed on nine knees with various combinations of changes made to the initial flexion angles, applied impact force, quadriceps and hamstrings pretensions, different valgus angles, and with or locked hip flexion (Hashemi J, 2007). For each combination the strain was measured using a DVRT.

The results from the study showed that a high level of quadriceps force prevented injury from occurring even under locked hip flexion conditions. The strain during injury causing events was recorded to be about 250%/s. There were a few limitations to this simulator such as the calf muscles, knee abductors/adductors, and the ankle being neglected. Another limitation was that the muscle force

consisted of a single pretension which is not how the muscles would react around the knee physiologically during jump landing.

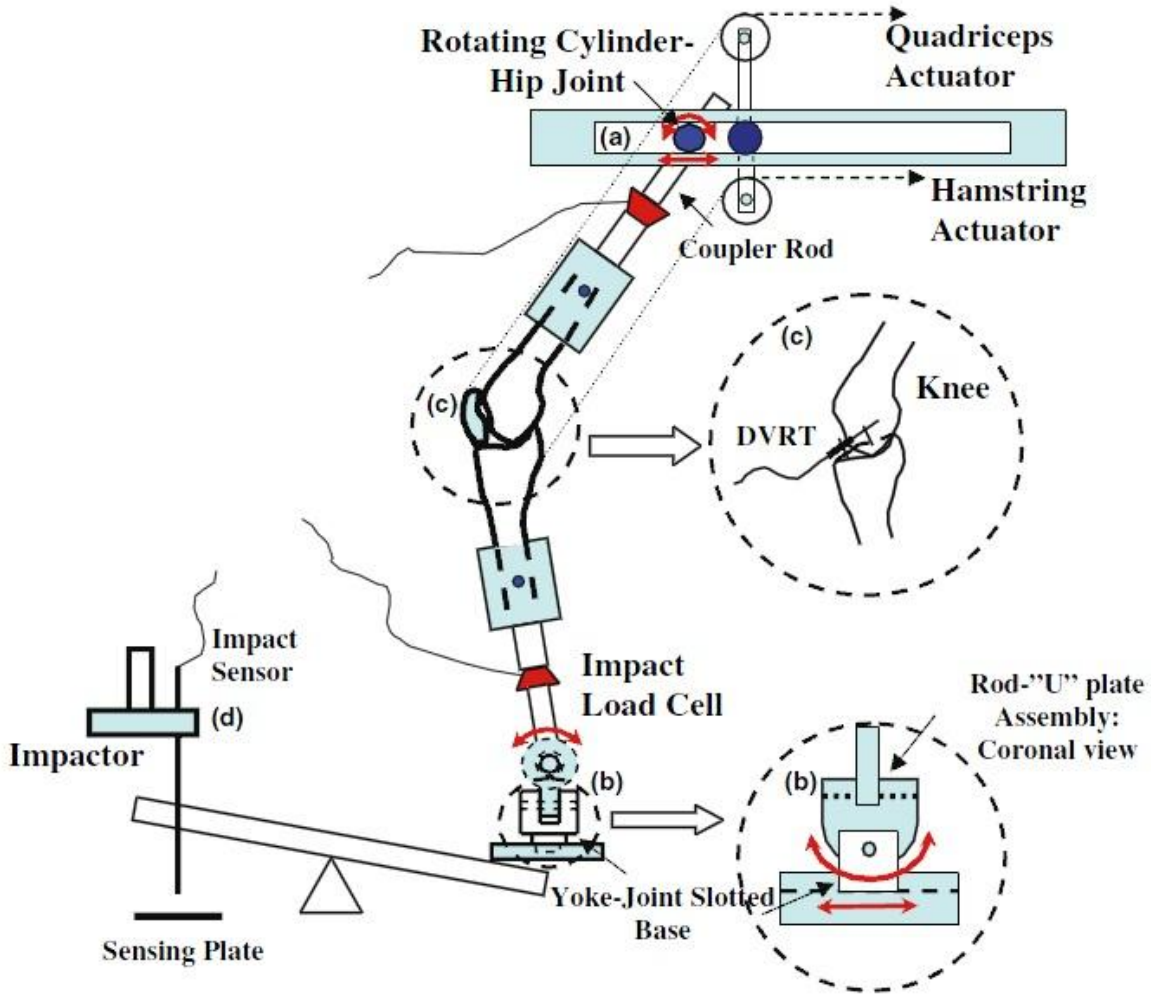

Figure 2.11: Schematic of Hashemi et al. dynamic knee injury simulator (Hashemi J, 2007).

Although these knee injury simulators allow for measurement of muscle forces and strains they lack the ability to replicate high speed movements and muscle forces seen in sports activities such as jump landing, rapid deceleration, and side stepping. Hashemi et al. and Withrow et al. attempted to study ACL strain during jump landing. Their studies were flawed in the sense that they lacked the

capability to apply muscle force-time history profiles. None of these studies were able to reproduce accurate knee kinematics with the muscles surrounding the knee to measure ACL strain. Not one study had the application of muscle force profiles of quadriceps, hamstrings, calf, and hip flexors which would be needed to accurately reproduce the kinematics of the knee during high speed activities like jump landing.

Chapter 3

Dynamic Knee Simulator and AnyBody Modeling Technology

The dynamic knee simulator that was used in the current study is designed to operate in the two dimensional sagittal plane. It takes into account the physiological muscle contributions of the leg at the knee joint during dynamic motions. The motion is driven by joint motion at the hips and ankle instead of knee joint angles or loading at the knee allowing for a more realistic reaction at the knee due to hip and ankle motions. Currently Anybody Modeling Technology software is used to model the simulations from motion capture to determine muscle contributions for the simulator.

3.1 : Design of dynamic knee simulator

Based on the experience gained through the first generation dynamic knee simulator (J. Hashemi, 2007), a second generation dynamic knee simulator was developed in our lab. It was designed on the principle that the strain in the ACL is related to ankle and hip joint positions (kinematics) and muscle forces in the lower limb (Kinetics). This simulator can simulate sagittal plane movements of a cadaver knee. The cadaver knee is secured to steel cups at its femoral and tibial ends; these steel cups are attached to the ends of turnbuckles which in turn are connected to ball and socket joints. These ball and socket joints simulate hip and ankle joints. The turnbuckle allows for customization of femoral and tibial length. The ball and socket joints at the ends of turnbuckles are mounted on to the crossheads of two belt actuators (position actuators). The vertical actuator moves the hip joint in the vertical direction while the horizontal actuator moves the ankle joint in the horizontal (antero-posterior) direction. The actuators are 14H Macron belt actuators (Macron Dynamics Inc., Croydon,PA) driven by Danaher Motion AKM73P brushless motors (Danaher Motion, Radford, VA). These actuators have the capability to move at a rate of 5 m/s.

The simulator also consists of four additional screw actuators (muscle actuators) to apply the muscle group forces. Three actuators, one each responsible for applying quadriceps, hamstring and gastrocnemius muscle group forces are connected to the respective muscle insertion sites through pull-pull control cables. The cable connects to the patella (at quadriceps muscle insertion point), femur (at gastrocnemius muscle insertion point) and tibia (at hamstring muscle insertion point). Aircraft cables are connected to the respective pull-pull cables responsible for that particular muscle group from their insertion point. Another actuator is connected by a hinge joint to the femoral turnbuckle distal to the surrogate hip joint through a push-pull control cable. This actuator is responsible for applying the flexor and extensor moment at the hip. A 2000 lb load cell (Honeywell, Columbus, OH) is connected in line with each actuator and control cable to measure the forces applied by these actuators. The muscle actuators are RSA32 model Tolomatic actuators (Tolomatic Inc., Hamel, MN) driven by AKM42J motors by Danaher Motion (Radford, VA). The actuators have the capability to apply 5000 N of force. The two position actuators and four force actuators are controlled by a six axis motion control board (Model DMC-4060, Galil Motion Control, Rocklin, CA) that is programmed directly through a computer. The position actuators are set to operate in velocity controlled mode while the force actuators are set to operate in closed loop force controlled mode.

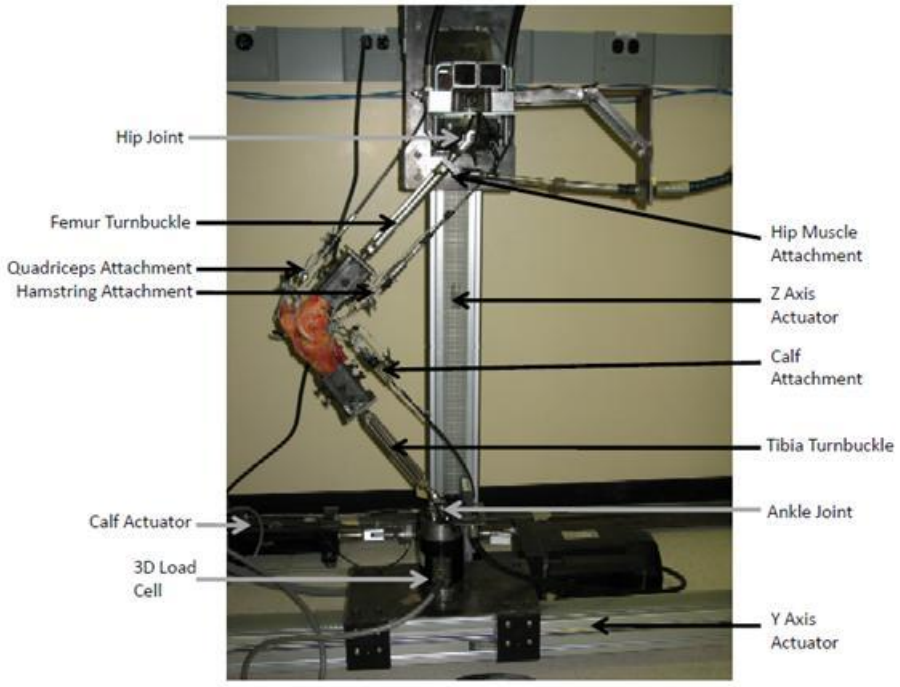

Figure 3.1: Initial design of dynamic knee injury simulator in sagittal view.

3.2 : Muscle Attachments

The muscle attachments were designed using pull/pull and push/pull cables from Cable Craft. The cables are attached from the actuator to the insertion point at the bone of the specimen. The cables have two anchors, one at each end allowing for easy attachment to the actuator and insertion point. For the quadriceps, three holes are drilled through the patella and a 1/8 inch aircraft cable is fed through the holes and attached to the pull/pull cable. The hamstrings attachment is made by drilling a hole through the tibial condyles where the hamstring tendons can be seen and feeding a 1/8 inch aircraft cable through the holes and attaching the cable to a pull/pull cable for the hamstrings actuator. The calf muscle attachment is performed by wrapping two steel wraps around the femur just above the condyles and attaching the steel wraps to the pull/pull cable using the 1/8 inch aircraft cable.

Finally the hip muscle attachment is rigidly mounted to the proximal end of the femur turnbuckle. The hip attachment uses a push/pull cable to consider the moment at the hip as opposed to the muscle force. For all of the muscle attachments there is a load cell installed in between the pull/pull and push/pull cables and the actuator to measure the force outputs of the actuators. The muscle attachments can be seen in Figure 3.2.

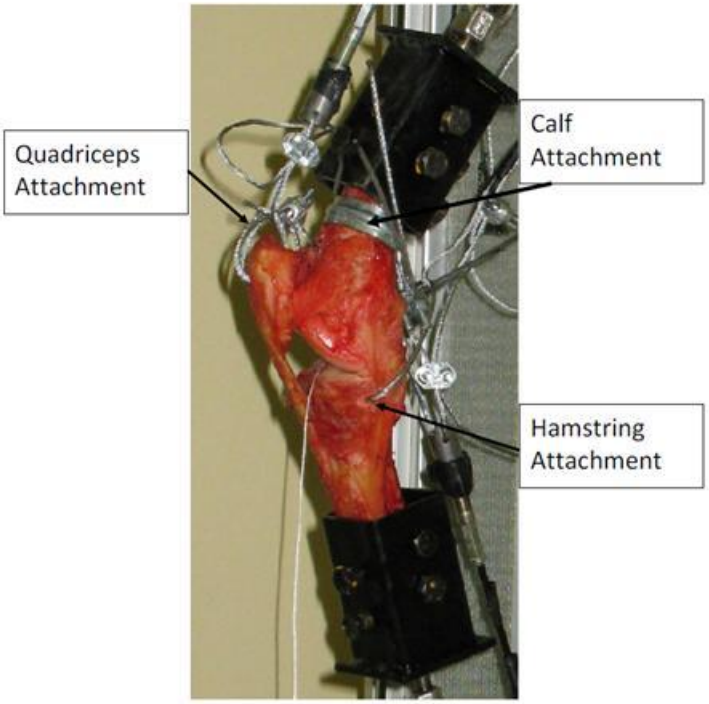

Figure 3.2: Initial muscle attachment sites.

3.3 Simulator modifications

3.3.1 : Hip modification

The initial design of the hip joint component where the hip muscle actuator's push/pull cable attached was made from 1/8 inch hot rolled steel. This design was ok for low forces such as the forces that act on the leg during gait. Although suitable for gait, when exposed to larger forces like jump landing

there was a greater hip moment causing the part to bend. As can be seen in Figure 3.3, the steel was a 1/8 inch and only had four metal strips welded to the main piece for support during bending stress.

Figure 3.3: Initial design of hip component.

The part was modified using a ¼ inch hot rolled steel. Two rectangular pieces were made and welded perpendicular to each other at the edges and reinforced with two triangular pieces also made of ¼ inch hot rolled steel. The Figure 3.4 and Figure 3.5 display the modified hip attachment component. It can be seen that this design is much more stable and is also able to handle a greater load as there is a greater surface area in the triangular elements to absorb the bending stress.

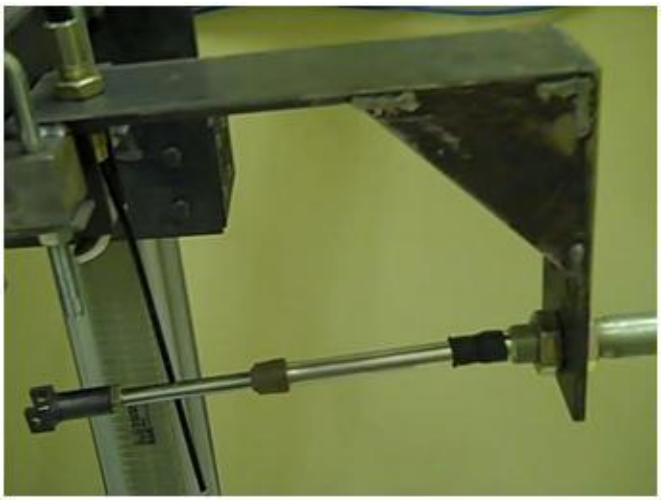

Figure 3.4: Modified hip component.

Figure 3.5: Triangular pieces used to reinforce hip component.

3.3.2 : Ankle joint modification

Since the current activities performed on the simulator are in the 2-dimensional sagittal plane, a few modifications were made to the ankle joint in order to ensure the internal/ external rotation of the leg is limited. This helps with the simulations as the initial design of the ankle joint and hip joint allowed the knee to rotate more than 90 degrees and would compromise some of the simulations.

The first modification was made to the plate at the ankle joint where the calf muscle actuator is fished through to its attachment site. The initial design was made with 1/8 inch hot rolled steel. This design was flawed as the plate was subjected to bending loads exceeding the maximum amount the plate could handle due to the calf muscle loads. The plate was reinforced with a thicker ¼ inch hot rolled steel plate. The modified plate at the ankle joint can be seen in Figure 3.6 and Figure 3.7.

Figure 3.6: Modified steel plate at ankle joint.

Figure 3.7: Side profile of modified plate at ankle joint.

The second modification was a new part that was made that acted as a stopper for internal/external rotation of the leg at the ankle. The part is made of ¼ inch hot rolled steel. It is designed to attach to

the ankle joint and to fit between the jaw of the tibia turnbuckle component of the leg. Figure 3.8 displays the design.

Figure 3.8: New part designed to restrict internal/ external rotation.

The third modification was made to remove the ball and socket joint at the ankle. This further reinforced the limitation of the internal/external rotation of the leg at the ankle. The ball and socket joint was removed and the new part is shown in Figure 3.9. This part was machined using a ¼ inch hot rolled steel. Four triangular elements were welded to the piece where the jaw attachment takes place to add strength to counteract any bending moment acting on the part.

Figure 3.9: Part designed to restrict internal/ external rotation.

When the modifications for the ankle joint are installed, sagittal plane motion is ensured by the limiting internal/external rotation to keep the motion in two dimensions. The issue with the polymer tape used as ligaments is that each time a simulation is performed the tape stretches and loses its ability to mimic the ligaments and they become lax. When the tape becomes lax the tibia and femur components of the simulator rotate at the ball and socket joints and move out of their initial position. This affects the outcome of the simulations. Therefore by replacing the ball and socket ankle joint with the new part the motion is more accurately captured by maintaining the two dimensional motion.

3.3.3 : Calf muscle actuator bracket redesigned

The calf muscle actuator bracket was initially made with two ¼ inch hot rolled steel plates welded together and installed as a t-bracket with a hole drilled through one end to mount the calf actuator cable. The issue with this design was that due to large loads from the calf muscle the bracket would bend since it did not have any lateral support when a large load was applied. Figure 3.10 and Figure 3.11 display the redesigned calf muscle actuator bracket. Two triangular pieces were cut and welded to each side of the T-bracket giving the bracket more stability and support during high loads on the calf muscle. The new design also used ¼ in hot rolled steel.

Figure 3.10: Redesigned calf muscle actuator bracket.

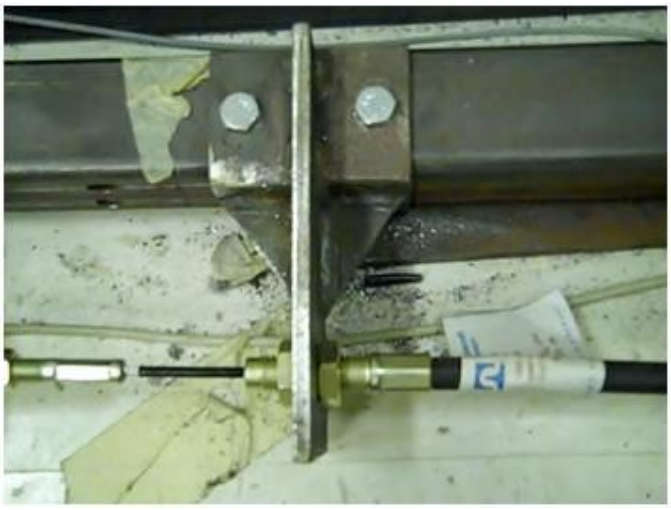

Figure 3.11: Top view of redesigned calf muscle actuator bracket.

3.3.4 : Vertical belt actuator mount

The initial design for the vertical belt actuator did not involve mounting the actuator. This is a cause for concern since large forces produce a moment that causes the actuator to move laterally and puts a strain on the belt actuator attachment to the frame. To fix this problem a large bracket was made to mount the actuator and keep it rigidly fixed. A square tube similar to the one used for the frame was selected and a flat piece of ¼ in hot rolled steel was welded at both ends. Then to add more stability under high loads triangular elements ¼ inch hot rolled steel were welded to both sides. Figure 3.12 and Figure 3.13 display the vertical belt actuator mount.

Figure 3.12: Vertical belt actuator mount.

Figure 3.13: Alternate view of vertical belt actuator mount.

3.4 : AnyBody Modeling Technology

AnyBody Modeling Technology was founded December 15, 2001, at Aalborg University (AnyBody Technology, 2011). It is software designed for creating musculoskeletal models. The software was developed with four goals in mind (Michael Damsgaard, 2006).

1) It should be a modeling system, i.e., a tool that allows users to construct models from scratch or use or modify the existing models to suit different purposes.
2) The system should facilitate model exchange and cooperation on model development, and it should allow models to be scrutinized.
3) If possible, it should have sufficient numerical efficiency to allow ergonomic design optimization on inexpensive computers.
4) The system should be capable of handling body models with a realistic level of complexity such as that shown in Fig. 1.

Figure 3.14: Full body model comprising several hundreds of muscles made with AnyBody (Michael Damsgaard, 2006).

AnyBody Modeling Technology's software consists of a Windows graphical user interface and a console application. Both have similar modeling facilities but are used in different ways. The console application can be called upon from other programs. The graphical user interface contains much more facilities for viewing the model and the results produced from it. The graphical user interface has a better foundation for developing models and analyzing them (Michael Damsgaard, 2006).

Modeling in AnyBody Technology is done by a text based input. AnyScript is the language that has been developed for modeling. The text based user input was chosen because it is easy to develop and maintain from the point of view of a software developer and it is also the only way to meet the four goals of the AnyBody system (Michael Damsgaard, 2006).

AnyBody Modeling Technology is software used to perform simulations that mimic the mechanics of the live human body with respect to its environment. The definition of the environment is in terms of external forces and boundary conditions (AnyBody Technology, 2011). The user can model any kind of posture or motion for the human body. This can be done either from a pre-existing model

from the AnyBody Managed Model Repository (AMMR) or from scratch. The AMMR is a library of models that contains a collection of detailed scalable template body models that mimic a variety of different activities of daily living. Users have access to the AMMR. The repository is regularly updated in concert with the new releases of the AnyBody Modeling System. For example a motion can be modeled using motion data from a c3d file and a pre-existing model from the model repository such as "GaitLowerExtremity.any". Performing a simulation allows AnyBody to calculate the mechanical properties of the body during the motion for the body-environment system (AnyBody Technology, 2011).

ChartFx2D contains all of the input and output data from the musculoskeletal model. Using ChartFx2D, results can be obtained from muscle forces of every muscle. ChartFx2D can also be used to calculate joint forces, moments, metabolism, elastic energy in tendons, antagonistic muscle actions and many more measurements. Models can be scaled to match anthropometric features of their human counterparts (AnyBody Technology, 2011).

Using AnyBody Modeling Technology one can handle body models with a high level of detail efficiently since there are over 1000 muscle elements. Knowledge on kinetics inside the body for a given environment can be obtained. Models can be customized using AnyScript. Design issues for various products can be solved by scaling and optimizing parametric models. Data from motion capture systems can be imported to drive AnyBody models. One can also export AnyBody data as input to Finite Element models (AnyBody Technology, 2011).

Chapter 4
Methodology

4.1 : Motion Capture

Motion capture is a term used to describe the process of recording movement and translating that movement on to a digital model. It is used in biomechanics, military, entertainment, sports, and medical applications, and for validation of computer vision and robotics (David Noonan, 2009). Optical motion capture systems use data captured from image sensors to triangulate the 3D position of a subject between multiple cameras. Markers are placed on a subject and attached to a data acquisition system which is connected to a force platform as well. The subject performs an activity and the position from the 3D markers and the ground reaction from the force platform are recorded using motion capture software. The Optotrak Certus motion capture system offers maximum flexibility for motion capture applications with its unsurpassed accuracy, high-speed marker frequency, portable design, and virtually wireless marker option (Nothern Digital Inc., 1996-2011). To simulate jump landing motion capture was performed with the help of the Kinesiology Department at the University of Waterloo. The Optotrak Certus motion capture system was used. The process of performing motion capture involves setup, marker placement, data collection, and data processing.

4.1.1 : Setup of Motion Capture System

The jump landing motion capture required four cameras, ODAU II data acquisition unit, Polaris system control unit, First Principles motion capture software, a wooden platform to jump off of, and a force plate. The force plate used for the motion capture was an OR6-6-2000 model designed by AMTI (Advance Mechanical Technology, Inc.). The OR6-6-2000 model is a high frequency force plate specifically designed for the precise measurement of ground reaction forces. The OR6-6-2000

measures the three orthogonal force components along the X, Y, and Z axes, and the moments about the three axes, producing six outputs, F_x, F_y, F_z, M_x, M_y, M_z (AMTI, 2011). The force plate was setup directly in front of the wooden platform as shown in Figure 4.1. The orientation and schematic of the setup of the force plate, cameras, and the jump platform is displayed in Figure 4.2.

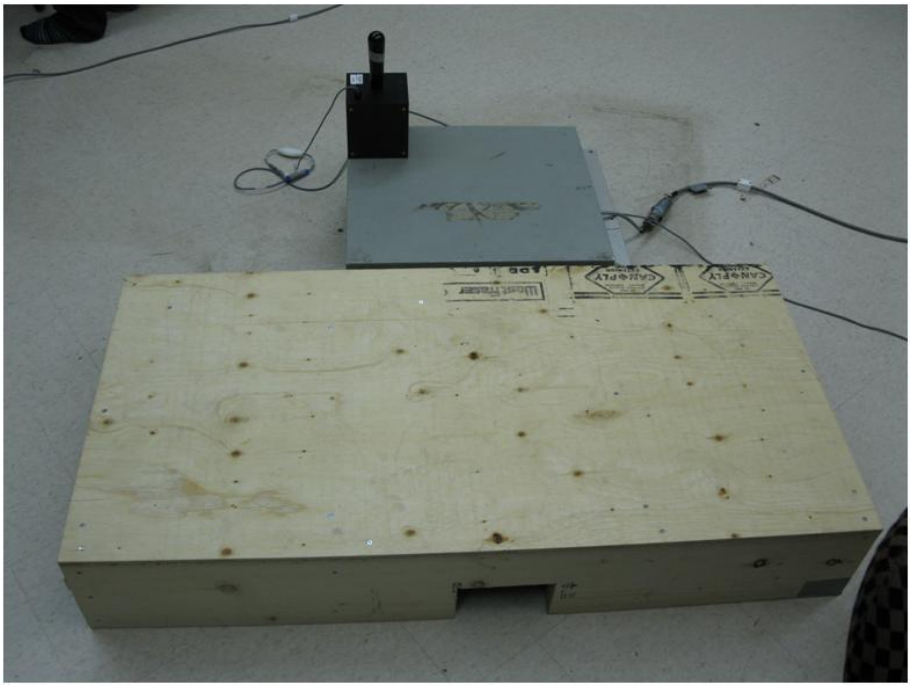

Figure 4.1: Orientation of force plate and jump platform during calibration.

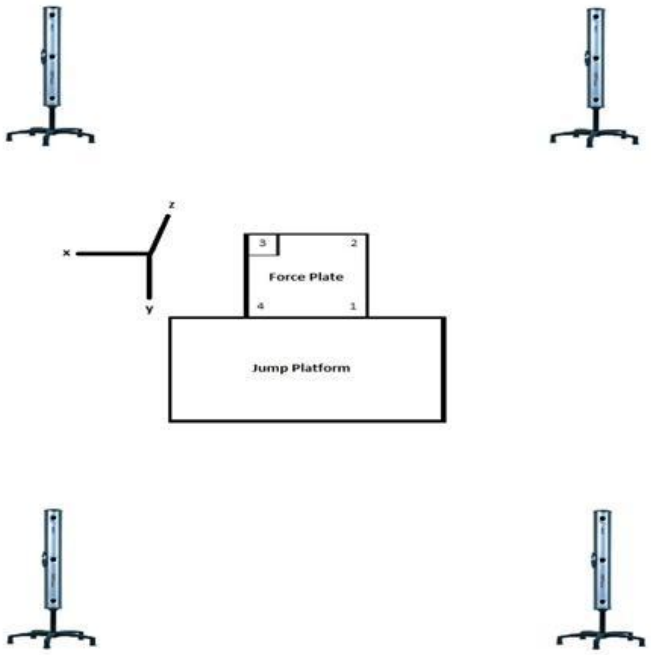

Figure 4.2: Schematic of motion capture setup

4.1.2 : Marker Placement

There were seven infrared markers placed on the subject (the author, 25 years, 170 lbs, 5' 7"). The markers were placed on the left trochanter, right trochanter, right femoral condyle, lateral malleolus, medial malleolus, 5th metatarsal, and the calcaneus. Optotrak Smart Markers were used because they are designed to allow fast and easy experimental setup with easy wire management, easy experiment reproducibility, and instant marker detection. Smart Markers simplify experiment execution by providing complete freedom of movement for research subjects. Figure 4.3 and Figure 4.4 display the positioning of the markers on the right leg.

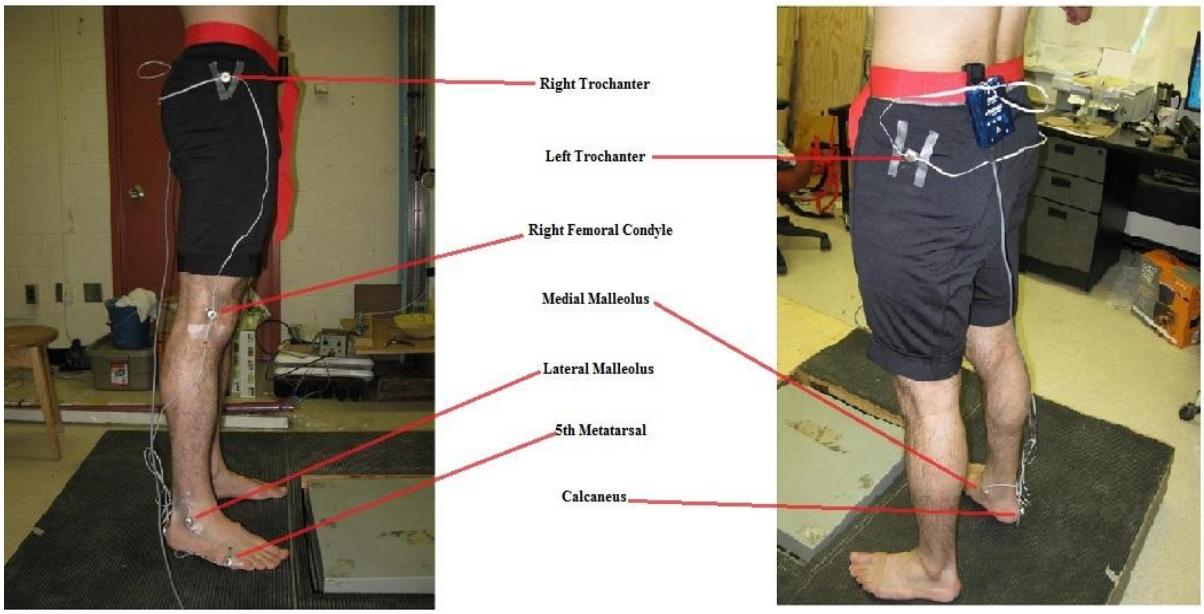

Figure 4.3: Marker placement.

4.1.3 : Jump Landing Activities

There were two different types of jump landing activities performed in the motion capture. Both jump landing activities involved landing on the right leg only making it a one legged landing from a jump. The first activity was to start from the wooden platform and jump vertically as high as possible and land on the force plate with the right leg only.

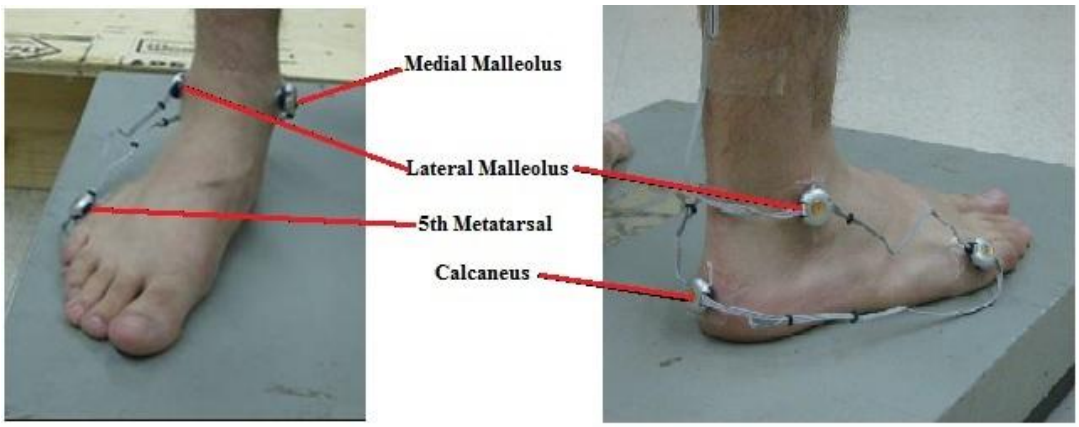

Figure 4.4: Marker placement around foot.

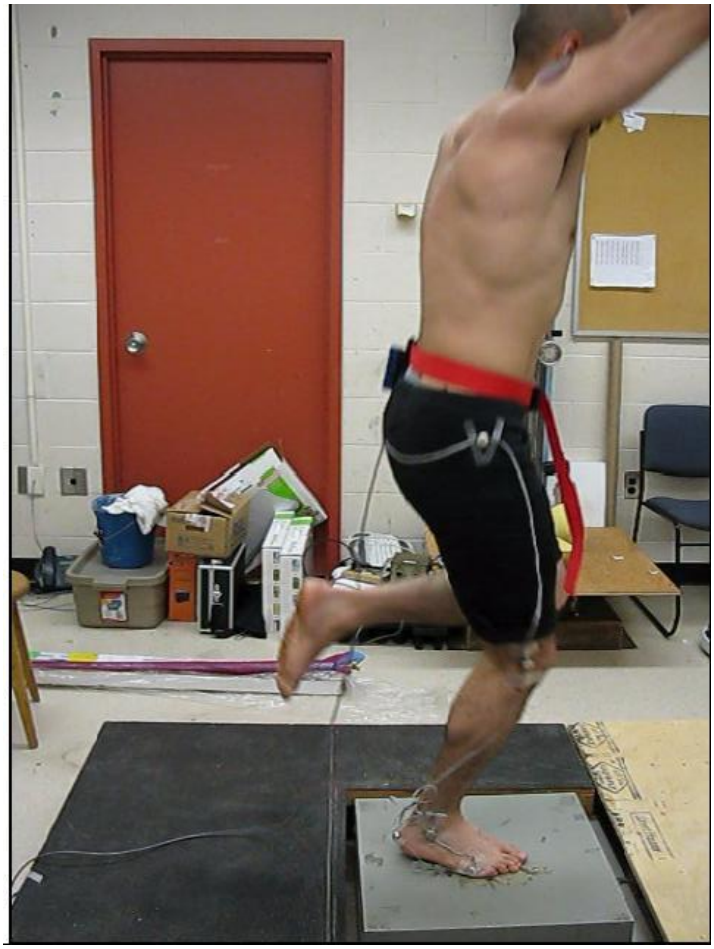

Figure 4.5: Sagittal view of jump landing motion capture.

The second activity involved jumping from a wooden stool which was placed on the wooden jump platform. This allowed for a more elevated jump landing. The stool is approximately 46cm in height. The setup is shown in Figure 4.6.

Figure 4.6: Setup with stool placed on jump platform.

4.1.4 : Data Collection

Data was collected in two forms. From the four cameras and the markers, position data was collected and sent to the system control unit. From the force plate analog data was collected from six channels that were connected to the ODAU II data acquisition system which sent the data to the system control unit. The ODAU II allows synchronization of the collection of analog and digital data with the Optotrak position data. The ODAU II uses a 16 bit converter to collect up to 16 single-ended input channels or 8 differential input channels (Nothern Digital Inc., 1996-2011). Feedback control to the motion capture subject can be achieved through the 8 digital I/O channels or 2 analog output channels (Nothern Digital Inc., 1996-2011). The Polaris system control unit provides an interface between the position sensor, the strobers and tools and the host computer (Nothern Digital Inc., 1996-2011). The

data travels from the system control unit to the host computer where NDI First Principles software is used for signal conditioning and processing the data into a model.

4.1.5 : Data Processing

The position data did not need any processing as it was stored within the C3D file. However the analog data collected from the jump landing motion capture trials required processing to determine the ground reaction forces and moments. There were six channels for Fx, Fy, Fz, Mx, My, and Mz. The data collected had 640 frames and a collection frequency of 128 Hz. The first step was to look up the force plate's calibration matrix to convert the voltage output from the force plate to N and Nm.

For each analog output array in the calibration file there is a certain point at which the output voltage readings drastically change and repeat for a certain number of frames. The time frame at which this occurs is different for analog channels 1-3 and channels 4-6. Table 4.1 displays the change in voltage and where the repetition begins.

Table 4.1: Constant voltage readings highlighted in calibration matrix.

Frame	Analog 1	Analog 2	Analog 3	Analog 4	Analog 5	Analog 6
93	0.001221	0	-0.00519	0.002136	-0.01221	0.001526
94	0.003967	0.005188	-0.00336	0.003662	-0.00885	0.004578
95	0.007324	7.274457	1.73553	0.003357	-0.01251	0
96	7.076703	7.039166	1.73614	0.005798	-0.00885	0.002441
97	7.075482	7.041608	1.73614	0.006104	-0.00824	0.001221
98	7.076093	7.038251	1.737666	0.003052	-0.00946	0.001221
99	7.074567	7.039166	1.737056	0.001831	-0.01068	0.003357
100	7.076093	7.037641	1.736751	0.003662	-0.00946	0.000916
101	7.077008	7.041303	1.736751	0.003052	-0.00977	0.004578
102	7.076703	7.038251	1.737056	0.003662	-0.00946	0.003052
103	7.074567	7.041303	1.738582	0.005188	-0.00702	0.002747
104	7.077008	7.040082	1.737361	0.003052	-0.00977	0.001831

The repeating voltage readings for analog channels 1-6 were then copied into a new excel sheet where the average voltage was calculated from the repeating voltages. Once the average voltage

readings were calculated from the calibration file, they were plotted against the force plate's shunt calibration values which were listed in Table 4.2.

Table 4.2: Shunt calibration values.

CAL SHUNT VALUES = microvolts/volt X cal matrix			
Fx	519.0 N	**Mx**	219.2 Nm
Fy	515.5 N	**My**	220.2 Nm
Fz	1009 N	**Mz**	105.1 Nm

From the plot, an equation of the line was found. This equation was used to calculate the ground reaction forces and moments produced during the jump landing activity. An example of the use of the average repeating voltage and shunt force value for F_y is shown in Table 4.3 and Figure 4.7. From the plot in Figure 4.7, the equation of the line was used to calculate the ground reaction force, F_y.

Table 4.3: Calibration data for F_y.

Fy	Voltage
0	0
515.5	7.040046

Using the equation of the linear line from Figure 4.7, Fy was calculated by applying the equation to the corresponding analog output array from the jump landing simulation. The same procedure was performed for Fx, Fz, Mx, My, and Mz. These were the input forces and moments used for the AnyBody jump landing simulation model.

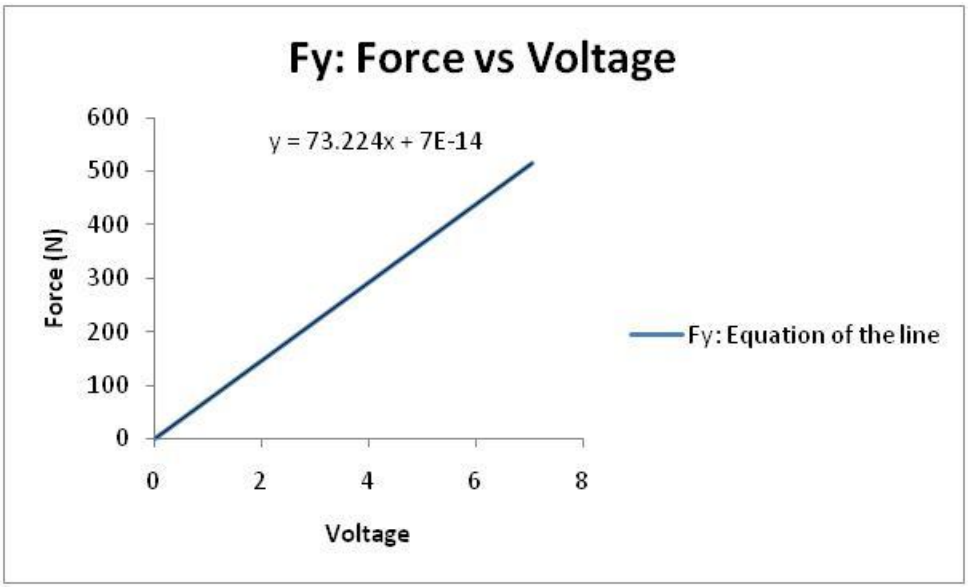

Figure 4.7: Calibration Force vs Voltage plot for F_y.

4.2 : Creating Jump Landing Model using AnyBody Modeling Technology

Using the motion capture data collected in C3D format a jump landing model was created. For the jump landing model, the start from wooden platform and land on the force plate scenario was used. In order to create this model the first step was to find a pre-existing model from the model repository that could be modified to simulate jump landing. The model that was chosen was "GaitLowerExtremity" from the AnyBody Managed Model Repository version 1.2 (AMMRV1.2). The gait lower extremity model was created to simulate the lower extremity of the body performing gait using motion capture data stored in C3D files.

4.2.1 : GaitLowerExtremity model background and usage of the model

This model is designed with two models within it that can be switched on and off in the main file. The first model is the "MotionAndParameterOptimizationModel" which is used for optimizing the motion and identifying model parameters such as segment lengths and local marker positions. The

output from this analysis is a set of parameters which are automatically saved and the optimized motion in terms of joint angles. These joint angles are automatically saved once the kinematic analysis is done. This model has no muscles applied to it.

The second model performs an inverse dynamics study which is driven by the optimized motion from the first model. This model includes muscles and allows one to calculate muscle forces and activity and many other parameters. It is recommended that only one model is active at a given time in order for the models to work.

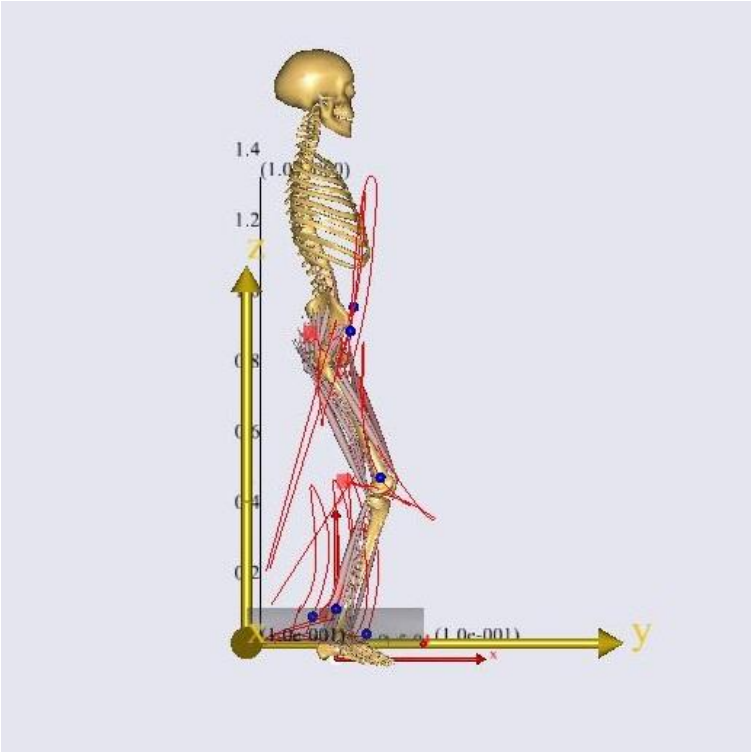

Figure 4.8: Sagittal view of jump landing model.

The models have to be run by first running the "RunMotionAndParameterOptimizationSequence" in the operation tree to optimize the model and save the joint angles. In order to run the sequence the "RunMotionAndParameterOptimizationSequence" must be set to 1 and the "InverseDynamicsModel" must be set to 0. The second step is to reload the model to read in the saved joint angles. Finally to

run the inverse dynamics sequence the “InverseDynamicModel” must be switched back to 1 and the motion and parameters optimization model should be switched back to 0. Then “InverseDynamicAnalysisSequence” should be selected from the operation tree and run.

4.2.2 : Modifications to GaitLowerExtremity model to simulate jump landing.

The first step in modifying the model to simulate jump landing was to exclude the environment file and comment out the inverse dynamics study to simplify the model to first get the kinematics analysis running. Once the kinematic analysis was running, the environment file including the force platform and the body parts setup including muscles could be applied to the model. In order to keep the model loading, only one feature at a time was applied to avoid complex debugging issues. The following sections describe the major files in the setup and different studies within the biomechanical model and the modifications made to simulate jump landing.

4.2.2.1 : Background of the major files in the biomechanical model

In the TrialSpecificData.any file one can input the name of the C3D file to be analyzed and set the start and end time for the analysis calculated from the C3D data. Also the anthropometrics data from the motion capture subject could be set and was used as the initial guess of the motion capture subject for the optimization algorithm. The optimization algorithm optimizes the initial guess and makes changes to the segment lengths to match the marker data. The initial position of the body can be modified here although it should only be modified if kinematics does not work in the first time step.

The “ModelSetup.any” file contains the marker topology of the data set used to link free floating markers with the markers on the human. At the top of the model setup file there are two macros, “SaveMacroOperation-Save.anymcr” and “RunMacroOperation-Save.anymcr”. The first saves a string into a macro file. The string provides the filename to save the design in. The string automatically sets the C3D filename and optimized parameters. The second macro saves the

optimized design into a file named according to the string operation: Main.Studies.MotionOptimization.Kinematics. The next portion of the model setup file involves the AnyInputC3D file. This is the input file to the analysis. It includes the C3D file name, marker properties, marker labels and a low pass filter. Once these parameters are set, the first and last frames in the simulation are set to the required time frames. The next portion of the model setup file is the Optimize Anthropometrics file. This file allows one to choose which segments of the body should be optimized such as the thigh length. The final part of the model setup involves the creation of markers, marker drivers, and design variables to optimize the marker location in the two models.

The BodyPartsSetup.any file allows one to modify the level of detail on different parts of the body. The file consists of modifiable body part setups for the trunk, trunk with neck, right arm, left arm, right leg, left leg, right leg touchdown, and left leg touchdown. Each of these part setups has a few options for example for the right leg, one can choose between the skeletal right leg, a right leg with a simple muscle model, and a right leg with a hill type muscle model. To choose whether to include a type of model, 1 is used to include and 0 is used to not include.

The Mannequin.any file calculates a guess for the initial position of the pelvis based on the ASIS and PSIS markers. This file also controls the initial position and the posture of the model. The mannequin file contains two major folders; the posture and posture velocity. The posture folder begins with the script for the pelvis position and rotation which can be modified to suit the desired initial pelvis position of the model. The posture velocity folder allows one to modify the pelvis position and rotation with respect to the global reference frame.

The Environment.any file is used to develop the environment surrounding the human model. This is where the force plate is configured and applied to the model.

4.2.2.2 : Modifications made to the major files

The trial specific data file was first modified to input the file name for the C3D file, "JumpTest_2010_10_ 14_144353_014". The anthropometrics were modified to first reflect the body mass and the body height. The rest of the anthropometrics which consisted of the segment lengths such as the thigh and shank length were left untouched as they were going to be optimized by the model. In the initial position portion of the trial specific data the pelvis rotation, hip flexion/abduction/external rotation, knee flexion, ankle plantar flexion, subtalar eversion can be modified.

The first modification to be made to the ModelSetup.any file was to modify the marker names. There are a total of seven markers: Right trochanter, left trochanter, right femoral condyle, lateral malleolus, medial malleolus, and right calcaneous. It was very important that the markers were labeled just as they were in the processed data folder to avoid errors from occurring. For example the right trochanter was labelled "r_troch". In order to reflect the markers for the jump landing simulation the create marker class was modified to include the marker name, the placement, optimization options, and coordinates of the marker to become concurrent with their respective marker.

In the Motion and Parameters optimization study the BodyPartsSetup.any and Mannequin.any files had to be modified. A trunk driver file had to be created as well to improve the kinematics of the biomechanical model. For the motion and parameters optimization study just the skeletal bone structure is required for the trunk and right leg. In the BodyPartsSetup.any file for the trunk just the skeletal trunk was included and for the right leg the touchdown model was included. For the purpose of the jump landing simulation only the trunk and right leg were required and all of the other body parts were not included. In the Mannequin.any file the posture of the pelvis was modified to fit the marker locations from the motion capture. Initially in the GaitLowerExtremity model, AnyParamFun functions for floating variables or single scalar quantities were created for the right and left ASIS and

PSIS using the XYZ marker coordinate data for the location of the markers throughout the entire motion capture from the C3D file. These functions were used to calculate the pelvis position triaxially using the coordinate data. Since the right and left ASIS and PSIS data were not collected the position of the pelvis was determined by manually manipulating the position of the pelvis until the model reached a proper fit to the motion capture. With these modifications the posture was set in the initial position required for the kinematics study to run. The rest of the mannequin file was left unmodified.

In the ModelEnvironmentConnection folder the TrunkDrivers.any file was created and included. The trunk driver was required since there aren't any markers located on the trunk. For this reason to control the posture of the trunk and motion, an include file was made and included for the trunk driver. Within the include file there is a driver for the neck, the thorax with respect to pelvis rotation driver, and a posture driver. The neck driver uses an AnyKinEqSimpleDriver which is a simple driver function that provides motion with constant acceleration. The thorax with respect to pelvis driver is also an AnyKinEqSimpleDriver. It utilizes the AnyKinMeasureOrg class which composes new kinematic measures from existing ones.

Once all of these changes had been made the kinematics analysis and the motion and parameters optimization study was completed.

In order to run the inverse dynamics the first modification to be made was to uncomment the inverse dynamics section in the main file and then add the environment file including the force platform and modify the body parts setup allowing muscles to be applied to the model. The inverse dynamics analysis is based on the optimized motion from the motion and parameters optimization model. The body parts setup file required one modification to the right leg touchdown, the simple muscles were included.

The first step in modifying the environment of the gait lower extremity model to better suit the jump landing model was to delete the EnvironmentAutoDetection.any file and create a new Environment.any file. The difference between the two files was that the already existing environment file had three force plates and automatically detected which foot was in contact with the force plate based on the C3D file data. The new Environment.any file that was created for the jump landing model was created to have one force plate and the foot in contact with the force plate had to be manually set within the file.

The first step in creating the environment was to create a reference frame for the force plate. The second step was to determine an appropriate force plate to be applied for this simulation. The Model Repository contains existing force plates of types 2, 3, and 4. Each force plate type has a different output into the analog channels. For example some force plates output the force Fx, Fy, Fz, into the first three channels and then have a different output such as center of pressure or moments into the next three channels. For the jump landing simulation the appropriate force plate type that was selected was the type 2 force plate. The output from the force plate was channels 1-6 which had Fx, Fy, Fz, Mx, My, Mz output respectively.

The type 2 force plate file consists of the force plate corners data, plate center, rotational transformation matrix, transducer location, plate graphics, plate origin, force plate drivers, plate foot reaction, lowpass butterworth filter, center of pressure, load, and moment. All of these factors play a large role in the inverse dynamics analysis. The first step in modifying the file was to manually input the coordinates of the four corners of the force plate. The corners data is used by the AnyGraphics application to draw the force platforms, force vectors, and center of pressure information in the correct locations relative to the 3D point data. The next step was to modify the transducer location. The AnyFloat Origins was modified to reflect the XYZ 3D coordinates of the origin of the force plate. The same step was repeated for the AnyFloat Origins folder. The origin vector is set up to

enable the transformation of the force vectors as measured by the transducers to the laboratory coordinate system. Finally, a plate to foot reaction force parameter was input using the AnyReacForce class referencing the limb and the force plate. This was done since the auto detecting force plate wasn't used.

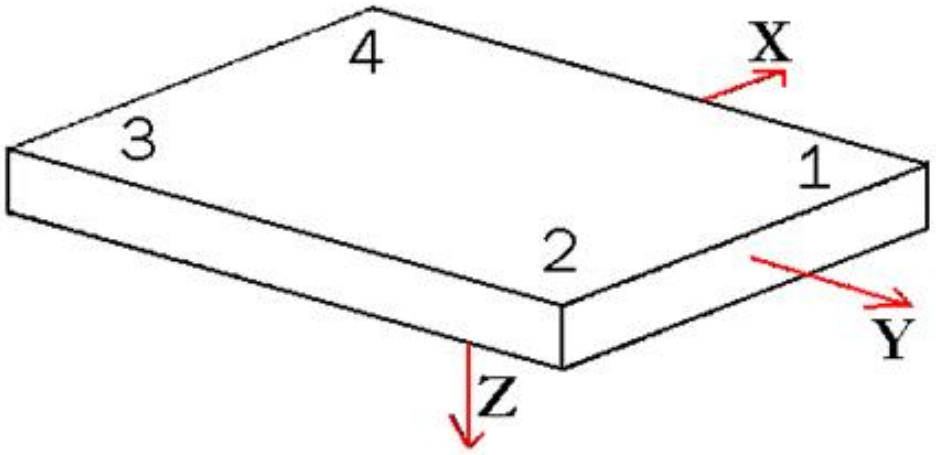

Figure 4.9: Force plate with corners.

Once the type 2 force plate was modified, the two additional force plates in the existing environment file were deleted. The remaining force plate type four was changed to the type two force plate that was modified and created for the jump landing simulation. The ground reaction forces and moments file paths had to be changed to reflect the file path of the input ground reaction forces and moments for the current simulation. Finally the calibration matrix was deleted as it was not needed in the method used to create the force plate.

Finally after the environment file was created, the inverse dynamics analysis could be completed. The results from the inverse dynamics analysis were used to determine the muscle forces to be input into the dynamic knee simulator.

4.3 : Extracting muscle forces from AnyBody Modeling Technology

Using ChartFX 2D, the muscle forces can be found from the output of the inverse dynamics analysis. ChartFX 2D allows one to obtain results on individual muscle forces, joint forces and moments, metabolism, elastic energy in tendons, antagonistic muscle actions and much more (AnyBody Technology, 2011).

4.3.1 : Using ChartFX 2D to obtain muscle forces

When opening ChartFX 2D, the model setup and studies folders are found. The model setup folder contains C3D file data and anthropometric data. The studies folder contains the output data from the inverse dynamics study and the load and parameters optimization study. Using ChartFX 2D the muscle forces were obtained from the output from the inverse dynamics study in the human model right leg folder under Mus. The Mus folder contains all of the muscles in the right leg. One can plot all of the muscle forces in the right leg by plotting a single muscle force and then modifying the file path of where the data is located. The Y data file path is located at the top of the plot and was modified with an asterisk to plot all of the muscles in the same plot. The Y-file path is: Main.Studies.InverseDynamicStudy.Output.HumanModel.Right.Leg.Mus.*.Fm, see Figure 4.10. Figure 4.11 displays all of the muscles in the right leg plotted. All of the plotted muscles were then copied to Microsoft Excel.

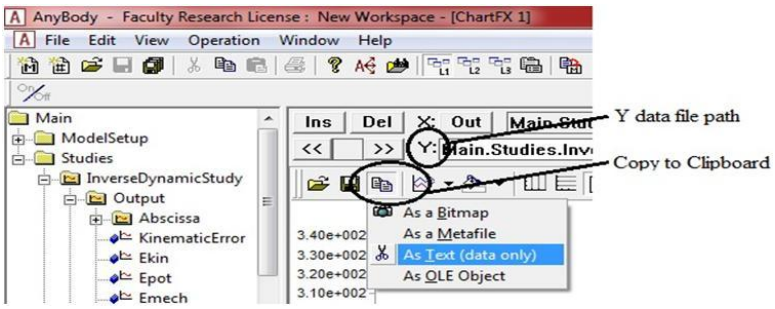

Figure 4.10: Data file path and copy to clipboard.

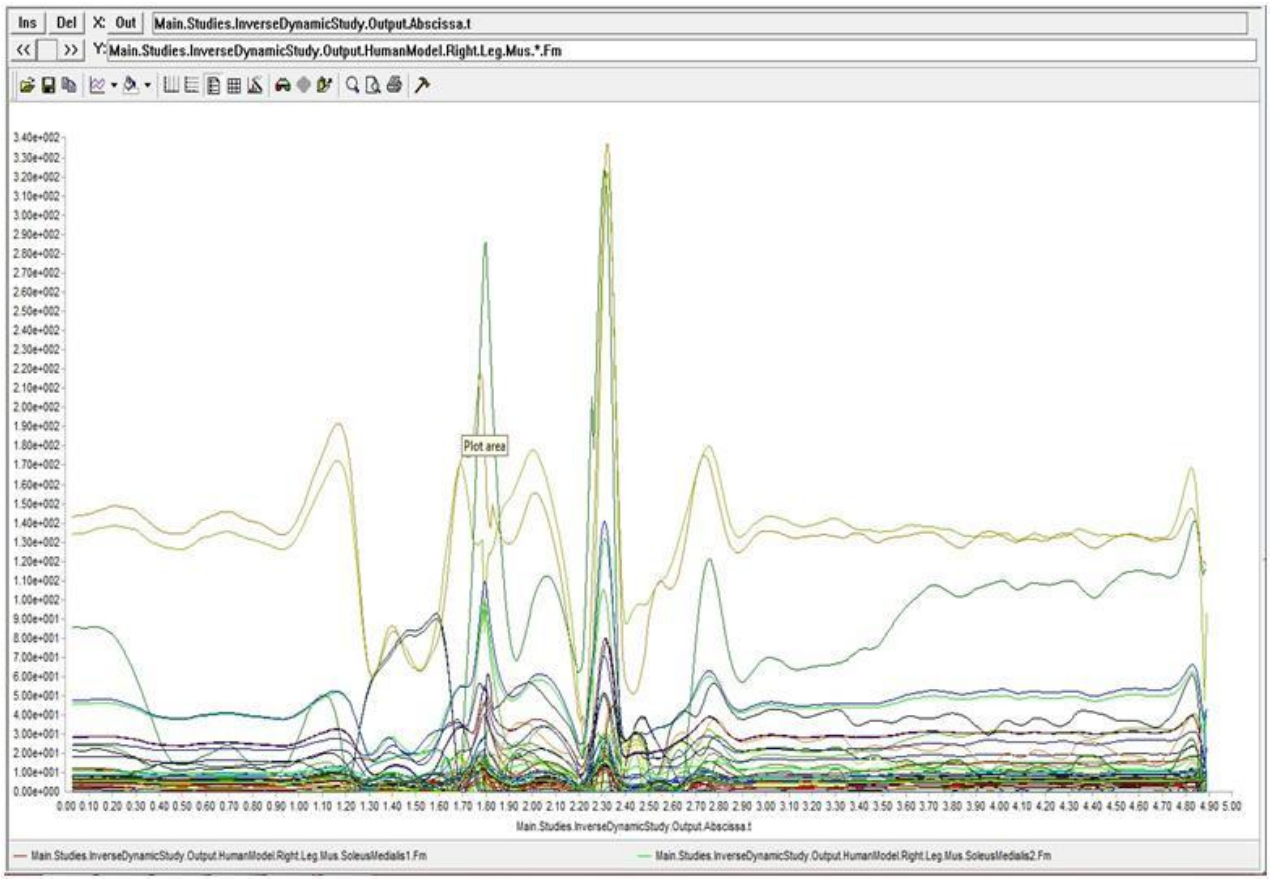

Figure 4.11: Plot displaying muscle forces for all of the muscles in the right leg.

4.3.2 : Using ChartFX 2D to obtain position data

The position data can be found by accessing the C3D data in the output tree of the inverse dynamics study. The position data for the right trochanter, right femoral condyle, and the lateral malleolus, is required for the calculation of the joint velocity of the ankle and hip. In the C3D data tree there is a model folder which contains position data on all of the markers used in the motion capture. When expanding the folders of the three required markers the Seg folder was selected and the variable, r, was selected to plot the position data of the marker. This process was done for the right trochanter, right femoral condyle, and the lateral malleolus.

4.4 : Processing the muscle force data

The extracted muscle force data for all of the muscles in the right leg was sorted into four muscle groups: hamstring, quadriceps, calf, and hip. In each muscle group the muscle forces were summed to take into account the contributions of each muscle within the group.

4.4.1 : Origin and insertion data

White et al. published muscle origin and insertion coordinates for all of the muscles in the lower extremities (SC White, 1989). The coordinates from White et al. were in the local coordinate system. Horseman et al. measured the global coordinates of the bony landmarks in the lower extremities (MD Klein Horsman, 2007). These values were used to convert the local coordinates of the muscle origin and insertion data of White et al. into global coordinates. Using the global coordinate data of the muscle origin and insertion the X, Y, and Z, angles for the line of action of each muscle was calculated. See Apendix D.

4.4.2 : Determining the muscle forces of each muscle group

To determine the combined muscle force of all of the muscles within a muscle group, each muscle's muscle force was broken into Fx, Fy, and Fz. Once all of the muscles were expressed in X, Y, and Z components, they were summed. Finally the resultant muscle force for each muscle group was calculated, F=$\sqrt{F_x^2 + F_y^2 + F_z^2}$. Each muscle force was converted to pounds. This process was performed for the quadriceps, hamstring, and calf muscle. For the hip muscle force a different method was used. The hip muscle moment had to be extracted from ChartFX 2D similar to the muscle forces under MomentMeasure and then it was converted to muscle force in pounds.

4.4.3 : Converting muscle force to encoder counts

For each muscle group the muscle forces were converted to encoder counts to be inserted into the Galil array. The Galil program reads the muscle forces in force control and in encoder counts. In order to convert the muscle forces to encoder counts, the encoder counts per pound was calculated. The encoder counts for each muscle force were calculated by finding the product of the muscle force in the pounds and the encoder counts per pound.

4.5 : Calculating joint motion from position data

Using the X, Y, and Z, position data of the hip and ankle the joint motion was calculated in the sagittal plane. The vertical hip position during the simulation was calculated by the change in the hip and ankle's vertical z-component. The horizontal ankle position during the simulation was calculated by the change in the hip and ankle's horizontal y-component. The position data was then converted to encoder counts. In order to do this the encoder counts per meter had to be calculated. This was done by using the Galil program to jog the horizontal position Macron 14H belt actuator used for the ankle joint motion and by measuring the change in encoder counts over a measured distance. It was determined that the actuators move at roughly 27235.23 encoder counts per meter. Using this value the position was calculated in encoder counts by multiplying the position data by the number of encoder counts per meter. In order to calculate the joint velocities the displacement had to be calculated from the position data. The Y displacement data was filtered to remove noise during the data collection. The displacements were divided by 0.01 seconds to get the encoder counts per second for the Y and Z joint velocities. 0.01 seconds was used because the data was collected and output in 10 millisecond time steps.

4.6 : Creating the Galil controller Input Matrix

With the muscle forces and joint velocities calculated for each muscle group and the ankle and hip joints, the calculated data had to be organized into a matrix that could be easily modified for various tests performed using the Galil controller. Thus far the data had been calculated for the entire simulation. For the Galil matrix it was important to only use the data in the time frame where the jump landing occurred. This was done by plotting the vertical ground reaction force to determine the time frame in which the landing occurred from the jump. The matrix can be found in Appendix E. The matrix can be easily manipulated to change the amount of muscle force or joint velocity in the muscles and joints. This is done by changing the percentage at the top of the matrix. The matrix has been programmed to automatically modify the data to the desired percentage of force or velocity required for a test. For example if one wanted to apply only 50 % of muscle force in all four muscle groups, the percentage at the top of the matrix would be changed from 100 % to 50%.

4.7 : Creating a Galil program for the jump landing simulation

The Galil program was created for 6 axes. Axis A, B, C, D, E, and F correspond to the hip, hamstring, quadriceps, calf, hip joint, and ankle joint respectively. Axis A, B, C, and D were all in force control mode. Axis E and F were placed in position control mode.

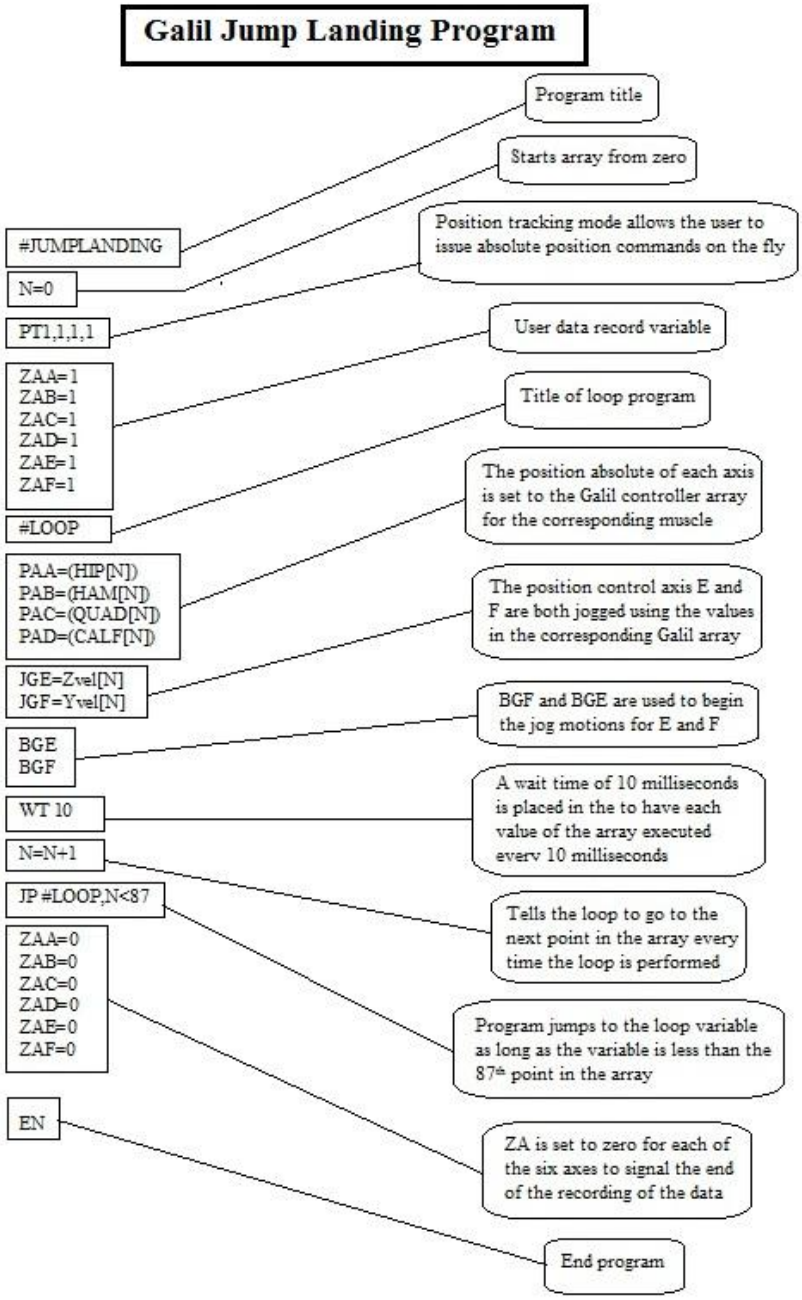

Figure 4.12: Detailed description of Galil jump landing program.

The first step in creating the Galil program for jump landing was to give the program an executable command title. The program was called # JUMPLANDING. The program was designed to read in an array and execute each row of the array every 10 milliseconds in a loop. The Galil input array is

saved as a comma separated values, csv, file that contains the array of muscle forces and joint velocities to be downloaded to the Galil controller. Figure 4.12 displays the Galil jump landing program with a detailed description.

The second part of the program involved the programming of the limit switches. The limit switch routine was designed to stop all of the axes when one limit switch it triggered. The routine begins with an ‘if’ statement. If the forward or the reverse limit switch for axis A is triggered then a message indicating limit switch A is triggered should appear and the program should be aborted and the motors should be turned off. Following this if statement is an else if statement which states if axis B is triggered than the program should be aborted and the motors should be turned off. Similarly, an else if statement was written for each of the other four axes.

4.8 : Calibrating load cell for test

In order to run the Galil program and produce accurate results, the load cells needed to be calibrated. The load cells are LC203-2K (Omega Engineering Inc., Stamford, CT). To calibrate each load cell that was connected to the muscle actuators, a load was placed on each pull/pull cable and the fine gain in the amplifier was adjusted to measure the load being placed accurately.

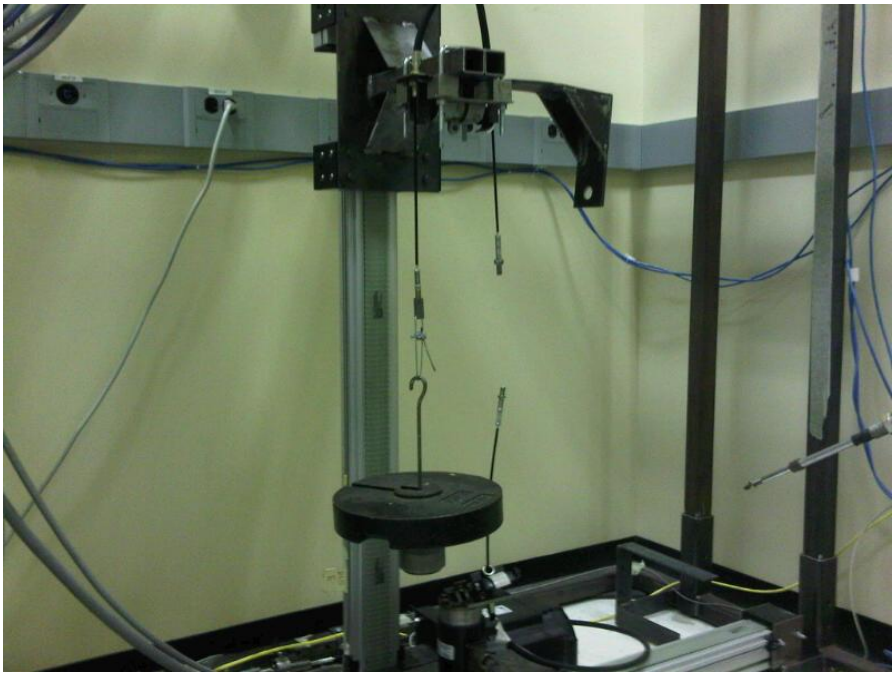

Figure 4.13: Calibrating load cell using weights.

A hook was attached to the end of the pull/pull cable by fishing a steel aircraft cable through the anchor and hooking on to it. The weights were placed on it as can be seen in Figure 4.13. With the load pulling on the load cell, voltage readings were found for each axis using "Galil Tools" software. The load cell should accurately output a voltage that is the same as the weight being placed on it. The load cells were calibrated to correspond to Table 4.4.

Table 4.4: Conversion chart.

Voltage	Encoder Counts	Pounds
10	2047	1000
1	204	100
0.1	20	10
0.01	2	1

For example if 0.25 V are read in Galil Tools, then 25 lbs of weight is being placed on the load cell. In order to make sure the load cell was measuring the load being applied accurately the fine gain in the Sensotec UV-10 in-line transducer amplifier, used in-line with the loadcell, was adjusted.

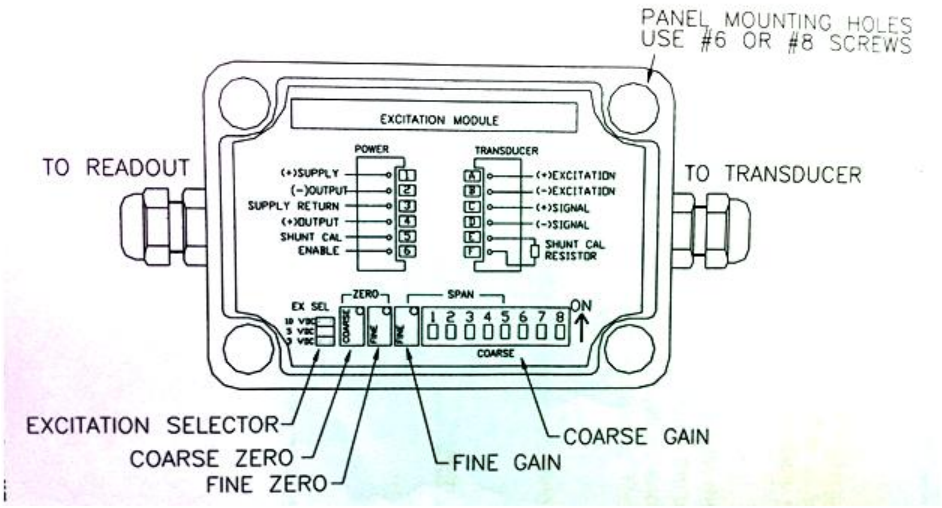

Figure 4.14: Amplifier schematic.

4.9 : Specimen Preparation

Before the cadaver knee could be used there were a few preparatory steps that were needed to be performed. First, a cadaver knee (49 years age, 120 lb. body mass) was thawed over night and then dissected. When dissecting, all of the muscles, skin, fat, and tendons were removed from the knee excluding the patellar tendon. The ACL, PCL, MCL, and LCL were left intact and undamaged. The quadriceps tendon was cut from the proximal end of the patella, leaving the patellar tendon intact. Excess tendon must be removed from the proximal end of the patella to ensure that it does not interfere with the testing. The fibula was attached to the tibia via a screw to keep it stabilized and maintain its natural position as seen in Figure 4.15. After stabilizing the fibula, below the screw the remaining bone of the fibula was sawed off since it was not needed.

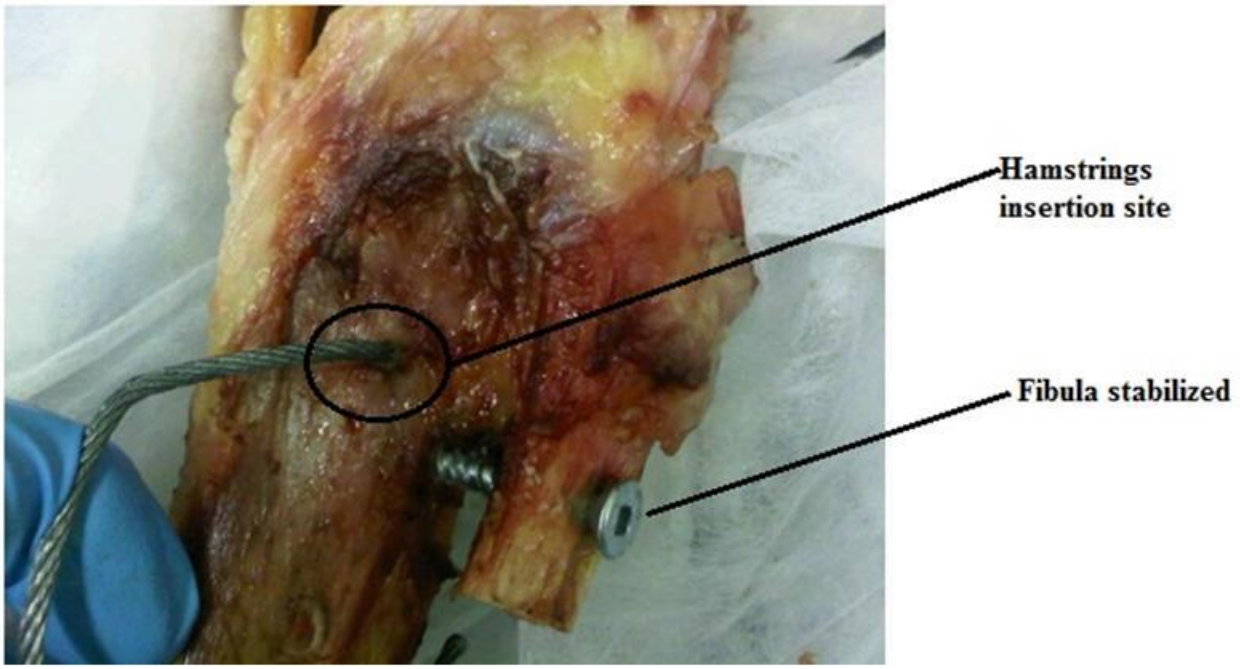

Figure 4.15: Stabilizing the fibula and location of hamstrings insertion site.

To simulate the quadriceps muscle, three holes were drilled through the patella and an aircraft cable was fished through the holes for connection to the quadriceps muscle actuator. Three holes were drilled in order to cover a larger surface area and offer more support to the patella when large pulling forces were placed on it by the quadriceps muscle actuator. Figure 4.16 displays the patella with the three holes drilled.

Figure 4.16: Patella preparation.

The calf muscle insertion was prepared by using a rigid steel wrap. The rigid steel wrap was bent around the femur just above the femoral epiphysis. For each knee a new steel wrap was used since it had to be molded to the shape and size of the femur on the knee being used. The steel wrap was bent and molded using pliers. The prepared calf muscle insertion can be seen in Figure 4.17 and Figure 4.18. The rigid steel wrap was used instead of drilling a hole through the calf muscle tendons on the femur because by doing so a greater surface area was used to distribute the load applied by the calf muscle around the shaft of the femur limiting the amount of damage caused when large forces were applied.

Figure 4.17: Front profile of knee with rigid steel wrap used for calf muscle insertion site.

Figure 4.18: Side profile of knee with rigid steel wrap used for calf muscle insertion site.

Finally the hamstrings muscle insertion was prepared by drilling a hole through the hamstrings tendons as seen in Figure 4.15.

4.10 : Installing knee into simulator

Before the knee could be installed on the simulator the tibial and femoral extensions had to be installed on their respective ends of the knee joint. This was done using eight screws to tighten the

femur and the tibia within the cups to ensure rigidity. Once the extensions were installed on the knee joint, the turnbuckle on each extension had to be adjusted to the appropriate length of the femur and tibia of the AnyBody model. The thigh length from the knee joint to the hip was 43.4 cm. The shank length from the knee joint to the ankle was 41.2 cm.

Before mounting the leg with the extensions adjusted to the required lengths onto the simulator, the Differential Variable Reluctance Transducer (DVRT, Microstrain Inc, Burlington, VT) had to be mounted. The DVRT is used to measure strain and is mounted similar to Hashemi et al (J. Hashemi, 2007). To mount the DVRT, the knee was bent and the patella was pulled back exposing the ACL. With the ACL exposed, forceps were used to install the DVRT onto the ACL. Figure 4.19 displays the DVRT installed on the ACL and Figure 4.20 shows a close up of the DVRT installed.

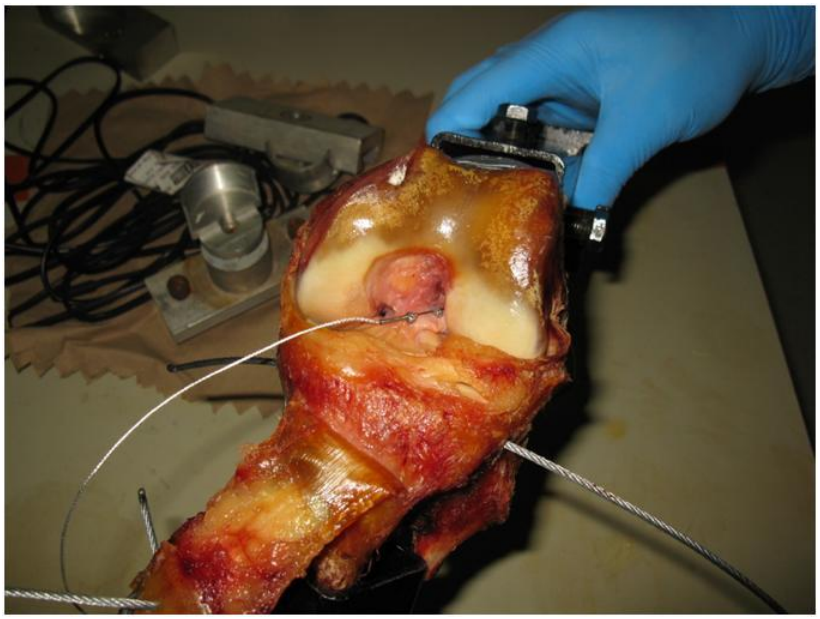

Figure 4.19: DVRT installed on the ACL.

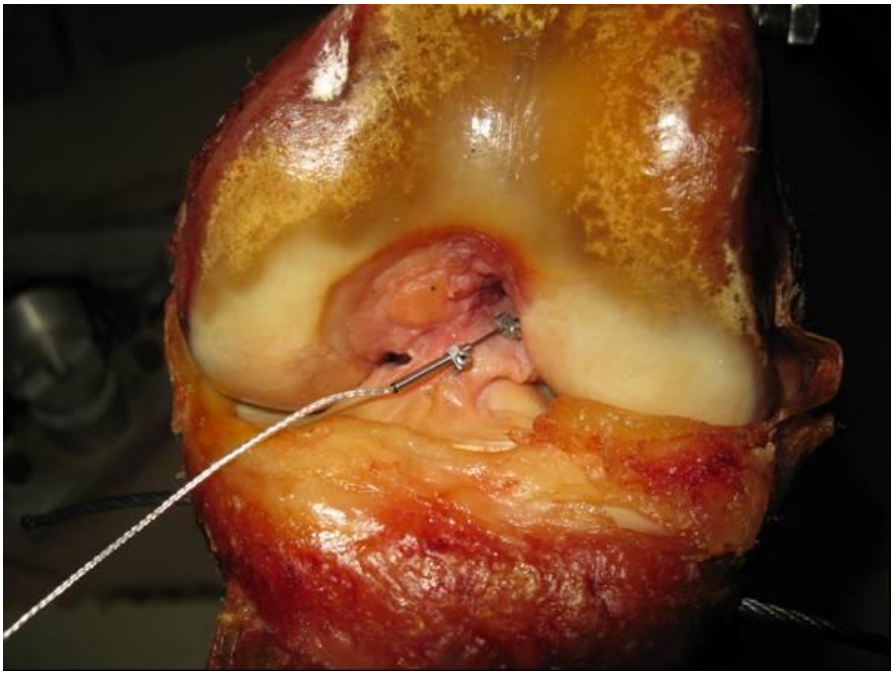

Figure 4.20: Close up of DVRT installed on ACL.

With the extensions and the DVRT installed on the knee, the leg could be installed onto the simulator. This was done by attaching the femur and tibial extensions to the ball and socket joint at the hip and the fixed joint at the ankle as seen in with the femur extension in Figure 4.21.

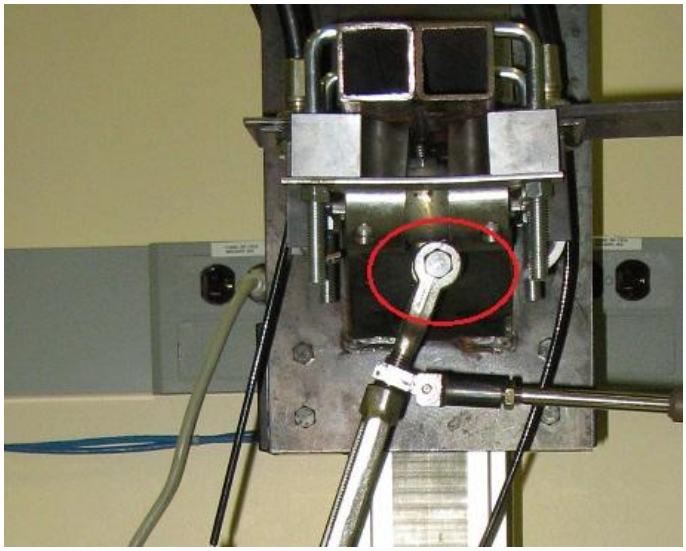

Figure 4.21: Femur extension attached to the ball and socket joint of the hip.

The tibial attachment to the ankle joint involves two parts. First the tibial extension's jaw is attached to the fixed ankle joint similarly to the femoral extension attachment to the hip ball and socket joint. Figure 3.9 displays the fixed ankle joint. The second part eliminates the internal and external rotation of the knee at the ankle joint allowing the motion to remain in the sagittal plane. The part and the attachment of the tibial extension are shown in Figure 4.22.

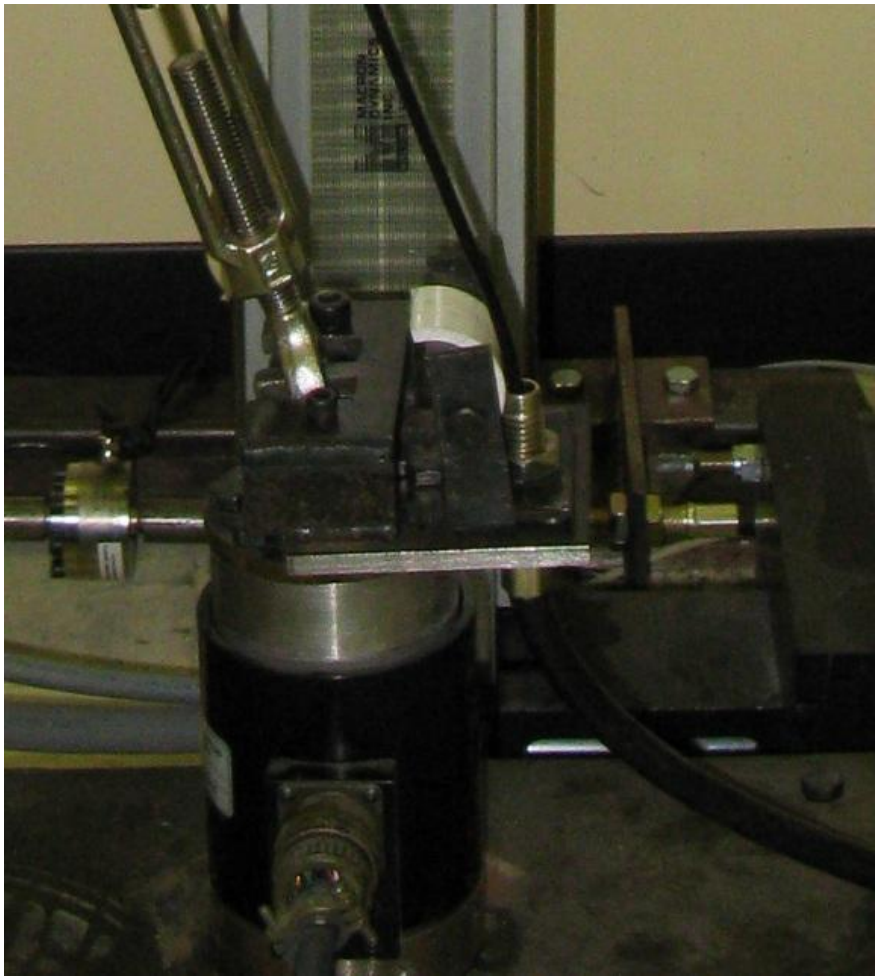

Figure 4.22: Attachment of tibial extension to the fixed ankle joint.

The hip muscle actuator was attached to the femoral extension by first feeding the push/ pull cable through a hole drilled through the hip joint as shown in Figure 4.23. The push/pull cable was then rigidly mounted to the proximal end of the turnbuckle on the femoral extension.

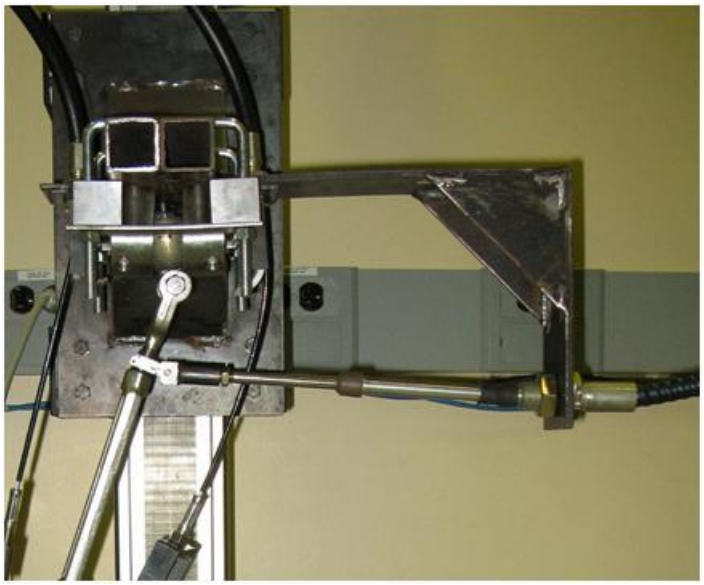

Figure 4.23: Hip component of the simulator.

The hamstring muscle actuator was attached at the muscle insertion site on the bone via a pull/pull cable. The pull/pull cable had a bracket attached to the end of it that connected to the specimen insertion site. The connection was made by fishing a 1/8 inch aircraft cable through the bone at the hamstring insertion site and then through a couple of holes drilled through the bracket. Figure 4.24 displays the knee joint mounted in the simulator with the muscle attachments connected at the insertion points. The calf muscle actuator's pull/pull cable had a bracket specially designed to simplify the connection to the insertion point as well. The bracket was connected to the calf muscle insertion site using an aircraft cable and two rigid steel wraps. The steel wraps were wrapped around the femur and connected to the bracket as shown in Figure 4.24.

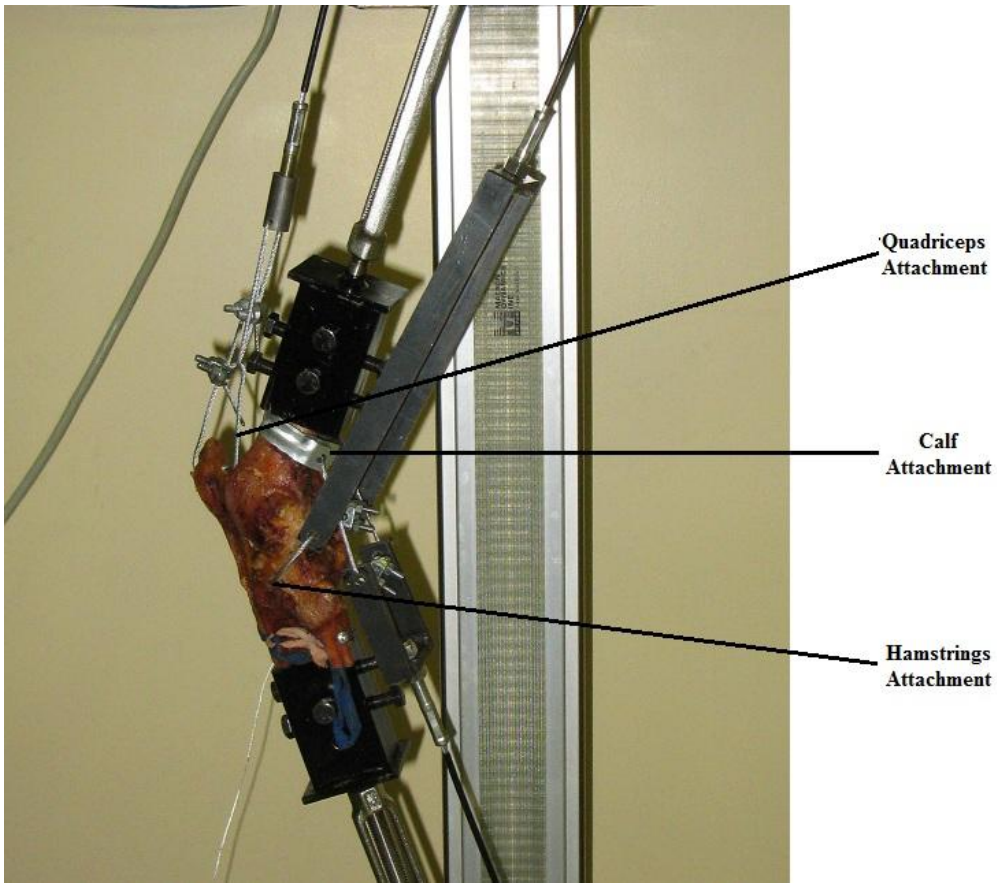

Figure 4.24: Muscle attachment sites.

The quadriceps muscle actuator was attached to the patella by connecting the anchor at the end of the pull/pull cable to the already prepared insertion site at the patella using a 1/8 inch air craft cable. The patella had three holes drilled in it with an aircraft cable fed through it for easy connection to the pull/pull cable. Figure 4.25 displays a detailed look at the dynamic knee simulator with the cadaver knee mounted.

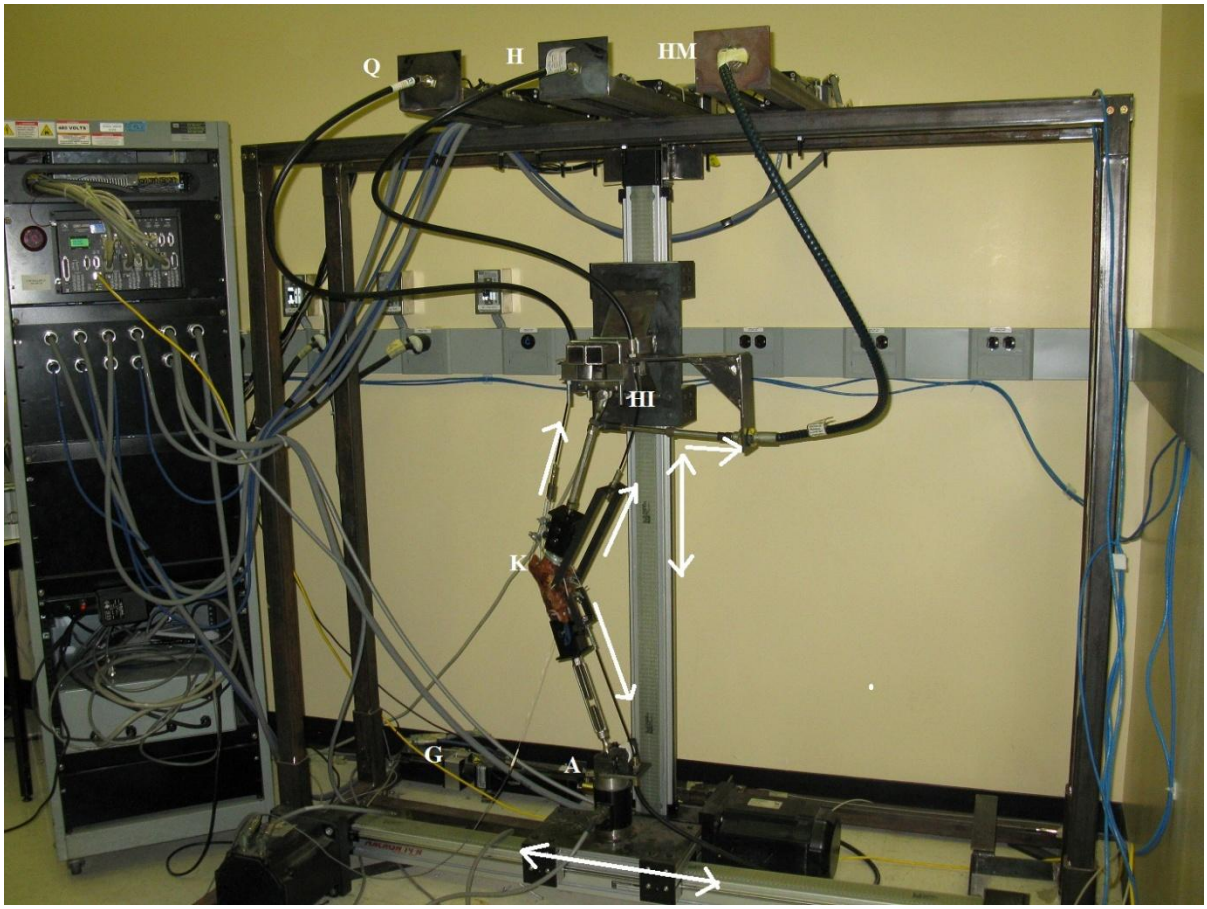

Figure 4.25: The dynamic knee simulator system. The cadaver knee (K) is connected to the turnbuckles that are connected to surrogate hip (HI) and ankle (A) joints. The hip joint moves in the vertical direction (dark double head arrow) and the ankle moves in the horizontal direction (white double head arrow). Three muscle force actuators (Q, H, and G) are connected to the knee and they apply dynamic quadriceps, hamstring, and gastrocnemius muscle forces (dark single head arrows). The hip moment actuator (HM) connected to the turnbuckle below the hip applies flexor-extensor moment.

4.11 : Setting up Galil for testing

Before setting up Galil for testing it is important to first turn on the power switches on the wall and then the Galil controller to ensure everything runs smoothly. The next step is to set up the WSDK. Galil's WSDK Servo Design Kit software is tuning software for Galil's prior generation controllers. These controllers include the DMC 40x0. A new tuning file was created with gain and torque limits modified.

Once the tuning file is loaded the Galil tools software is opened and the controller is connected. With the controller connected the first step is to make sure the four tolomatic muscles actuators are in load control and the two belt joint actuators are in position control. This is done by entering the AF command for analog feedback. Galil should return six numbers separated by commas. If Galil returns a "1" then the axis is in load control. If it returns a "0" then the axis is in position control.

Following the AF interrogation, the DMC program file was downloaded. Depending on the test sequence a new array was downloaded to Galil before running each test. For example if 50% of the muscle forces are to be applied the array is updated and downloaded to Galil. For the jump landing simulation, the acceleration, deceleration, and the acceleration feedforward coefficient for the hip and ankle joint actuators had to be modified. The acceleration and deceleration for the hip joint were set to 750k counts/s^2 and for the ankle joint they were 5 million counts/s^2. The feedforward coefficient, when scaled by the acceleration, adds a torque bias voltage during the acceleration phase and subtracts the bias during the deceleration phase of a motion. The coefficient for the hip is 80 and for the ankle it is 120.

With the Galil software setup for testing, the program was now ready to be executed. The motors were turned on and the absolute positions for the four load control actuators were set to the initial

encoder counts from their corresponding arrays in the Galil array. This applied the initial force for each muscle upon executing the program. The program was now ready for execution.

4.12 : Test Setup

Before running tests, the jump landing and gait simulations were run to compare the input versus output of the muscle forces and hip and ankle motion profiles. The first test scenario involved five tests of the landing phase of jump landing and gait simulations with 100% speed and muscle forces applied. The gait simulation was setup the same way as it was setup in Cassidy's study (Cassidy, 2009). The data for the gait simulation was obtained from the GaitVaughan model using AnyBody Modeling Technology. The five trials were evaluated to validate the repeatability of the results and the accuracy of the muscle actuators and the position actuators. The output force of the muscle actuators and speed of the position actuators was compared to the input muscle forces and speed to check accuracy. The DVRT voltage output was used to measure the strain and compare the results over the five trials to display repeatable results.

The second scenario involved varying the firing patterns for the jump landing simulation. For each trial one of the muscles was subjected to 0%, 50%, and 150% of the muscle force while the other muscles were firing with 100% muscle force. The strain results were compared.

The third scenario involved testing the jump landing simulation with zero muscle forces, with the muscle actuators slack(not preloaded to the first load of the input array for each muscle actuator), and finally with 200% hip muscle forces applied. The strain results were compared.

4.13 : Data Collection

The data was collected using LabVIEW (NI LabVIEW, Austin TX, USA). The LabVIEW program was setup to collect the load cell and strain gauge data. The program read the four 1 D load cells, the

six channels of the 3D load cell and the DVRT. The program attached a time stamp as well. The time stamp made it easier to compare the output muscle force from the actuators to the input muscles forces. The Galil motion control had a LabVIEW virtual instrument that allowed LabVIEW to directly record the output from Galil.

The 1 D load cells were used for the muscle actuators since they pull in one direction. The load cells are rated for 2000 lbs of force for tension and compression and are made by Omega Engineering (Omega Engineering, Connecticut, USA).

The 3 D load cell is designed by Bertec INC (Bertec Corp, MI, USA). It has six channels used to measure the F_x, F_y, F_z, M_x, M_y, and M_z. The 3 D load cell was used to measure the ground reaction forces and moments at the ankle joint during the jump landing simulation.

Finally the DVRT as mentioned in the specimen preparation was mounted on the anterior side of the ACL.

4.14 : Processing the output data

The output from LabVIEW was stored in a LabVIEW Measurement (`.lvm`) format which is a text-based file format for one-dimensional data that one can use with the Read LabVIEW Measurement File and Write LabVIEW Measurement File Express Vis (National Instruments, 2010). The `.lvm` file is designed so it is easy to parse and easy to read when imported into a spreadsheet program, such as Microsoft Excel. The voltage results from the simulation were converted to muscle forces and strain.

The muscle forces were converted based on the calibration of the actuators. For every volt there is 204.7 encoder counts or 100 lbs of force applied. So the voltage was multiplied by 100 to get the

output muscle force in pounds. For comparison purposes the results were converted to Newtons. This process was performed for each of the four muscles.

For measuring strain the first step was to measure the initial voltage and the distance between the prongs of the DVRT. A LabVIEW virtual instrument was created to view the DVRT voltage change in real time. Using this virtual instrument an initial recording was taken of the initial voltage before the loads were applied prior to executing the Galil program. The initial voltage is used as a reference voltage that is used for calculating the displacement of the DVRT from the initial position. For every trial the DVRT has a new initial position and it is important to take into account the change in position from the first measurement. The change in voltage is converted to displacement in mm by multiplying by -0.36 mm/V which was specified on the DVRT calibration sheet. The new initial length is then calculated by adding the displacement to the initial distance between the prongs. With the new initial voltage and length the strain could be calculated. The strain was calculated by subtracting the initial voltage from each output voltage in the output array from the simulation and multiplying by -0.36 mm/V. These values were then divided by the new initial length and multiplied by 100 to get the percent strain.

Chapter 5

Results

5.1 : Jump landing simulation

5.1.1 : Muscle force profiles from AnyBody Modeling Technology

Error! Reference source not found. displays the muscle force profiles of the four major muscle groups surrounding the knee joint calculated from AnyBody Modeling Technology. These muscle force profiles were input into the dynamic knee simulator.

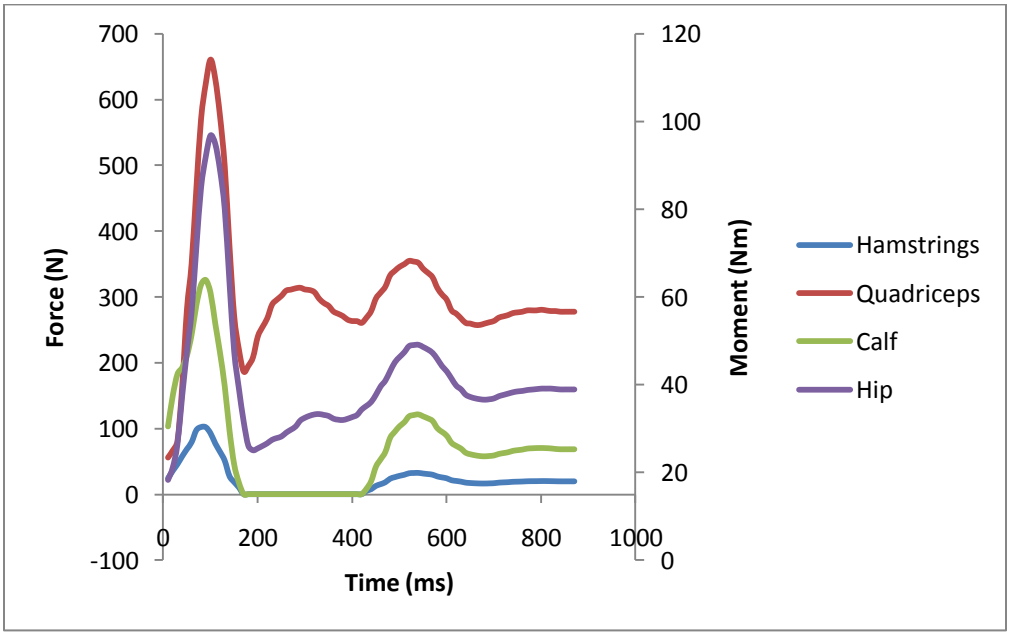

Figure 5.1: Muscle force profiles from AnyBody Modeling Technology.

5.1.2 : Relative Joint motion from AnyBody Modeling Technology

Figure 5.2 displays the joint motion of the hip and ankle determined from the AnyBody model of jump landing. These profiles display the movement of the hip and ankle throughout the simulation.

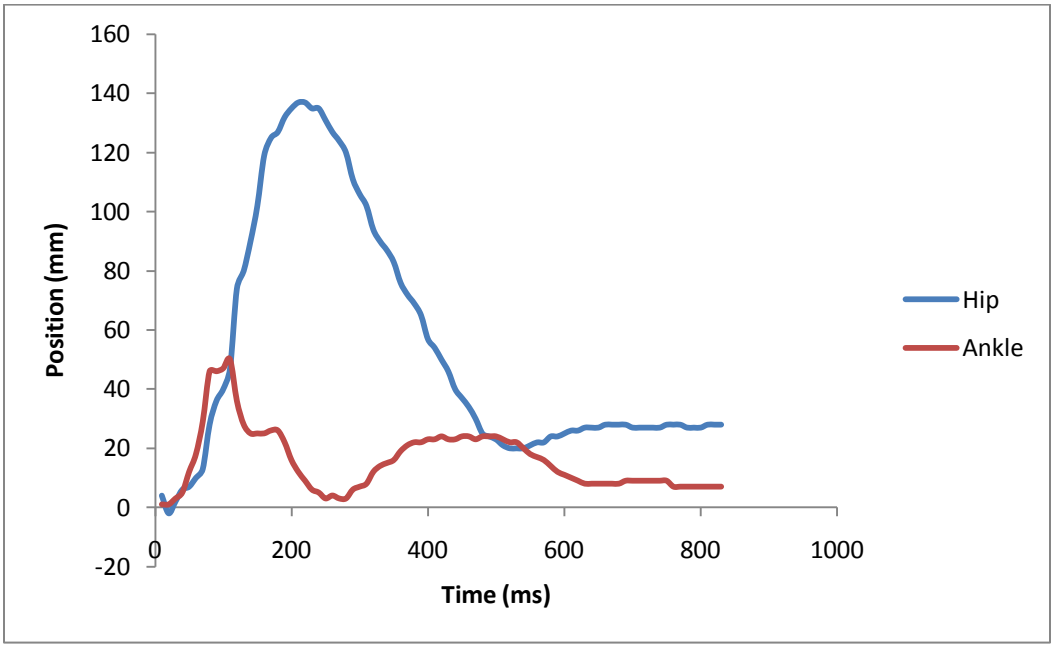

Figure 5.2: Joint motion from AnyBody Modeling Technology.

5.1.3 : Comparison of muscle force profiles with simulated muscle forces

The muscle forces that were output from the load cells of the simulator based on the input muscle force profiles are shown in Figure 5.3. It can be seen that the simulator has the ability to follow the input profiles very well. The output muscle forces have been filtered to remove electrical and mechanical noise.

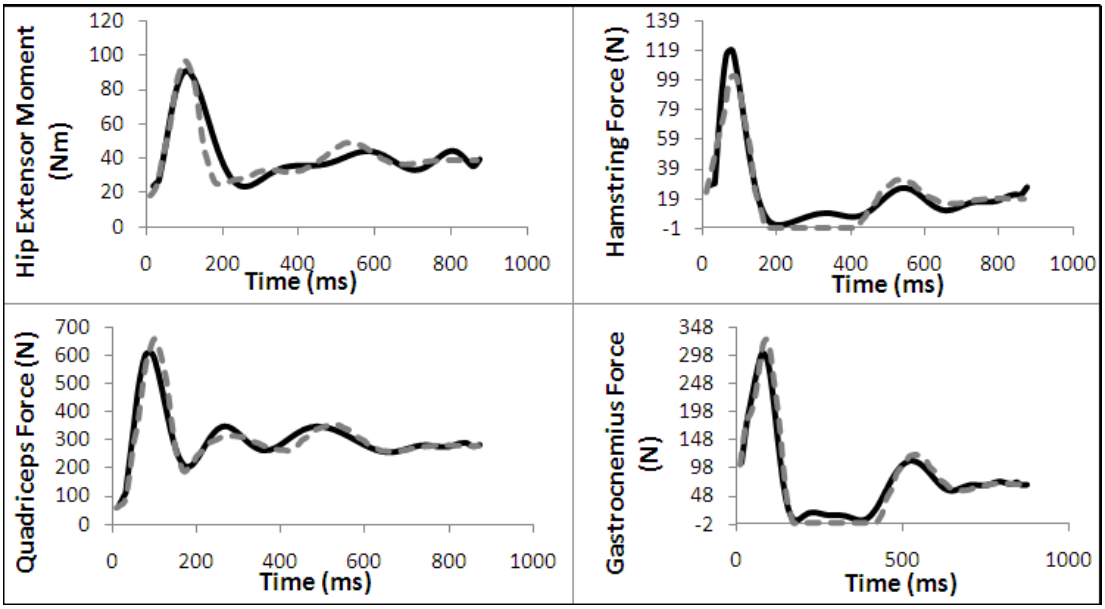

Figure 5.3: The applied muscle force profiles (solid line) of hamstring, quadriceps, gastrocnemius(calf) muscle group forces and the applied hip extensor moment. The input to the actuators is shown as dotted grey lines. The data is filtered to remove electrical and mechanical noise.

5.1.4 : Comparison of joint position

In Figure 5.4 and Figure 5.5 the joint motion is compared between the input profile from AnyBody Modeling Technology and the output from the simulator. It can be seen in Figure 5.4 that the hip motion follows the AnyBody input position very well but slightly lags in the time taken to reach the desired position. The ankle output from the simulator reaches the desired input positions but has a 40 millisecond lag at the beginning of the simulation and slightly over shoots the desired position as can be seen in Figure 5.5.

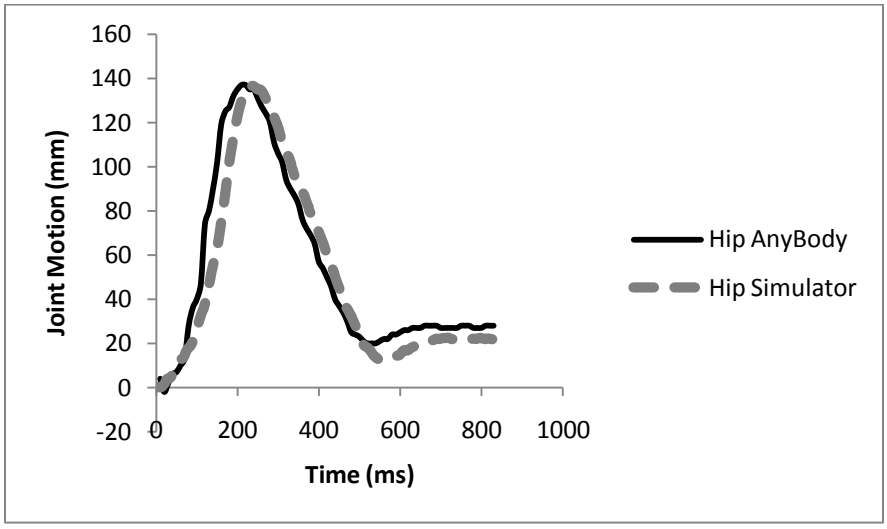

Figure 5.4: Comparison of hip motion.

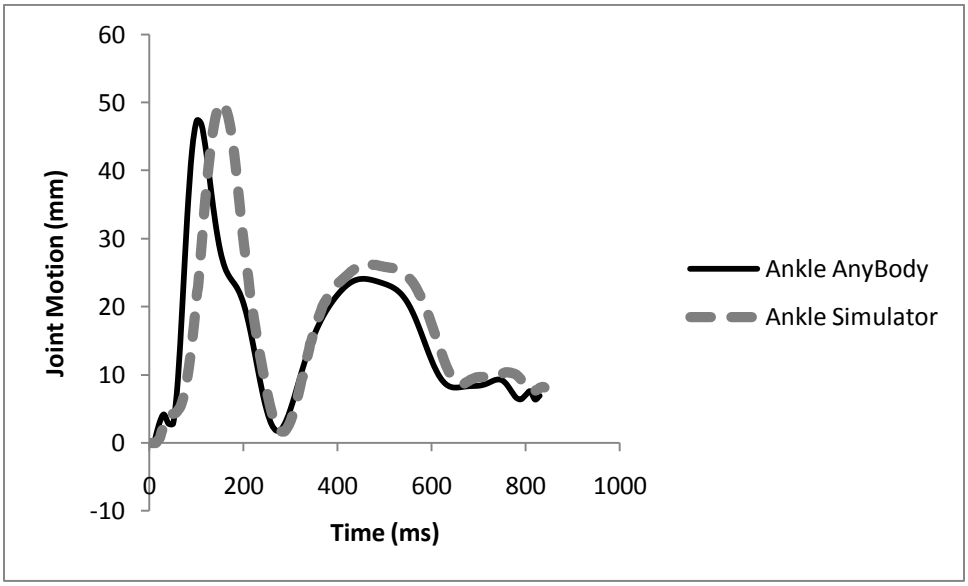

Figure 5.5: Comparison of ankle motion.

5.1.5 : ACL strain from 5 trials of jump landing

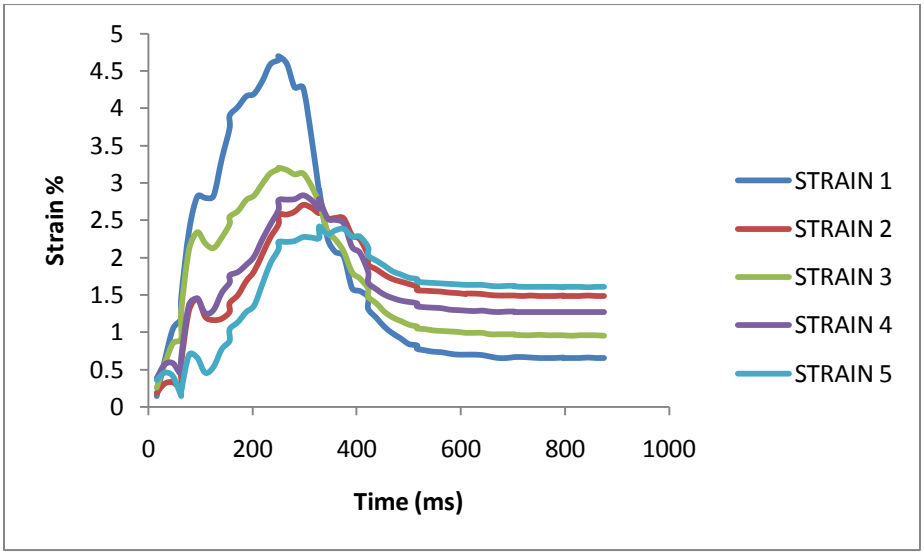

Figure 5.6: Comparison of ACL strain from 5 trials of jump landing.

In Figure 5.6 the ACL is measured and compared between five trials of the jump landing simulation. It can be seen that the strain results are reproducible. The average peak strain was about 3%. The average strain rate was 17%/s.

5.2 : Comparison of ACL strain during jump landing under various firing patterns

Various firing patterns of muscle forces were tested to study the effects on ACL strain. In each test ACL strain was measured while a certain muscle group's firing pattern was altered to fire with 0%, 50%, and 150% muscle force meanwhile the other muscles fired at 100% muscle force. These results were compared with the ACL strain with all of the muscles firing at 100% muscle force and with all of the muscles not firing at all. The results can be seen in Figure 5.7, Figure 5.8, Figure 5.9, and Figure 5.10.

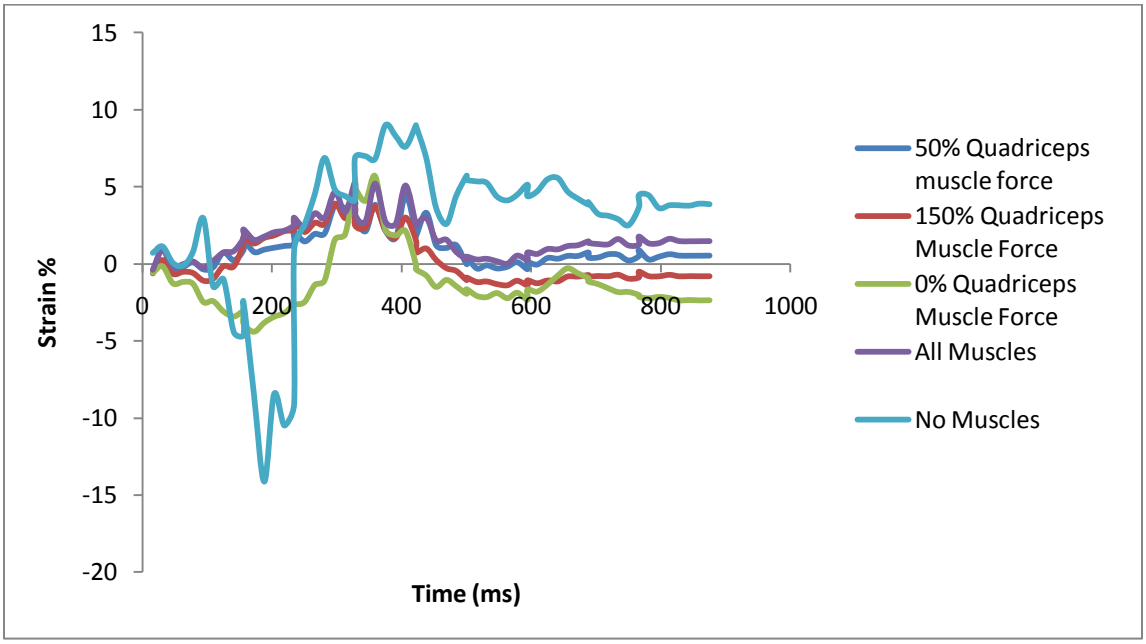

Figure 5.7: Quadriceps muscle force- strain characteristics.

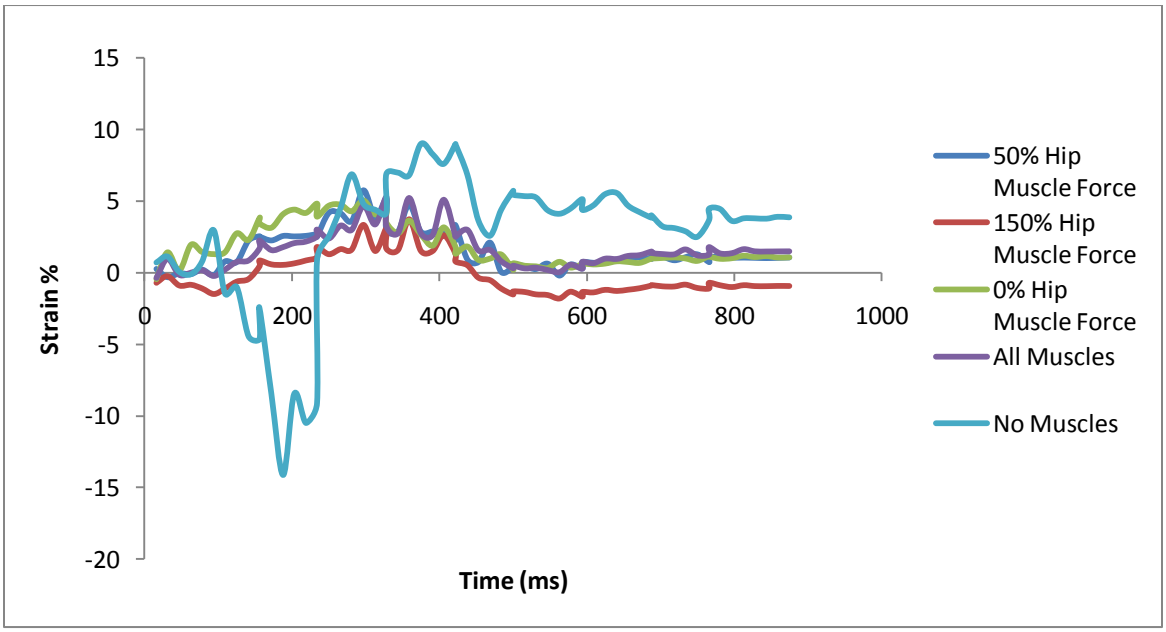

Figure 5.8: Hip muscle force- strain characteristics.

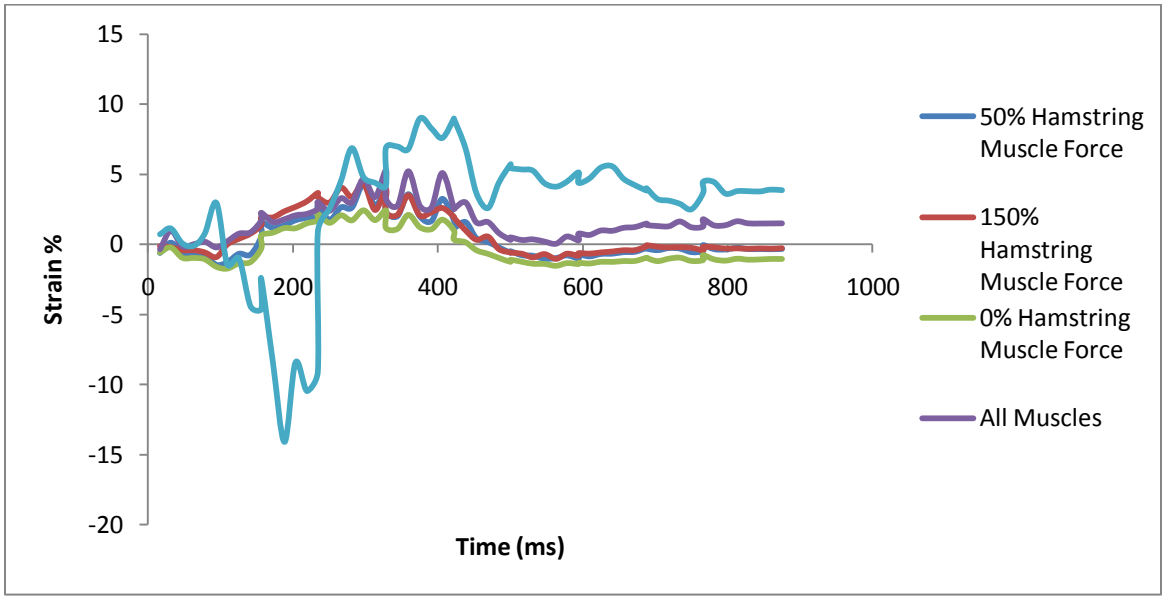

Figure 5.9: Hamstring muscle force- strain characteristics.

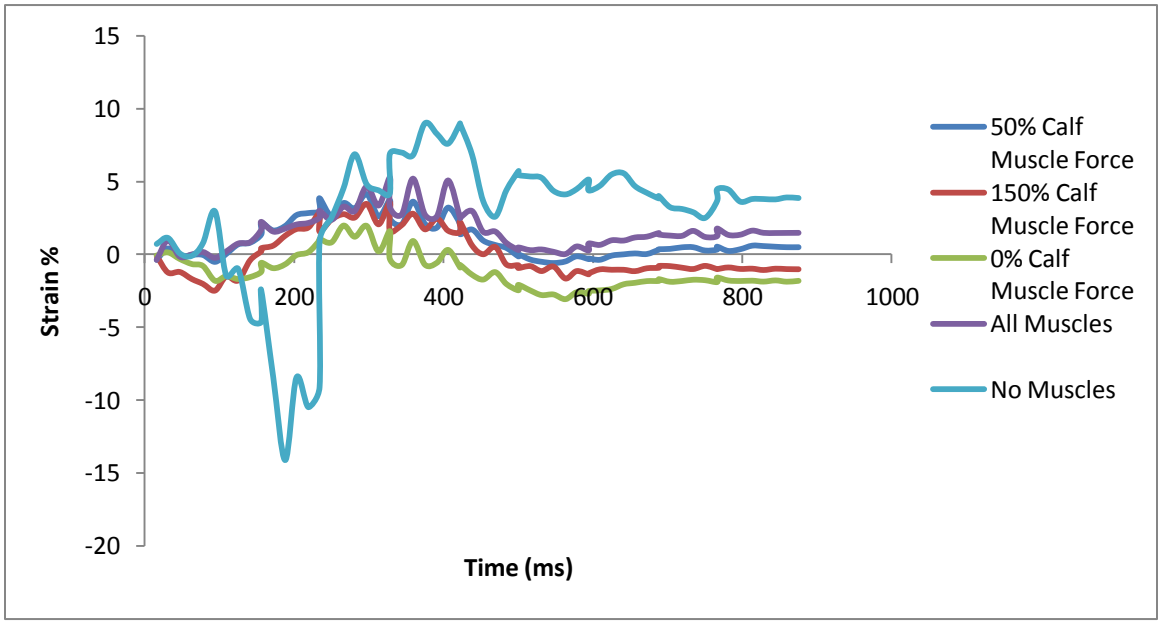

Figure 5.10: Calf muscle force- strain characteristics.

From the results it can be seen that there is a significant increase in strain when no muscles are applied. When all of the muscles fire with 100% muscle force the peak strain is roughly around 5% at 359 milliseconds.

At 50% of the quadriceps force the peak strain is about 4.45% at 406 milliseconds. At 150% quadriceps muscle force the peak strain is 3.9% and reached at 297 milliseconds. When the quadriceps muscle does not fire the peak strain is 5.71 % at 359 milliseconds.

At 50% hip flexion the peak ACL strain is measured to be 5.8% at 297 milliseconds. When the hip flexor fires with 150% muscle force the peak ACL strain is 3.72 % at 359 milliseconds. When the hip flexor muscle does not fire the peak ACL strain is 5.1% at 297 milliseconds. It can be seen that the strain increases at a higher rate when the hip flexor-extensor is not firing.

At 50% hamstrings muscle force the peak ACL strain is measured to be 4.27% at 297 milliseconds. When the hamstrings fire at 150% muscle force the peak ACL strain is measured to be just slightly higher at 4.34% at 297 milliseconds. When the hamstrings are not firing the peak strain decreases to 2.41% at the same time.

The calf muscle at 50% muscle force produced a peak ACL strain of 4.1% at 297 milliseconds. At 150% applied calf muscle force the peak ACL strain was measured to be 2.1% at 328 milliseconds. When the calf muscle was turned off the peak ACL strain produced by the jump landing simulation was 2% at 266 milliseconds.

5.3 : Gait Simulation

In addition to simulating jump landing, gait was also simulated to compare and validate that the output from the load cells followed the input muscle force profiles. As can be seen in Figure 5.11 the output from the load cells follow the muscle force profiles very well.

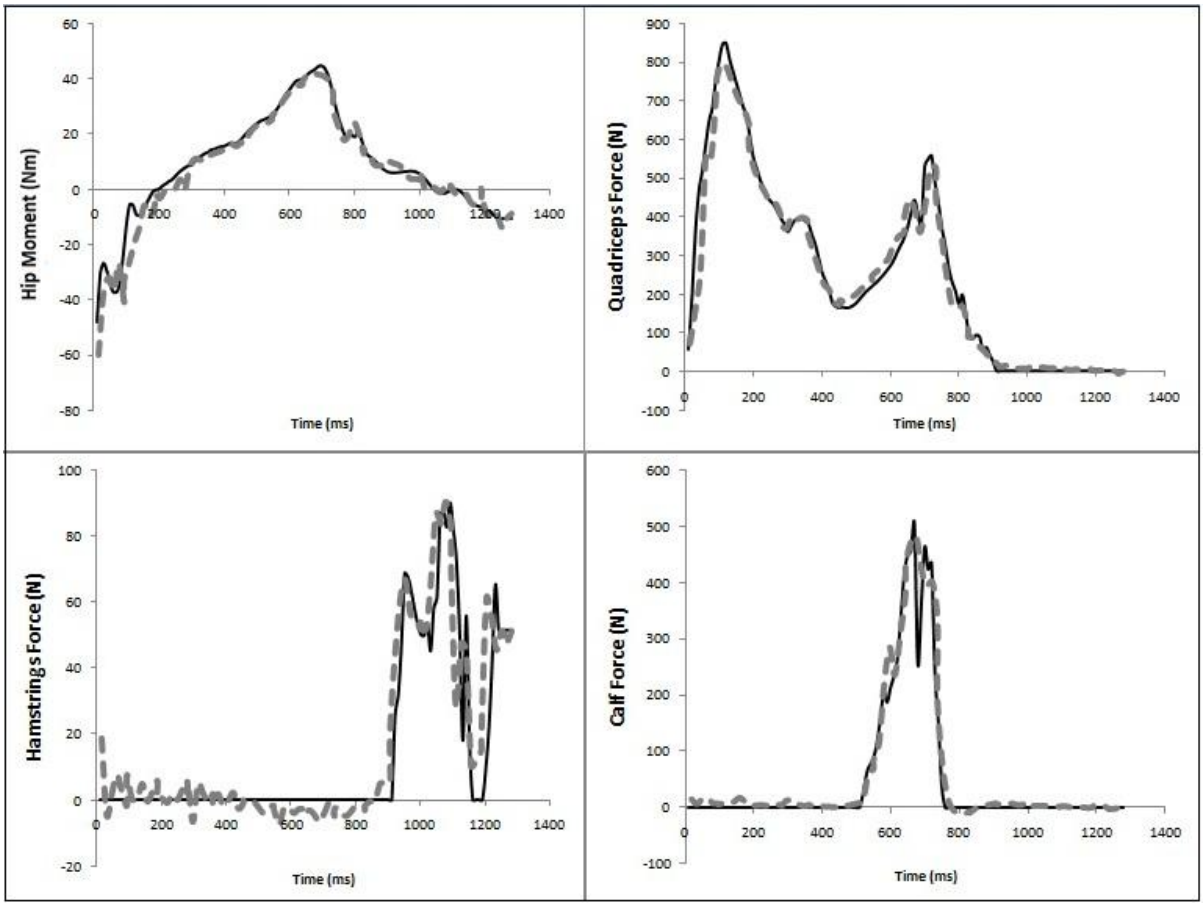

Figure 5.11: The applied muscle force profiles (solid line) of hamstring, quadriceps, gastrocnemius(calf) muscle group forces and the applied hip extensor moment. The input to the actuators is shown as dotted grey lines.

In Figure 5.12 the ACL strain is measured and compared between five trials of the gait simulation. It can be seen that the strain results are reproducible. The average peak strain was about 2.71%.

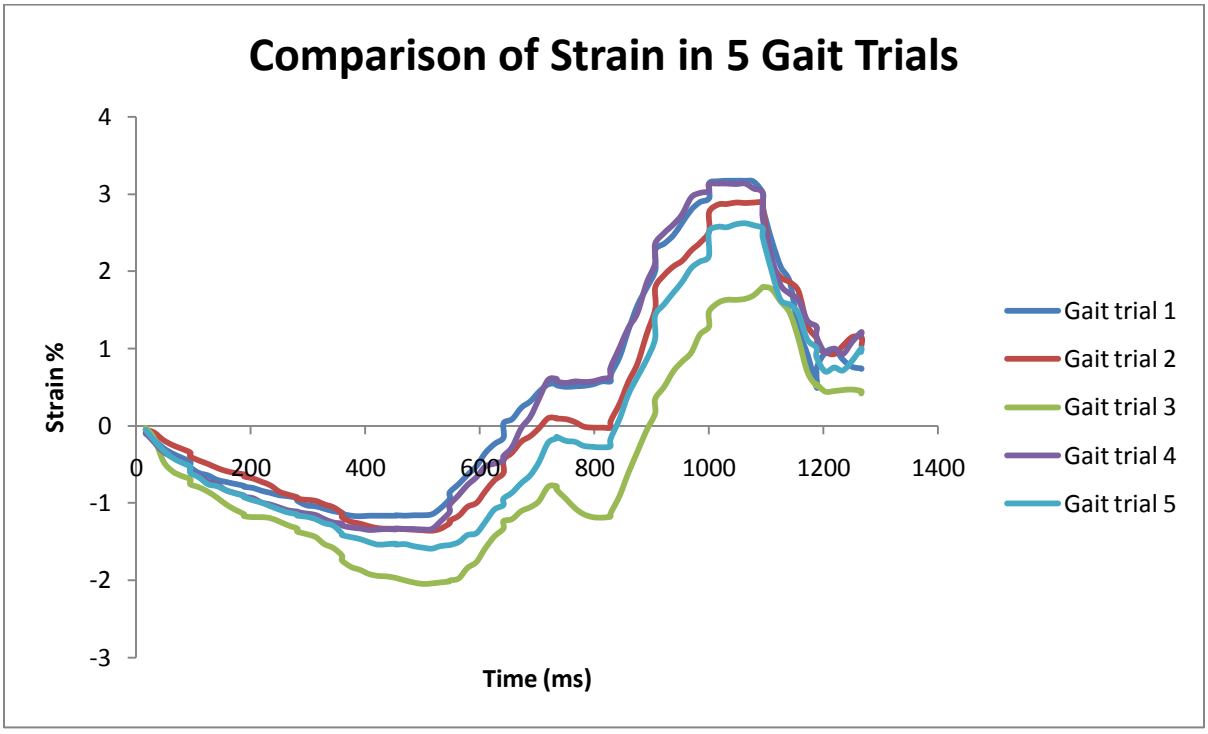

Figure 5.12: Comparison of ACL strain from 5 trials of gait.

5.4 : Discussion

The results from the jump landing simulations show that the dynamic knee injury simulator is capable of replicating the physiological motion of jump landing. The 6 axes of the simulator compared very well with the input muscle force and joint motion velocity profiles. In the past, simulators such as the ones designed by Hashemi et al. and Withrow et al. have not been able to replicate the high speed motions and active muscle profiles necessary to study the effects of muscle contraction on the ACL for activities such as jump landing and rapid deceleration. Furthermore our simulator utilizes powerful electromechanical actuators and powerful multi-axis motion control with a two millisecond response time to apply muscle force and velocity profiles accurately. The previous generation simulator from Hashemi et al. had the ability to apply quadriceps and hamstrings muscles forces (Hashemi J, 2007), but could not simulate the motion of the hip and ankle as well as the muscle force

contributions from the hip moment and the gastrocnemius (calf) muscle group. The hip and ankle motion are very important in replicating the physiological motion as they contribute to the firing patterns of the muscle forces.

The peak quadriceps muscle force was found to be 650 N. In comparison to recent studies this quadriceps force is a bit low. Domire et al. performed a study in which they investigated the effects of the quadriceps muscle force on the anterior cruciate ligament using a simple simulation of a landing activity (Domire ZJ, 2011). They found that the upper bound of quadriceps force was 2000 N in the first 50 milliseconds which is the time frame in which injury occurs. Weinhold et al. found the quadriceps muscle force to be roughly 1 to 1.5 times the body weight of the person landing from the jump. In the case of our study, the subject used in the motion capture and the musculoskeletal model was 170 lbs. This would mean the quadriceps force according to Weinhold et al would be between 750 N and 1125 N. A possible reason for the low quadriceps force calculated in our study, is that during the motion capture the subject had a soft landing to avoid injury. The subject had performed numerous one legged jump landings so it was evident that to prevent injury the subject landed softly rather than stiff. The entire landing simulation took about 750 milliseconds as can be seen in the plot of the ground reaction force seen in Figure 5.13. In our simulation the knee was flexed about 60 degrees during landing while Withrow et al. determined that peak knee flexion occurs at about 31 degrees (Withrow TJ, 2006). The results from Withrow et al. indicate a stiff landing.

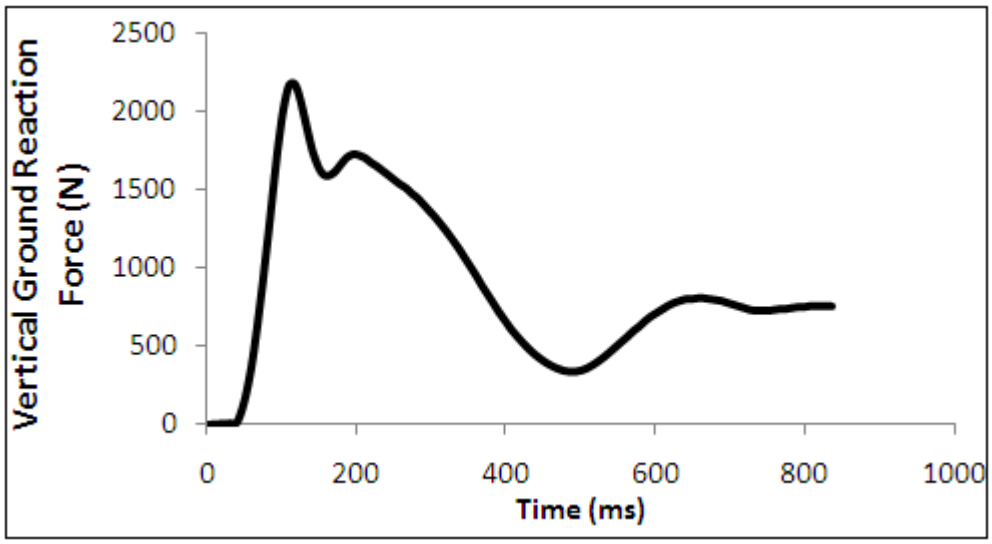

Figure 5.13: Ground reaction force during the landing phase of the jump landing simulation.

While the simulators muscle force outputs followed the input muscle force profiles well, the hip and ankle motion did a great job following their input profiles. The hip profile followed the input very well but the ankle lagged a bit in following the profile. This is due to the required high linear acceleration. By increasing the voltage input this problem can be solved.

In the five trials of jump landing, the strain results were repeatable and the average peak strain was found to be 3%. Weinhold et al. found ACL strain to be roughly 1.5-4% for a male knee (Weinhold PS, 2007). Withrow et al. found ACL strain to be roughly 4% during jump landing (Withrow TJ, 2006). Shin et al. found ACL strain to be around 2-2.5% from their jump landing simulation (Shin CS, 2007). Zhang et al. and Taylor et al. found similar results. All of these results agree with the results we obtained in our jump landing simulations. The results could be more accurate if the DVRT is installed at 20 degree flexion. Our results were determined based on the initial position being recorded when the ACL was stretched due to difficulty installing the DVRT. These results came from the use of one knee. A better comparison can be made when the results are compared amongst a few

knees. Our study simply shows that the simulator is capable of simulating jump landing and measuring ACL strain.

When varying the firing patterns of each of the four muscle groups it was evident that the most significant effects on ACL strain came from the hip moment and the quadriceps force. When the hip moment was decreased to 50 % of its capability the peak ACL strain increased from 5.28% to 5.77%. When the hip moment was turned off and the muscle group didn't fire the ACL strain was roughly the same as when all of the muscles fire at 100% but the strain rate increased and reached peak strain much faster. When the hip flexor was increased to 150%, the peak ACL strain decreased significantly to 3.7%. Hashemi et al. believe that the hip muscles are crucial in developing strain in the ACL and could actually cause increased ACL strain (Hashemi J, 2010). From our study it is found that the ACL strain decreases with increasing hip flexion. The quadriceps had the most significant influence on the ACL strain. When the quadriceps did not fire the peak ACL strain increased to 5.7%. As the quadriceps force was applied and increased the peak strain decreased to 4.44% at 50% force and 3.9% at 150% force. The results of the hamstrings showed that at 50% and 150% the peak ACL strain decreased to about 4.34% from 5.28%. And when the hamstrings did not fire the strain decreased to 2.4%. The calf muscle displayed a decrease in peak ACL strain of 4.12% when the calf fired at 50% force. The peak strain decreased even more to 3.6% when the calf muscle fired at 150 % and finally down to 1.9% when the calf muscle was turned off.

It must be noted that this data is based on a controlled jump landing which was performed with the subject's intention not to get injured. Therefore the landing was soft as opposed to stiff. For this reason all of the muscles fired in a fashion to protect the ACL from injury. This explains why when increasing the quadriceps force the strain decreases. If the subject landed in a non-controlled manner the ground reaction force would be directed posteriorly to increase flexion of the knee, this would cause the body to resist the excessive flexion therefore increasing the quadriceps load which would

increase the ACL strain and potentially cause injury (Hashemi J B. R.-O., 2010). In that kind of loading situation the muscles surrounding the knee would fire in a more unstable fashion. If the same tests of variable muscle contraction were performed on those kinematics then there would be more significant effects on ACL strain when a certain muscle is fired with more force or less.

When performing the gait simulations, it can be seen that the results from the gait simulations show that the 6 axes of the simulator compared very well with the input muscle force and joint motion velocity profiles. The strain results were repeatable as well with an average strain of 2.71 %. Although the results of the muscle force and velocity profiles were favourable the kinematics seemed to be quite unrealistic. This could be due to the gait biomechanical model used to obtain the kinematic data.

Although the simulator is able to simulate gait and jump landing there are a few limitations to be considered. Currently the motion is only in the sagittal plane. Motions in the coronal plane cannot be taken into account. Therefore all simulations have been simplified to one plane of motion. The DVRT installation is also something that needs to be more fine tuned, a new method for installing the DVRT must be determined as currently it is installed when the knee is flexed to the point where the ACL is stretched a significant amount.

Although there are a few limitations the simulator is a significant improvement over current simulators. It has been validated that the simulator can perform simple gait and more complex jump landing simulations. This shows that it is capable of performing high speed motions with rapid decelerations. There is definitely room for improvement in the simulator, but it is has the potential to make significant contributions to the study of ACL injuries. As further improvements are made, more accurate studies of the ACL injury mechanisms can be performed.

Chapter 6
Conclusion and Future Work

6.1 : Conclusion

a) The aim of this study was to simulate jump landing using the dynamic knee injury simulator. The simulation is physiological as it replicates the kinematics from motion capture and muscle force profiles from the AnyBody Modeling Technology musculoskeletal model. There were a few improvements made to the simulator to help it withstand the effects of higher forces and speeds during activities such as jump landing.

b) The simulator has proven to be able to simulate both gait and jump landing. The muscle actuators tracked the input muscle profiles very well. The joints traveled smoothly and compared very accurately to the input motion profiles. The ankle joint lagged a bit in catching up to the speed of the input motion profile but this can be fixed by increasing the input voltage. The jump landing simulation required a few modifications to the simulator to reinforce the parts but it simulated the motion accurately and resembled the jump landing performed in the motion capture when compared to the video. ACL strain agreed with published data on jump landing.

c) AnyBody model is an excellent tool to use for calculating muscle force profiles. The muscle forces are very difficult to calculate. The AnyBody model allows us to perform motion capture and input the kinematic data and anthropometric data and receive the muscle forces through the inverse dynamics analysis. This method allows us to determine the muscle force profiles for any type of activity such as rapid deceleration or sidestepping.

6.2 : Future Work

6.2.1 : Mounting the DVRT

Currently the DVRT is mounted on the ACL by using surgical forceps. This is a very difficult task as the DVRT's sliding transducer core slides and rotates while using the forceps. Another issue is that the knee has to be flexed a significant amount to use the forceps and get the hands close enough to install the DVRT. It is recommended that a device be created to help ease the installation of the DVRT. This would decrease the time required to get the DVRT installed in a suitable position on the ACL.

6.2.2 : Muscle attachments

The muscle attachments currently still use aircraft cables to attach the pull/pull cables to the muscle attachment sites on the knee joint. Although the attachments are improved from the previous generation attachments, it is recommended that the aircraft cables be discarded of and that steel brackets are designed to directly attach from the pull/pull cables to the attachment sites. This would ensure that there is no slack in the attachment prior to testing.

6.2.3 : Motion capture for rapid deceleration

The majority of noncontact motions that put the ACL at a high-risk of injury include rapid deceleration, directional change, and jump landing (B. Yu, 2007). Since the dynamic knee simulator is currently capable of performing simulations in the sagittal plane it is recommended that a new motion capture study be performed for rapid deceleration. New data will be stored in C3D format containing analog, position, and important force plate data. With this information a new AnyBody musculoskeletal model can be created.

6.2.4 : Creation of AnyBody model for rapid deceleration

Using the GaitLowerExtremity model a new model can be created by inputting the C3D file from the motion capture of the rapid deceleration task. Additional changes would have to be made to change the model from a gait simulation to the required rapid deceleration model. Changes can be made similarly to the changes made to the model for jump landing as outlined in Chapter 4.

Appendix A

RSA Actuator Specification

RSA/RSM32 Series

ACME SCREW SPECIFICATIONS

RSA32 ACME SCREW CRITICAL SPEED AND PV LIMITS

CRITICAL SPEED WITH 0.75" 1TPI ENGLISH ACME SCREW

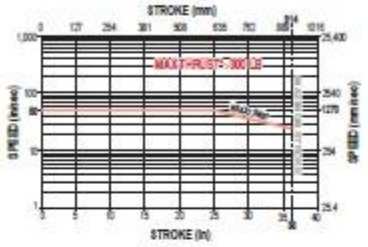

PV LIMITS: 0.75" 1TPI ENGLISH ACME SCREW

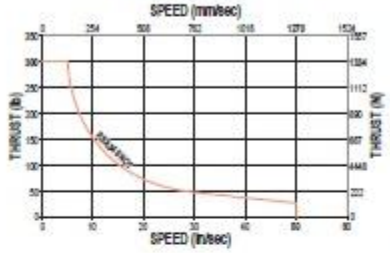

CRITICAL SPEED WITH 0.75" 2TPI ENGLISH ACME SCREW

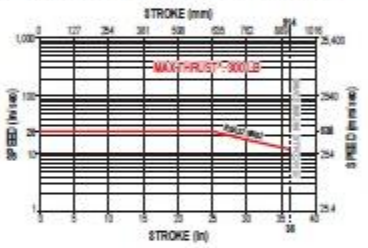

PV LIMITS: 0.75" 2TPI ENGLISH ACME SCREW

CRITICAL SPEED WITH 0.75" 10TPI ENGLISH ACME SCREW

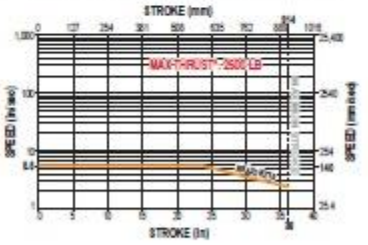

PV LIMITS: 0.75" 10TPI ENGLISH ACME SCREW

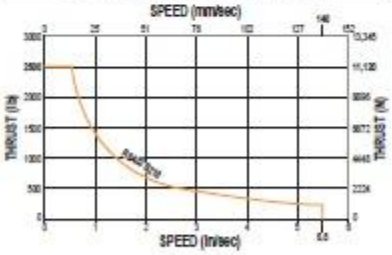

SN – Solid Nut *BZ – Bronze Nut*

** Maximum thrust is the maximum continuous dynamic thrust subject to Thrust x Velocity limitation.*

PV LIMITS: Any material which carries a sliding load is limited by heat buildup. The factors that affect heat generation rate in an application are the pressure on the nut in pounds per square inch and the surface velocity in feet per minute. The product of these factors provides a measure of the severity of an application.

$$\left(\frac{P}{\text{(Max. Thrust Rating)}}\right) \times \left(\frac{V}{\text{(Max. Speed Rating)}}\right) \leq 0.1$$

$$\leq 0.1$$

ROD SCREW

RSA/RSM32 Series

- Acme screw critical speed and PV limits

RSA/RSM32 Series

BALL SCREW SPECIFICATIONS

RSA32 BALL SCREW CRITICAL SPEED AND LIFE CALCULATIONS

CRITICAL SPEED WITH 0.75" 2TPI ENGLISH BALL SCREW

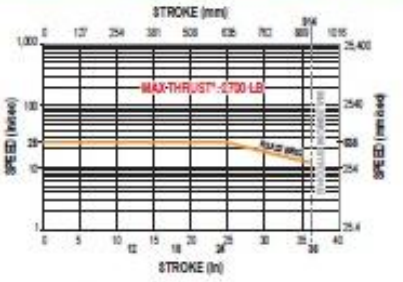

LIFE CALCULATION: 0.75" 2TPI ENGLISH BALL SCREW

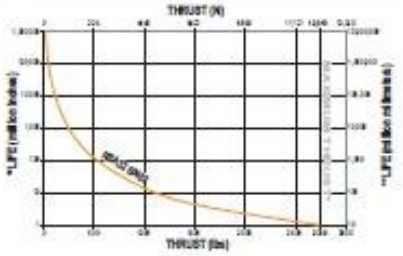

CRITICAL SPEED WITH 0.75" 5TPI ENGLISH BALL SCREW

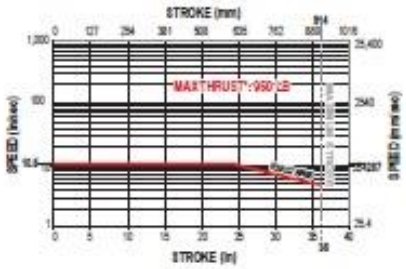

LIFE CALCULATION: 0.75" 5TPI ENGLISH BALL SCREW

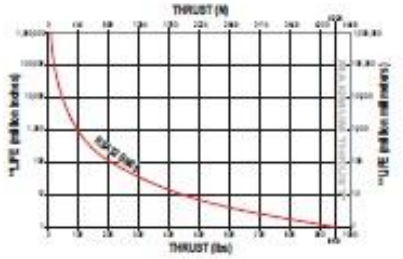

ROD SCREW

RSA/RSM32 Series

- Ball screw critical speed and life calculations

BN – Ball Nut

⚠ ** Maximum thrust reflects 90% reliability for 1 million linear inches of travel.*

***Life indicates theoretical maximum life of screw only, under ideal conditions and does not indicate expected life of actuator.*

Appendix B

Macron Acuator Specification

MACRON Product	PULLEY	BELT	BEAM OPTION	CART WEIGHT/LBS
MACRON PSC-28	28	12H	28X38	.35 (5.6oz)*
MACRON Mini 6-28	28	12S, 12H	28 x n	1.156*
MACRON 6	40	25S	40 x n	3.406*
MACRON 6 Z	40	25S	40 x n	N/A
MACRON 135	40	25S, 25H	40 x 80 Track	1.594*
MACRON 14	40 or 80	25S, 25H, 50S, 50H	40/80 x n	7.811*
MACRON 14 Z	40	25S, 50S	40/80 x n	N/A
MACRON 14 H	40 or 80	25, 50 (S,H)	40/80 x n	12.00*
MACRON Rail	28, 40, 80	12, 25, 50 (S,H)	40/80 x n	App. Specific
MACRON Rail All Stainless	28, 40, 80 28	12, 25, 50 (S,H)	App. Specific	App. Specific
MACRON Single Belt Drive 12	28	12H	28 x n	N/A
MACRON Single Belt Drive 25	40	25S, 25H	40/80 x n	N/A
MACRON Single Belt Drive 50	40	50S, 50H	80 x n	N/A
MACRON Single Belt Drive 50 H	80	50H	80 x n	N/A
MACRON Dual Independent Belt Drive	40	25S, 25H	80 x n	N/A

S = Standard, H = Heavy

n = See MacFRAME Section for Extrusion Options

Note: Cart Type Determines Actuator Style
* Weight shown is for standard cart only.

Contact factory for other cart weights.

SHAFTED PULLEY ASSEMBLY Options
A = Single Shafted Pulley

B = Double Shafted Pulley

EXAMPLE	Product	PULLEY	BELT WIDTH	BEAM OPTION	SHAFT & LOCATIONS
(in bold)	**6**	**40**	**25S**	**40×80**	A1
	14H	**80**	**50H**	**80×88**	A3

Pulley Specifications

Note: All Shafted Pulleys are Machined as one piece from a solid bar of stress proof steel

	Belt Width						Pulley Weight		
'A' Dim	12mm	26mm	60mm	Teeth	Pitch	Travel/Revolution	Shafted	Idler	Double Shafted
28mm	x			21	5mm	105mm (4.134 in)	4.7 oz	4.3 oz	5.4 oz
40mm		x		15	10mm	150mm (5.906 in)	11.3 oz	7.7 oz	17 oz
40mm			x	15	10mm	150mm (5.906 in)	28.4 oz	26.4 oz	31.5 oz
80mm			x	28	10mm	280mm (11.020 in)	105 oz	92.0 oz	119.0 oz

Pulley Diameter = Travel/Revolution divided by 3.1415

All Belts are made of Polyurethane material and steel cords

Belt and Pulley Assembly

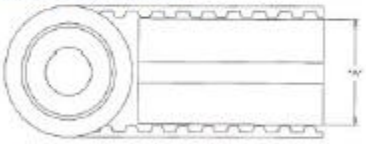

A Dim = 28, 40, 80 mm

Recommended Running Load

Using Safety Factor of 4

		Belt Width		
		12mm	26mm	60mm
Belt Type	S	NA	1945 N 437 Lbs	5118 N 1150 Lbs
	H	1282 N 288 Lbs	4570 N 1027 Lbs	12015 N 2700 Lbs

Belt Weight

	Belt Width		
	12mm	26mm	60mm

BELT TENSIONING TOOL
Belt can be adjusted to a +/- 5 lbs-in range for smooth motion using Macron Belt Tensioning Tool

BUY ORDER ON-LINE

Belt Tensioning Procedures

Belt Tension 'Recommended Max Preload Range'
Belt can be adjusted to a +/- 5 lbs-in range

		Belt Width		
		12mm	26mm	60mm
Belt Type	S	NA	890 N 200 Lbs	1335 N 300 Lbs
	H	445 N 100 Lbs	1335 N 300 Lbs	1780 N 400 Lbs

Ultimate Tensile Strength For Belts

	Belt Width		
	12mm	26mm	60mm

Belt Type					
	S	NA	.076 Lb/Ft .114 Kg/M	.160 Lb/Ft .235 Kg/M	
	H	.029 Lb/Ft .043 Kg/M	.121 Lb/Ft .181 Kg/M	.226 Lb/Ft .336 Kg/M	

Belt Type					
	S	NA	7787 N 1750 Lbs	20470 N 4600 Lbs	
	H	5117.5 N 1150 Lbs	18280 N 4108 Lbs	48040 N 10800 Lbs	

S=Standard, H=Heavy, N=Newtons

Belt And Pulley Assembly Dimensional Drawing

28-12 Pulley Assembly – (Single and Double Shafted)
28-12C Pulley Assembly – (Single and Double Shafted)
28-12H Pulley Assembly – (Single and Double Shafted)
40-25 Pulley Assembly – (Single and Double Shafted)
40-50 Pulley Assembly – (Single and Double Shafted)
80-50 Pulley Assembly – (Single and Double Shafted)
80-50M Pulley Assembly – (Single and Double Shafted)

Comments (0) View Related Posts In: Product Specifications

Appendix C

Danaher Motor Specification(AKM73P and AKM42J)

KOLLMORGEN

Performance Data - AKM4x Frame

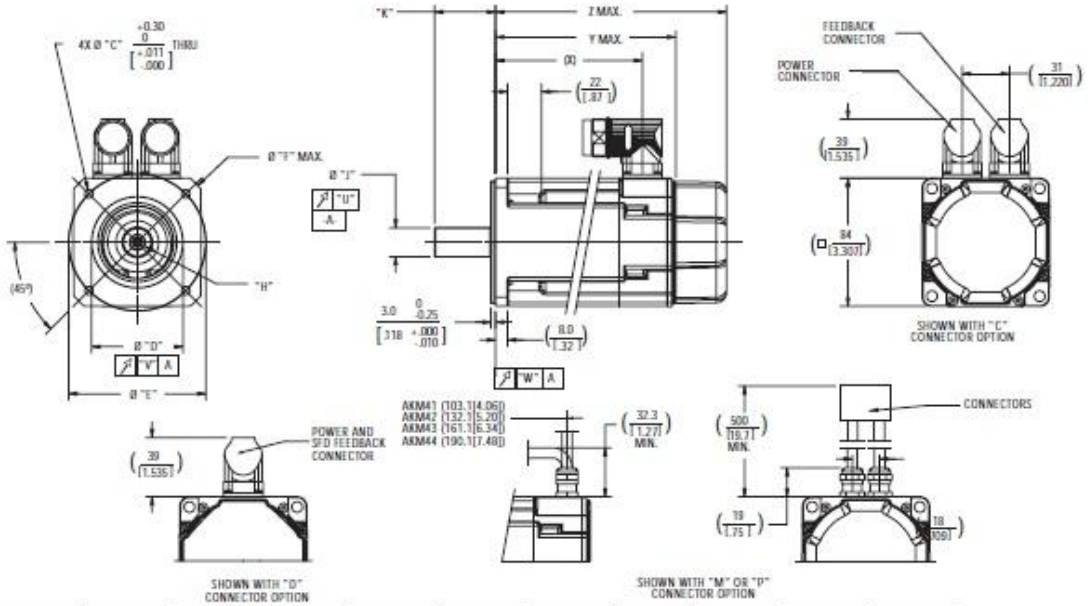

MOUNTING CODE	"C"	"D"	"E"	"F"	"H"	"J"	"K"	"L"	"M"	"N"
AC	7 [.276]	60 +0.012 +0.004 [2.362 +.0004 +.0001] JS	100 [3.937]	–	D M6 DIN 332	19 +0.015 +0.002 [.748 +.0006 +.0001] N6	40.0 [1.57]	–	–	–
AN	7 [.276]	60 +0.012 +0.004 [2.362 +.0004 +.0001] JS	100 [3.937]	–	D M6 DIN 332	19 +0.015 +0.002 [.748 +.0006 +.0001] N6	40.0 [1.57]	–	–	–
BK	5.54 [.218]	73.025 +0.025 +0.000 [2.8750 +.0010 +.0000]	98.43 [3.875]	–	–	15.875 +0.013 +0.002 [.6250 +.0005 +.0001]	52.40 ± 0.78 [2.063 ± .031]	17.02 +0.43 +0.00 [.670 +.017 +.000]	4.762 +0.025 +0.000 [.1875 +.0010 +.0000]	34.93 ± 0.25 [1.375 ± .010]
CC	5.54 [.218]	60 +0.012 +0.004 [2.3622 +.0004 +.0001] JS	90 [3.543]	109 [4.291]	D M6 DIN 332	19 +0.015 +0.002 [.748 +.0006 +.0001] N6	40.0 [1.57]	–	–	–
CN	5.54 [.218]	60 +0.012 +0.004 [2.3622 +.0004 +.0001] JS	90 [3.543]	109 [4.291]	D M6 DIN 332	19 +0.015 +0.002 [.748 +.0006 +.0001] N6	40.0 [1.57]	–	–	–
EK	5.54 [.218]	73.025 +0.025 +0.000 [2.8750 +.0010 +.0000]	98.43 [3.875]	–	–	12.700 +0.013 +0.002 [.5000 +.0005 +.0001]	31.75 ± 0.25 [1.250 ± .010]	14.09 +0.43 +0.00 [.555 +.017 +.000]	3.175 +0.050 +0.000 [.1250 +.0020 +.0000]	19.05 ± 0.25 [.750 ± .010]

MOUNTING CODE	"P"	"R"	"S"	"T"	"U"	"V"	"W"
AC	21.5 +0.13 +0.08 [.846 +.005 +.003]	0 +0.025 +0.001 [.000 +.001 +.000] No	4.00 [1.57]	32 +0.38 +0.00 [1.260 +.015 +.000]	0.040 [.0015]	0.080 [.0031]	0.080 [.0031]
AN	–	–	–	–	0.040 [.0015]	0.080 [.0031]	0.080 [.0031]
BK	–	–	–	–	0.051 [.0020]	0.10 [.004]	0.10 [.004]
CC	21.5 +0.13 +0.08 [.846 +.005 +.003]	0 +0.025 +0.001 [.000 +.001 +.000] No	4.00 [1.57]	32 +0.38 +0.00 [1.260 +.015 +.000]	0.040 [.0015]	0.080 [.0031]	0.080 [.0031]
CN	–	–	–	–	0.040 [.0015]	0.080 [.0031]	0.080 [.0031]
EK	–	–	–	–	0.051 [.0020]	0.10 [.004]	0.10 [.004]

(X)	Y MAX.	Z MAX. (W/ BRAKE)	MODEL
96.4 [3.80]	116.8 [4.60]	152.3 [6.00]	AKM41
125.4 [4.94]	147.8 [5.82]	181.3 [7.14]	AKM42
154.4 [6.08]	176.8 [6.96]	210.3 [8.28]	AKM43
183.4 [7.22]	205.8 [8.10]	239.3 [9.42]	AKM44

Dimensions are in mm [inches].
Product designed in metric.
English conversions provided for reference only.

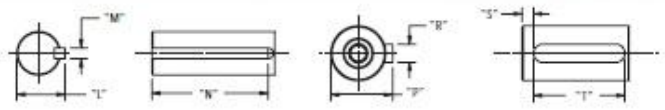

Performance Data - AKM4x Frame

AKM4x - Up to 640 VDC

See system data beginning on page 8 for typical torque/speed performance.

	PARAMETER	Tol	SYMBOL	UNITS	AKM41 C	AKM41 E	AKM41 H	AKM42 C	AKM42 E	AKM42 G	AKM42 J	AKM43 E	AKM43 G	AKM43 K	AKM44 E	AKM44 G	AKM44 J
	Max Rated DC Bus Voltage	Max	V_{bus}	Vdc	640	640	320	640	640	640	320	640	640	320	640	640	640
	Continuous Torque (Stall) for ΔT winding = 100°C ①②③④⑤	Nom	T_{cs}	N-m	1.95	2.02	2.06	3.35	3.42	3.53	3.58	4.70	4.80	4.90	5.70	5.88	6.00
				lb-in	17.3	17.9	18.2	29.6	30.3	31.2	31.5	41.6	42.5	43.4	51.0	52.0	53.1
	Continuous Current (Stall) for ΔT winding = 100°C ①②③④⑤	Nom	I_{cs}	A_{rms}	1.46	2.85	5.60	1.40	2.74	4.80	8.40	2.76	4.87	9.60	2.9	5.0	8.8
	Continuous Torque (Stall) for ΔT winding = 60°C ②	Nom	T_{cs}	N-m	1.56	1.62	1.65	2.68	2.74	2.82	2.86	3.76	3.84	3.92	4.61	4.70	4.80
				lb-in	13.8	14.3	14.6	23.7	24.2	25.0	25.2	33.3	34.0	34.7	40.8	41.6	42.5
	Max Mechanical Speed ⑤	Nom	N_{max}	rpm	6000	6000	6000	6000	6000	6000	6000	6000	6000	6000	6000	6000	6000
	Peak Torque ①②	Nom	T_p	N-m	6.12	6.28	6.36	11.1	11.3	11.5	11.6	15.9	16.1	16.3	19.9	20.2	20.4
				lb-in	54.2	55.6	56.3	98.8	99.7	102	103	141	142	144	176	179	181
	Peak Current	Nom	I_p	A_{rms}	5.8	11.4	22.4	5.61	11.0	19.2	33.7	11.0	19.5	38.3	11.4	20.0	35.2
75VDC	Rated Torque (speed) ①②③④⑤⑥		T_{rtd}	N-m	-	-	1.99	-	-	-	-	-	-	-	-	-	-
				lb-in	-	-	17.6	-	-	-	-	-	-	-	-	-	-
	Rated Speed		N_{rtd}	rpm	-	-	1000	-	-	-	-	-	-	-	-	-	-
	Rated Power (speed) ①②③④⑤⑥		P_{rtd}	kW	-	-	0.21	-	-	-	-	-	-	-	-	-	-
				Hp	-	-	0.28	-	-	-	-	-	-	-	-	-	-
160VDC	Rated Torque (speed) ①②③④⑤⑥		T_{rtd}	N-m	-	1.94	1.86	-	-	-	3.03	-	-	4.08	-	-	-
				lb-in	-	17.2	16.5	-	-	-	26.8	-	-	36.1	-	-	-
	Rated Speed		N_{rtd}	rpm	-	1200	3000	-	-	-	3000	-	-	2500	-	-	-
	Rated Power (speed) ①②③④⑤⑥		P_{rtd}	kW	-	0.24	0.58	-	-	-	0.95	-	-	1.07	-	-	-
				Hp	-	0.33	0.78	-	-	-	1.28	-	-	1.43	-	-	-
320VDC	Rated Torque (speed) ①②③④⑤⑥		T_{rtd}	N-m	1.88	1.82	1.62	-	3.12	2.90	2.38	4.24	4.00	2.62	5.22	4.90	3.84
				lb-in	16.6	16.1	14.3	-	27.6	25.7	21.1	37.5	35.4	23.2	46.2	43.4	34.0
	Rated Speed		N_{rtd}	rpm	1200	3000	6000	-	1800	3500	6000	1500	2500	6000	1200	2000	4000
	Rated Power (speed) ①②③④⑤⑥		P_{rtd}	kW	0.24	0.57	1.02	-	0.59	1.06	1.50	0.67	1.05	1.65	0.66	1.03	1.61
				Hp	0.32	0.77	1.36	-	0.79	1.42	2.00	0.89	1.40	2.21	0.88	1.38	2.16
560VDC	Rated Torque (speed) ①②③④⑤⑥		T_{rtd}	N-m	1.77	1.58	-	3.10	2.81	2.35	-	3.92	3.01	-	4.80	3.76	2.75
				lb-in	15.7	14.0	-	27.4	24.9	20.8	-	34.7	26.6	-	42.5	33.3	24.3
	Rated Speed		N_{rtd}	rpm	3000	6000	-	1500	3500	6000	-	2500	5000	-	2000	4000	6000
	Rated Power (speed) ①②③④⑤⑥		P_{rtd}	kW	0.56	0.99	-	0.49	1.03	1.48	-	1.03	1.58	-	1.01	1.57	1.73
				Hp	0.75	1.33	-	0.65	1.38	1.98	-	1.38	2.11	-	1.35	2.11	2.32
640VDC	Rated Torque (speed) ①②③④⑤⑥		T_{rtd}	N-m	1.74	1.58	-	3.02	2.72	2.35	-	3.76	2.57	-	4.56	3.19	2.75
				lb-in	15.4	14.0	-	26.7	24.1	20.8	-	33.3	22.7	-	40.4	28.2	24.3
	Rated Speed		N_{rtd}	rpm	3500	6000	-	2000	4000	6000	-	3000	6000	-	2500	5000	6000
	Rated Power (speed) ①②③④⑤⑥		P_{rtd}	kW	0.64	0.99	-	0.63	1.14	1.48	-	1.18	1.61	-	1.19	1.67	1.73
				Hp	0.85	1.33	-	0.85	1.53	1.98	-	1.58	2.16	-	1.60	2.24	2.32
	Torque Constant ①	±10%	K_t	N-m/A_{rms}	1.34	0.71	0.37	2.40	1.26	0.74	0.43	1.72	0.99	0.52	2.04	1.19	0.69
				lb-in/A_{rms}	11.9	6.3	3.3	21.2	11.2	6.5	3.8	15.2	8.8	4.6	18.1	10.5	6.1
	Back EMF constant ④	±10%	K_e	V/K_{rpm}	86.3	45.6	23.7	154	80.9	47.5	27.5	111	63.9	33.2	132	76.6	44.2
	Resistance (line-line) ④	±10%	R_m	Ω	21.7	5.7	1.51	27.52	7.22	2.38	0.80	8.04	2.61	0.70	8.08	2.65	0.88
	Inductance (line-line)		L	mH	66.1	18.4	5.0	97.4	26.8	9.2	3.1	32.6	10.8	2.9	33.9	11.5	3.8
	Inertia		J_m	kg-cm²	0.81			1.5				2.1			2.7		
	(includes Resolver feedback) ⑤			lb-in-s²	7.2E-04			1.3E-03				1.8E-03			2.4E-03		
	Optional Brake Inertia		J_m	kg-cm²	0.068			0.068				0.068			0.068		
	(additional)			lb-in-s²	6.0E-05			6.0E-05				6.0E-05			6.0E-05		
	Weight		W	kg	2.44			3.39				4.35			5.3		
				lb	5.4			7.5				9.6			11.7		
	Static Friction ①⑥		T_f	N-m	0.014			0.026				0.038			0.05		
				lb-in	0.12			0.23				0.34			0.44		
	Viscous Damping ①		K_{dv}	N-m/K_{rpm}	0.009			0.013				0.017			0.021		
				lb-in/K_{rpm}	0.08			0.12				0.15			0.19		
	Thermal Time Constant		TCT	minutes	13			17				20			24		
	Thermal Resistance		R_{thw-a}	°C/W	1.04			0.89				0.78			.71		
	Pole Pairs				5			5				5			5		
	Heatsink Size				10"x10"x¼" Aluminum Plate			10"x10"x¼" Aluminum Plate				10"x10"x¼" Aluminum Plate			10"x10"x¼" Aluminum Plate		

Notes:
1. Motor winding temperature rise, ΔT=100°C, at 40°C ambient.
2. All data referenced to sinusoidal commutation.
3. Add parking brake if applicable for total inertia.
4. Motor with standard heatsink.
5. May be limited at some values of Vbus.
6. Measured at 25°C.
7. Brake motor option reduces continuous torque ratings by 0.12 N-m.
8. Non-Resolver feedback options reduces continuous ratings by:
   AKM41 – 0.1 N-m AKM42 – 0.1 N-m
   AKM43 – 0.2 N-m AKM44 – 0.3 N-m
9. Motors with non-Resolver feedback and Brake option, reduce continuous torque by::
   AKM41 – 0.22 N-m AKM42 – 0.36 N-m
   AKM43 – 0.55 N-m AKM44 – 0.76 N-m
10. For motors with optional shaft seal, reduce torque shown by 0.071 N-m (0.63lb-in), and increase T_f by the same amount.

Performance Data - AKM7x Frame

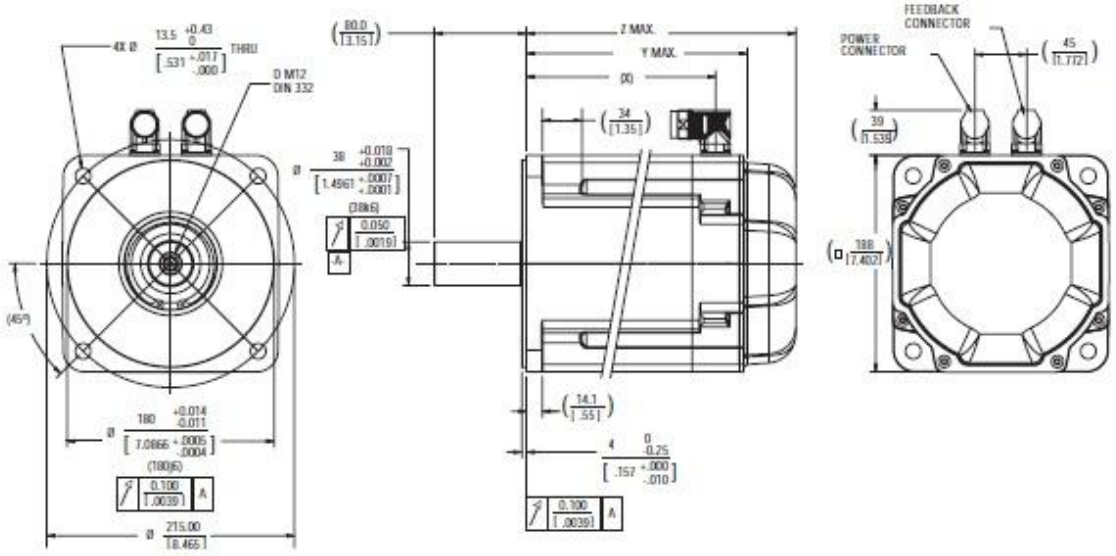

MOUNTING CODE	"T"	"U"	"V"	"W"
AC	10 [.3937]	41 [1.614]	5.00 [.197]	70 [2.756]
AN	-	-	-	-

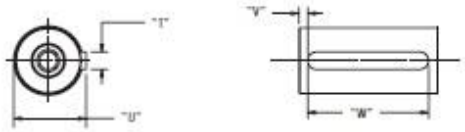

Z MAX.	Z MAX.	QQ	Y MAX.	Z MAX.	MODEL
201.7 [7.94]	253.3 [9.97]	164.5 [6.48]	197.5 [7.58]	234.5 [9.23]	AKM72
235.7 [9.38]	287.3 [11.31]	198.5 [7.81]	226.5 [8.92]	268.5 [10.57]	AKM73
269.7 [10.62]	321.3 [12.65]	232.5 [9.15]	260.5 [10.26]	302.5 [11.91]	AKM74

Dimensions are in mm [inches].
Product designed in metric.
English conversions provided for reference only.

AKM7x - Up to 640 VDC

See system data beginning on page 8 for typical torque/speed performance.

	PARAMETER	Tol	SYMBOL	UNITS	AKM72 K	AKM72 M	AKM72 P	AKM73 M	AKM73 P	AKM74 L	AKM74 P
	Max Rated DC Bus Voltage	Max	V_{bus}	Vdc	640	640	640	640	640	640	640
	Continuous Torque (Stall) for ΔT winding = 100°C ①②④⑤⑥	Nom	T_{cs}	N-m	29.7	30.0	29.4	42.0	41.6	53.0	52.5
				lb-in	263	266	260	372	368	469	465
	Continuous Current (Stall) for ΔT winding = 100°C ①②④⑤⑥	Nom	I_{cs}	A_{rms}	9.3	13.0	18.7	13.6	19.5	12.9	18.5
	Continuous Torque (Stall) for ΔT winding = 60°C ②	Nom	T_{cs}	N-m	23.8	24.0	23.5	33.6	33.3	42.4	42.0
				lb-in	211	212	208	297	295	375	372
	Max Mechanical Speed ⑨	Nom	N_{max}	rpm	6000	6000	6000	6000	6000	6000	6000
	Peak Torque ①②	Nom	T_p	Nm	79.2	79.7	78.5	113	111	143	142
				lb-in	701	705	695	997	985	1269	1253
	Peak Current	Nom	I_p	A_{rms}	27.8	38.9	56.1	40.8	58.6	38.7	55.5
75VDC	Rated Torque (speed) ①②④⑤⑥ ⑩		T_{rtd}	N-m	-	-	-	-	-	-	-
				lb-in	-	-	-	-	-	-	-
75VDC	Rated Speed		N_{rtd}	rpm	-	-	-	-	-	-	-
75VDC	Rated Power (speed) ①②④⑤⑥		P_{rtd}	kW	-	-	-	-	-	-	-
				Hp	-	-	-	-	-	-	-
160VDC	Rated Torque (speed) ①②④⑤⑥ ⑩		T_{rtd}	N-m	-	-	-	-	-	-	-
				lb-in	-	-	-	-	-	-	-
160VDC	Rated Speed		N_{rtd}	rpm	-	-	-	-	-	-	-
160VDC	Rated Power (speed) ①②④⑤⑥		P_{rtd}	kW	-	-	-	-	-	-	-
				Hp	-	-	-	-	-	-	-
320VDC	Rated Torque (speed) ①②④⑤⑥ ⑩		T_{rtd}	N-m	-	-	23.8	-	34.7	-	-
				lb-in	-	-	211	-	307	-	-
320VDC	Rated Speed		N_{rtd}	rpm	-	-	1800	-	1300	-	-
320VDC	Rated Power (speed) ①②④⑤⑥		P_{rtd}	kW	-	-	4.49	-	4.72	-	-
				Hp	-	-	6.01	-	6.33	-	-
560VDC	Rated Torque (speed) ①②④⑤⑥ ⑩		T_{rtd}	N-m	25.1	23.6	20.1	33.8	28.5	43.5	39.6
				lb-in	222	209	178	299	252	385	350
560VDC	Rated Speed		N_{rtd}	rpm	1500	2000	3000	1600	2400	1200	1800
560VDC	Rated Power (speed) ①②④⑤⑥		P_{rtd}	kW	3.94	4.94	6.31	5.31	7.16	5.47	7.46
				Hp	5.29	6.63	8.46	7.12	9.60	7.33	10.01
640VDC	Rated Torque (speed) ①②④⑤⑥ ⑩		T_{rtd}	N-m	24.0	22.1	18.2	32.1	26.3	41.5	35.9
				lb-in	212	196	161	284	233	367	318
640VDC	Rated Speed		N_{rtd}	rpm	1800	2500	3500	1800	2800	1400	2000
640VDC	Rated Power (speed) ①②④⑤⑥		P_{rtd}	kW	4.52	5.79	6.67	6.05	7.71	6.08	7.52
				Hp	6.06	7.76	8.94	8.11	10.34	8.16	10.08
	Torque Constant ①	±10%	K_t	N-m/A_{rms}	3.23	2.33	1.58	3.10	2.13	4.14	2.84
				lb-in/A_{rms}	28.6	20.6	14.0	27.4	18.9	36.6	25.1
	Back EMF constant ④	±10%	K_e	V_{krpm}	208	150	102	200	137	266	183
	Resistance (line-line) ④	±10%	R_m	Ω	1.22	0.64	0.33	0.68	0.35	0.85	0.43
	Inductance (line-line)		L	mH	20.7	10.8	5.0	12.4	5.9	16.4	7.7
	Inertia (includes Resolver feedback) ③		J_m	kg-cm²	65			92		120	
				lb-in-s²	0.057			0.082		0.11	
	Optional Brake Inertia (additional)		J_m	kg-cm²	1.64			1.64		1.64	
				lb-in-s²	1.46×10^{-3}			1.46×10^{-3}		1.46×10^{-3}	
	Weight		W	kg	19.7			26.7		33.6	
				lb	43.4			58.8		74.0	
	Static Friction ①⑩		T_f	N-m	0.16			0.24		0.33	
				lb-in	1.4			2.1		2.9	
	Viscous Damping ①		K_{dv}	N-m/krpm	0.06			0.13		0.2	
				lb-in/krpm	0.5			1.2		1.8	
	Thermal Time Constant		TCT	minutes	46			53		60	
	Thermal Resistance		R_{thw-a}	°C/W	0.43			0.37		0.33	
	Pole Pairs				5			5		5	
	Heat Sink Size				10"x10"x½" Aluminum Plate			10"x10"x½" Alum. Plate		10"x10"x½" Alum. Plate	

Notes:
1. Motor winding temperature rise, ΔT = 100°C, at 40°C ambient.
2. All data referenced to sinusoidal commutation.
3. Add parking brake if applicable for total inertia.
4. Motor with standard heatsink.
5. May be limited at some values of Vbus.
6. Measured at 25°C.
7. Brake motor option reduces continuous torque ratings by 1 N-m.
8. Non-Resolver feedback options reduce continuous torque ratings by:
   AKM72 = 2.0 N-m AKM73 = 2.7 N-m
   AKM74 = 3.4 N-m
9. Motors with non-Resolver feedback and Brake option, reduce continuous torque by:
   AKM72 = 3.9 N-mAKM73 = 5.1 N-m
   AKM74 = 6.2 N-m
10. For motors with optional shaft seal, reduce torque shown by 0.25 N-m (2.21 lb-in), and increase T_f by the same amount.

Appendix D

Muscle Origin and Insertion

		Origin				Insertion			
Muscle	**Group**	x(cm)	y(cm)	z(cm)		X(cm)	y(cm)	z(cm)	
RFEM	QUAD	-2.4	-4	-1.7	A	0	0	0	C
VASLAT	QUAD	-0.3	-3	-2.2	B	0	0	0	C
VASINT	QUAD	1.7	-14.7	-4	B	0	0	0	C
VASMED	QUAD	-0.3	-9	-4.4	B	0	0	0	C
BIFEMS	HAMS	-0.4	-18.6	-4.1	B	-3.9	1.2	3.1	C
BIFEML	HAMS	-12.1	-9.8	-4.8	A	-3.9	1.2	3.1	C
SEMTEN	HAMS	-12.2	-10	-4.9	A	-2.3	-0.5	-1.9	C
SEMMEM	HAMS	-11	-9.9	-4.4	A	-4.6	1.4	-1.5	C
MEDGAS	CALF	-2	-38	-7.9	B	0.5	0	0.2	D
LATGAS	CALF	-2.6	-39.3	-4.9	B	0.5	0	0.2	D
SOLEUS	CALF	-4.2	-3.2	0.1	C	1	0	0.2	D

Global Reference Frame

	x	y	z
A	3.76	8.78	4.15
B	-5.98	-3.66	5.12
C	1.26	-45.65	5.21
D	10.51	-83.41	6.16

Global Origin			Global Insertion			Length				Angle of Line of Action		
x(cm)	y(cm)	z(cm)	x(cm)	y(cm)	z(cm)	X(cm)	Y(cm)	Z(cm)	Length	cosX	cosY	cosZ
1.36	4.78	2.45	1.26	-45.65	5.21	0.1	50.43	2.76	50.50557	0.00198	0.998504	0.054647
-6.28	-6.66	2.92	1.26	-45.65	5.21	7.54	38.99	2.29	39.77833	0.18955	0.980182	0.057569
-4.28	-18.36	1.12	1.26	-45.65	5.21	5.54	27.29	4.09	28.1454	0.196835	0.969608	0.145317
-6.28	-12.66	0.72	1.26	-45.65	5.21	7.54	32.99	4.49	34.13725	0.220873	0.966393	0.131528
-6.38	-22.26	1.02	-2.64	-44.45	8.31	3.74	22.19	7.29	23.65434	0.158111	0.938094	0.308189
-8.34	-1.02	-0.65	-2.64	-44.45	8.31	5.7	43.43	8.96	44.70947	0.12749	0.971383	0.200405
-8.44	-1.22	-0.75	-1.04	-46.15	3.31	7.4	44.93	4.06	45.71595	0.161869	0.982808	0.088809
-7.24	-1.12	-0.25	-3.34	-44.25	3.71	3.9	43.13	3.96	43.48665	0.089683	0.991799	0.091062
-7.98	-41.66	-2.78	11.01	-83.41	6.36	18.99	41.75	9.14	46.76775	0.406049	0.892709	0.195434
-8.58	-42.96	0.22	11.01	-83.41	6.36	19.59	40.45	6.14	45.36155	0.431864	0.891724	0.135357
-2.94	-48.85	5.31	11.51	-83.41	6.36	14.45	34.56	1.05	37.47397	0.385601	0.92224	0.028019

Appendix E

Galil Program Array

Time	Hip	Ham	Quad	Calf	Hip [vel]	Ankle [vel]
2.23	-140.12	-11.12	-25.84	-47.40	0	0
2.24	-161.66	-16.34	-30.73	-68.77	10894.09	7267.0525
2.25	-202.67	-21.04	-37.28	-84.00	-16341.1	3850.41909
2.26	-287.14	-26.58	-75.36	-88.61	10894.09	-3687.496782
2.27	-364.56	-31.61	-129.18	-96.92	10894.09	113.2309706
2.28	-434.63	-36.50	-161.48	-111.69	2723.523	17395.84913
2.29	-546.46	-44.90	-213.62	-132.23	8170.569	31471.64856
2.3	-651.63	-47.12	-262.51	-146.77	8170.569	34064.99386
2.31	-706.27	-46.98	-287.43	-150.00	40852.85	25848.97471
2.32	-743.09	-42.74	-304.04	-141.00	21788.18	12117.1808
2.33	-728.41	-35.63	-290.66	-119.54	10894.09	-1365.880886
2.34	-682.90	-29.81	-264.82	-99.23	19064.66	-10748.52131
2.35	-614.51	-23.54	-229.76	-75.69	73535.12	-14738.37165
2.36	-487.29	-12.74	-174.15	-44.92	16341.14	-14118.61283
2.37	-365.38	-8.51	-125.03	-20.86	27235.23	-10791.34934
2.38	-300.37	-4.77	-101.50	-8.12	32682.28	-6834.992728
2.39	-243.04	0.00	-86.06	0.00	46299.89	-3841.768326
2.4	-199.88	0.00	-89.95	0.00	16341.14	-2613.719351
2.41	-192.05	0.00	-96.05	0.00	5447.046	-3170.845856
2.42	-195.44	0.00	-110.39	0.00	13617.62	-4963.682773
2.43	-199.69	0.00	-117.12	0.00	8170.569	-7171.063255
2.44	-204.27	0.00	-123.13	0.00	5447.046	-8984.071316
2.45	-210.27	0.00	-132.63	0.00	0	-9812.457232
2.46	-213.37	0.00	-136.08	0.00	-5447.05	-9387.081389
2.47	-216.16	0.00	-138.86	0.00	0	-7762.868102
2.48	-222.83	0.00	-142.53	0.00	-10894.1	-5247.189227
2.49	-228.02	0.00	-143.24	0.00	-10894.1	-2287.831291
2.5	-233.62	0.00	-144.14	0.00	-8170.57	645.6357767
2.51	-244.14	0.00	-144.54	0.00	-10894.1	3160.371099
2.52	-249.09	0.00	-143.33	0.00	-24511.7	5002.519582
2.53	-252.53	0.00	-142.93	0.00	-13617.6	6078.261335
2.54	-254.83	0.00	-141.44	0.00	-10894.1	6438.163772
2.55	-255.46	0.00	-136.82	0.00	-21788.2	6235.832707
2.56	-253.88	0.00	-133.87	0.00	-10894.1	5674.670271

2.57	-252.08	0.00	-131.85	0.00	-8170.57	4956.186409
2.58	-247.36	0.00	-127.98	0.00	-10894.1	4240.259501
2.59	-245.58	0.00	-126.35	0.00	-19064.7	3623.307113
2.6	-245.03	0.00	-124.75	0.00	-10894.1	3135.532796
2.61	-247.18	0.00	-122.24	0.00	-8170.57	2753.99541
2.62	-250.23	0.00	-121.26	0.00	-10894.1	2425.775343
2.63	-253.78	0.00	-121.21	0.00	-21788.2	2093.580259
2.64	-263.51	-0.01	-120.01	0.00	-8170.57	1717.449144
2.65	-269.76	-2.27	-123.64	-3.79	-10894.1	1287.586857
2.66	-276.65	-3.51	-128.26	-9.14	-10894.1	825.4843964
2.67	-289.17	-5.83	-137.02	-19.20	-16341.1	375.3790269
2.68	-303.82	-7.03	-141.18	-24.37	-8170.57	-12.27530751
2.69	-314.01	-8.39	-145.33	-29.59	-8170.57	-299.4460473
2.7	-330.39	-10.85	-153.17	-39.42	-10894.1	-475.157786
2.71	-345.89	-11.95	-156.40	-43.71	-13617.6	-564.23595
2.72	-355.22	-12.88	-159.17	-47.54	-2723.52	-624.4478041
2.73	-363.55	-13.61	-161.02	-50.31	-2723.52	-735.659311
2.74	-374.33	-14.68	-163.32	-54.46	-5447.05	-974.138882
2.75	-376.22	-14.86	-162.86	-55.39	-2723.52	-1397.164663
2.76	-376.69	-14.95	-161.94	-55.85	0	-2015.354249
2.77	-372.76	-14.49	-157.79	-54.46	0	-2787.016479
2.78	-368.33	-14.12	-155.02	-53.08	2723.523	-3611.626513
2.79	-362.45	-13.66	-151.79	-51.23	2723.523	-4356.401029
2.8	-351.68	-12.46	-144.41	-46.15	0	-4871.472539
2.81	-339.27	-11.77	-139.79	-43.57	5447.046	-5039.624342
2.82	-330.09	-11.12	-136.10	-40.89	0	-4791.250893
2.83	-317.49	-9.78	-128.72	-35.91	2723.523	-4141.933263
2.84	-305.15	-9.29	-126.41	-33.74	2723.523	-3195.282428
2.85	-298.80	-8.81	-123.18	-31.89	0	-2119.101356
2.86	-289.27	-8.10	-119.95	-28.99	2723.523	-1102.19747
2.87	-285.32	-7.84	-119.49	-27.92	0	-323.5232825
2.88	-282.95	-7.64	-118.57	-27.19	0	133.181003
2.89	-281.37	-7.52	-118.57	-26.68	2723.523	256.182266
2.9	-280.55	-7.49	-119.49	-26.49	0	177.3555517
2.91	-281.31	-7.58	-120.42	-26.72	0	71.78137507
2.92	-282.84	-7.72	-121.34	-27.09	0	111.8170535
2.93	-286.67	-8.10	-123.64	-28.15	-2723.52	352.8913257
2.94	-288.98	-8.28	-124.57	-28.75	0	665.468277
2.95	-291.28	-8.43	-125.49	-29.35	0	888.8759799

2.96	-293.58	-8.69	-126.87	-30.32	0	567.6910465
2.97	-295.13	-8.79	-127.34	-30.79	0	-289.8893675
2.98	-295.91	-8.89	-127.80	-31.20	2723.523	-1712.9515
2.99	-297.49	-9.06	-128.72	-31.89	0	-2733.29765
3	-298.30	-9.12	-128.72	-32.12	0	-2500.979674
3.01	-299.10	-9.14	-128.72	-32.26	-2723.52	-659.244356
3.02	-299.95	-9.20	-129.18	-32.31	0	1634.685045
3.03	-299.98	-9.20	-128.72	-32.22	0	1592.641482
3.04	-300.00	-9.14	-128.26	-32.03	2723.523	-3301.035809
3.05	-299.26	-9.07	-128.26	-31.66	0	1474.055263
3.06	-298.51	-9.01	-127.80	-31.43	0	211.5589931

Bibliography

AMTI. (2011). *OR6-6 brochure.pdf.* Retrieved from AMTI Force and Motion: http://www.forceandmotion.com/select%20product%20PDFs/Biomechanics%20force%20platforms/OR6-6%20brochure.pdf

AnyBody Technology. (2011). *AnyBody Technology: AnyBody Modeling System*. Retrieved from AnyBody Technology: http://www.anybodytech.com/index.php?id=26

B. Yu, W. G. (2007). Mechanisms of non-contact ACL injuries. *British Medical Journal* , 47-51.

Bohdanna T. Zazulak, T. E. (2007). Deficits in Neuromuscular Control of the Trunk Predict Knee Injury Risk. *American Journal of Sports Medicine* , 1123-1130.

Cassidy, K. (2009). *Design and Validation of Dynamic Knee Injury Simulator.* Waterloo: University of Waterloo.

Cerulli G, B. D. (2003). In vivo anterior cruciate ligament strain behaviour during rapid deceleration movement : case report. *Knee Surg Sports Traumatol Arthrosc.* , 11(5): 307-11.

Chappell JD, Y. B. (2000). A comparison of knee kinetics between male and female recreational athletes in stop-jump tasks. *American Journal of Sports Medicine* , 28:234-40.

David Noonan, P. M.-Z. (2009). A Stereoscopic Firbroscope for Camera Motion and 3D Depth Recovery During Minimally Invasive Surgery. *2009 IEEE International Conference on Robotics and Automation,* (pp. 4463-4468). Kobe.

DeMorat G, W. P. (2004). Agressive quadriceps loading can induce noncontact anterior cruciate ligament injury. *American Journal of Sports Medicine* , 32(2): 477-83.

Domire ZJ, B. R. (2011). An exsamination of possible quadriceps force at the time of anterior cruciate ligament injury during landing: A simulation study. *Journal of Biomechanics* , 17:44(8):1630-2.

Elias JJ, F. A. (2003). The soleus muscle acts as an agonist for the anterior cruciate ligament. An in vitro experimental study. *American Journal of Sports Medicine* , 31(2):241-6.

Fleming BC, B. B. (1999). Strain behavior of the anterior cruciate ligament during stair climbing: an in vivo study. *Arthroscopy* , 15(2): 185-91.

Gerwyn Hughes, J. W. (2006). A Risk Factor Model for Anterior Cruciate Ligament injury. *Sports Med* , 411-428.

Hashemi J, B. R.-O. (2010). Increasing pre-activation of the quadriceps muscle protects the anterior cruciate ligament during the landing phase of a jump: An in vitro simulation. *The knee* , 235-241.

Hashemi J, C. N. (2007). An Alternative Mechanism of Non-contact Anterior Cruciate Ligament Injury During Jump-landing. *Experimental Mechanics* , 47: 347-354.

Kernozek TW, R. R. (2008). Estimation of anterior cruciate ligament tension from inverse dynamics data and electromyography in females during drop landing. *Clinical Biomechanics* , 23, 1279-1286.

Laughlin WA, W. J. (2011). The effects of single-leg landing technique on ACL loading. *Journal of Biomechanics* .

Maletsky LP, H. B. (2005). Simulating dynamic activities using a five-axis knee simulator. *Journal of Biomechanics* , 127(1):123-33.

Markolf KL, O. G. (2004). Effects of applied quadriceps and hamstrings musle loads on forces in the anterior and posterior cruciate ligaments. . *American Journal of Sports Medicine* , 32(5):1144-9.

McKinley, M. (2008). *Human Anatomy Second Edition.* McGraw Hill.

McLean CA, A. A. (1993). Design and development of an unconstrained dynamic knee simulator. *Journal of Biomechanics* , 115(2):144-8.

MD Klein Horsman, H. K. (2007). Morphological muscle and joint parameters for musculoskeletal modelling of the lower extremity. *Clinical Biomechanics* , 239-247.

Michael Damsgaard, J. R. (2006). Analysis of musculoskeletal system in the AnyBody Modeling System. *Simulation Modelling Practice and Theory 14* , 1100-1111.

Michael McKinley, V. O. (2008). *Human Anatomy* . McGraw-Hill.

National Instruments. (2010, July 7). *Specification for the LabVIEW Measurement File(.lvm).* Retrieved June 9, 2011, from National Instruments: Test, Measurement, and Embedded Systems: http://zone.ni.com/devzone/cda/tut/p/id/4139

Nothern Digital Inc. (1996-2011). *Features of the Optotrak Certus Research-Grade Motion Capture System*. Retrieved from NDI- Accurate Measurement Solutions for Medical, Industrial, and Life Sciences Applications: http://www.ndigital.com/lifesciences/certus-benefits.php

SC White, H. Y. (1989). A three-dimensional musculoskeletal model of gait analysis. *Journal of biomechanics* , 22(8-9):885.

Shin CS, C. A. (2007). The influence of deceleration forces on ACL strain during single leg landing: A simulation study. *Journal of Biomechanics* , 40(5):1145-52.

Taylor KA, T. M. (2011). Measurement of in vivo anterior cruciate ligament strain during dynamic jump landing. *Journal of Biomechanics* , 44(3):365-71.

Thomas W. Kernozek, M. R. (2005). Gender Differences in Frontal and Sagittal Plane Biomechanics during Drop Landings. *Medicine and Science in Sports and Exercise* .

Timothy E. Hewett, G. D. (2005). Biomechanical Measures of Neuromuscular Control and Valugus Loading of the Knee Predict Anterior Cruciate Ligament Injury Risk in Female Athletes: A Prospective Study. *American Journal of Sports Medicine* , 33:492.

Weinhold PS, S. J. (2007). The influence of gender-specific loading patterns of the stop-jump task on anterior cruciate ligament strain. *Injury Biomechanics* , 38(8):973-8.

Withrow TJ, H. L.-M. (2006). The effect of an impulsive knee valgus moment on in vitro relative ACL strain during a simulated jump landing. *Clinical Biomechanics* , 21(9):977-83.

Zhang Y, L. G. (2011). Biomechanical simulation of anterior cruciate ligament strain for sports injury prevention. *Comput Biol Med.* , 41(3):159-63.